The Dissertation Committee for Edmund Locke Frost III Certifies that this is the approved version of the following dissertation:

FACIES HETEROGENEITY, PLATFORM ARCHITECTURE AND FRACTURE PATTERNS OF THE DEVONIAN REEF COMPLEXES, CANNING BASIN, WESTERN AUSTRALIA

Committee:

Charles Kerans, Supervisor

Scott Tinker

William Fisher

Xavier Janson

Phillip Playford

FACIES HETEROGENEITY, PLATFORM ARCHITECTURE AND FRACTURE PATTERNS OF THE DEVONIAN REEF COMPLEXES, CANNING BASIN, WESTERN AUSTRALIA

by

Edmund Locke Frost III, B.A.

Dissertation

Presented to the Faculty of the Graduate School of

The University of Texas at Austin

in Partial Fulfillment

of the Requirements

for the Degree of

Doctor of Philosophy

The University of Texas at Austin

December, 2007

Dedication

This work is dedicated to my wife Annie and to my family for their unfaltering support during this process and to the late Bob Goldhammer for introducing me to the world of carbonate stratigraphy and for setting me on this path.

Acknowledgements

The author would like to thank Charlie Kerans, for his support, guidance and friendship throughout this project and for taking me on as student during a chaotic time. Philip Playford of the Geologic Survey of Western Australia is graciously thanked for his invaluable input and help with this project, for introducing me to the Canning Basin and for directing me towards two spectacular field localities. Thanks to my Ph.D. committee: Charlie Kerans, Scott Tinker, Phillip Playford, Xavier Janson, and William Fisher, for their input on this work.

Steve Rogers, Annie Frost, Sam Scott, Ted Playton, Wayne Narr and Eric Flodin are thanked for their assistance and camaraderie in the field. Xavier Janson and Jerry Bellian are graciously thanked for their help with gOcad and Polyworks. Roger Hocking is thanked for providing me with GIS and cycle data from the Canning Basin and for candid discussions in the field. Wayne Narr, Eric Flodin Dan Carpenter, Ed Kosa and Chris Zahm (RCRL) are thanked for enlightening discussions on syndepositional fractures. Leonel Gomez and Randy Marrett are helped me understand the “ins and outs” of fracture clustering. Annette George is thanked for discussions on the Famennian of the Canning Basin.

The Bureau of Economic Geology’s Reservoir Characterization Research Laboratory and its sponsors provided significant financial support that allowed for this research to be conducted in the remote Australian outback. The Geological Survey of Western Australia provided key field and logistical support in the form of a vehicle and camping gear for two field seasons. Satellite imagery was graciously provided by ExxonMobil Upstream Research. This research was funded in part by grants and fellowships from: the Jackson School of Geosciences Foundation,

ConocoPhillips, Chevron, the Geological Society of America and the American Association of Petroleum Geologists. Land access was provided by Western Australia's Conservation and Land Management Agency (CALM) and by Peter Leutenegger of the Napier Downs station. Peter Leutenegger is graciously thanked for a helicopter flight over the Northern Napier Range. Western Metals Ltd. is thanked for access to the Napier Downs core shed and the NRD-88 core.

FACIES HETEROGENEITY, PLATFORM ARCHITECTURE AND FRACTURE PATTERNS OF THE DEVONIAN REEF COMPLEXES, CANNING BASIN, WESTERN AUSTRALIA

Publication No._____

Edmund Locke Frost III, Ph.D.
The University of Texas at Austin, 2007

Supervisor: Dr. Charles Kerans

Carbonate facies patterns and stratal architecture are the product of the complex interaction of internal (e.g., reef-building biota, sediment production) and external drivers (e.g., tectonics, climate, and relative sea level). In the Canning Basin of Western Australia, many of these drivers are in flux across the Late Devonian Frasnian–Famennian (F–F) boundary and significant variations in reef-building biota and long-term accommodation are observed. This study documents the evolution of the Canning Basin's Devonian reef complexes across the F–F boundary and proposes a new interpretation of the stratal architecture and paleobathymetric profile of the Famennian. Data presented here demonstrate the evolution of a shelf-crest system in the Famennian, with beds expanding basinward and

the reef growing in water depths of approximately 5-15 m. The paleobathymetric profile of the Famennian described by this study represents a departure from the well-documented barrier-reef system of the Frasnian. Digital outcrop models help capture the heterogeneity of the Famennian system and allow for characterization of the Devonian reef complexes across the F–F boundary.

Syndepositional fractures are a ubiquitous feature of high-relief, reef-rimmed carbonate systems and these features exert a profound influence on many facets of platform evolution. This study documents strong variability in syndepositional fracture patterns as a function of lithofacies and depositional setting and evidence for the temporal evolution of the mechanical properties of the Devonian reef complexes is presented. A statistically significant relationship is documented between syndepositional fracture development and variations in stratigraphic architecture, approximated here by platform-margin trajectory. This relationship implies a significant stratigraphic control on syndepositional deformation in carbonate platforms and suggests that external drivers are not required to generate early fractures in high-relief carbonate platforms.

Table of Contents

List of Figures

Tables

Chapter One: Introduction

SCOPE OF PROJECT

The Devonian reef complexes of Western Australia's Canning Basin represent one of the world's best-preserved and exposed examples of an ancient reef system. The reef complexes occur as a rugged northwest to southeast trending, 350 km long outcrop belt on the northeastern margin of the Canning Basin (Figure 1.1). The Devonian reef complexes have been subjected to limited amounts of structural and diagenetic overprinting and much of the original depositional architecture is well-preserved and easily accessible (Figure 1.2). The goals of this field-based study are as follows:

- Characterize the spatial variability of facies patterns, stratal architecture, and cyclicity of the late Frasnian and Famennian reef complexes of the Canning Basin.
- Determine if variations in platform architecture occur across the Late Devonian Frasnian–Famennian mass extinction boundary.
- Acquire high-resolution, ground-based LIDAR (LIght Detection and Ranging) data from the Devonian reef complexes and create outcrop-calibrated geocellular facies models.
- Investigate the spatial and temporal variability of syndepositional fractures in the Devonian reef complexes.
- Test the hypothesis that syndepositional fracture patterns vary systematically as a function of changes in stratigraphic architecture.

Each of the following chapters have been written as stand-alone manuscripts, which

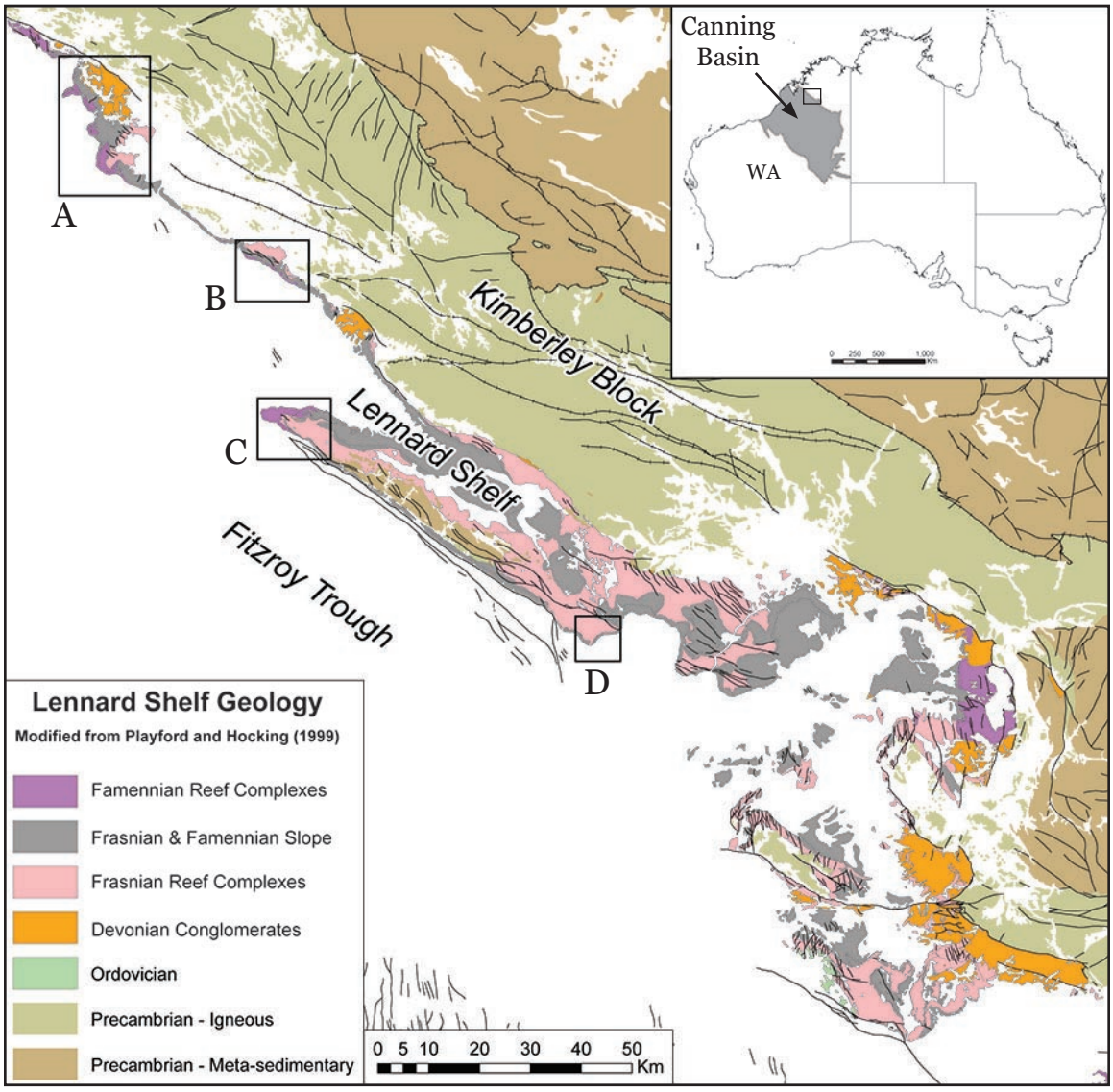

Figure 1.1: Geology of the Lennard Shelf and study area locations.

Primary study areas: (A) the northern Napier Range, (B) Windjana Gorge, (C) the northern Oscar Range, and (D) the southern Oscar Range. Geology modified from Playford and Hocking (1999).

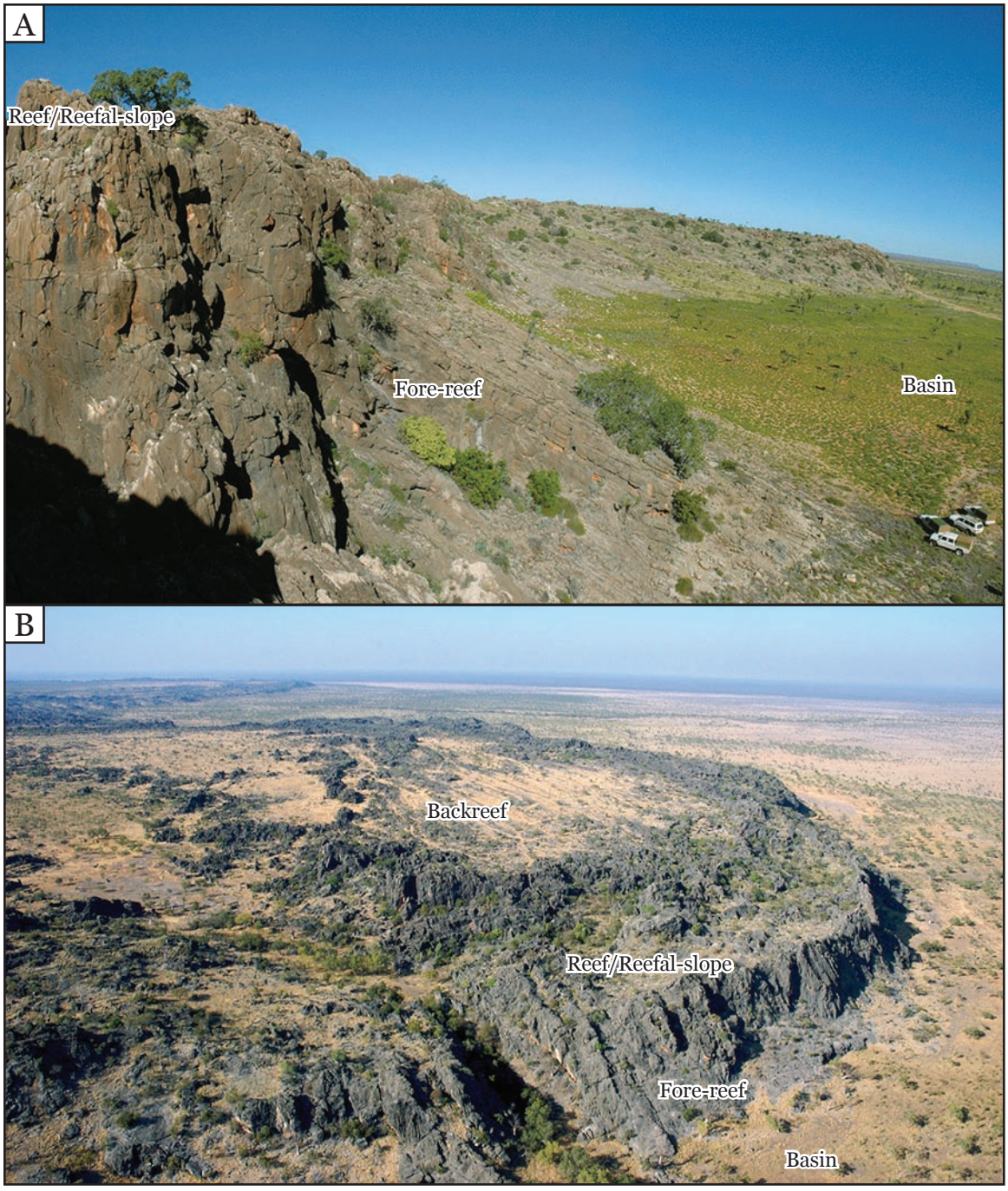

Figure 1.2: Outcrop exposures of the Devonian reef complexes.

(A) Middle Frasnian reef to basin exposures, Nadji Cave area (vehicles provide scale). (B) Exposures of a series of Famennian platforms along the northern Napier Range, cliffs are 40-60 m tall. In both cases, the modern cliff-line represents the relatively undeformed depositional topography of the Devonian reef complexes.

are in the process of being submitted to peer-reviewed journals for publication.

STUDY AREA AND DATASET

The Devonian reef complexes of the Canning Basin outcrop in the sparsely populated West Kimberley region of Western Australia. The Devonian reef complexes are surrounded by open, grass-covered savanna plains lined with boab and gum trees, while spinifex covers the karsted tops of the rugged limestone ranges and lush tropical riparian areas line the region's river gorges. The climate of the Kimberley is warm and dry during the Southern Hemisphere's winter months and wildfires are common. Heavy rains inundate the area during the summer "wet-season" months and temperatures often exceed 110° F. The spectacular landscape of the Devonian reef complexes is home to three national parks: Windjana Gorge, Tunnel Creek, and Geikie Gorge, which draw tourists and geologists from around the world.

The field areas selected for this study include: the northern Napier Range, Windjana Gorge, and the northern and the southern Oscar Range (Figure 1). Data for this study were collected over the course of four field seasons from 2004 – 2007 (seven months in total). Fieldwork was conducted each year between the months of May and August, durring the Canning Basin's "dry-season". The Devonian reef complexes were accessed from the town of Derby, via the Gibb River and Fairfield Leopold roads. Access to the northern Napier Range was granted by the Napier Downs station, Windjana Gorge was accessed via the CALM (Conservation and Land Management) national park entrance, and access to the northern Oscar Range was permitted by the Kimberley Diamond Company. Due to the rugged topography of most field areas, outcrops were typically approached by foot.

Data for this study consists of either field data (e.g., mapping, measured

sections, core description and 1D fracture scanlines) or remote sensing data (LIDAR pointclouds, satellite imagery, and photomosaics). Detailed field mapping was conducted in the Billy Munro Gorge area of the northern Napier Range and in Windjana Gorge during the 2005 and 2006 field seasons. Fifteen measured sections were acquired from the northern Napier Range (Billy Munro Gorge and Limestone Spring), Windjana Gorge and the northern Oscar Range between 2004-2005 and base-metal exploration core that penetrated Famennian reef to basinal strata in the Billy Munro Gorge area was described during the 2005 field season. During the 2006 field season, twelve 1D fracture scanlines were collected along the polished canyon walls of Windjana Gorge and Tunnel Creek recording over 1700 fractures.

Satellite imagery was utilized to measure syndepositional fracture orientations in each of the study areas and over 2900 fracture traces and eleven 1D fracture scanlines were mapped in ArcGIS. LIDAR data was collected along the canyon walls of Windjana Gorge and Billy Munro Gorge during the 2004-2005 field seasons. This data along with the stratigraphic data collected by this study were used to generate outcrop-calibrated geocellular models. Methods and data specific to each study will be discussed in more detail in the following chapters.

PREVIOUS WORK

The Devonian reef complexes of the Canning Basin have had a long history of investigation beginning with oil exploration carried out by Wade in 1924, who was the first to recognize the Devonian reef complexes as ecologic reefs (Playford, 1980). Teichert (1941, 1943, 1947) established the initial biostratigraphic zonations for the Devonian reef complexes, while Guppy et al. (1958) outlined the Paleozoic stratigraphy of the Canning Basin. Playford and Lowry (1966) defined the general lithostratigraphic units and provided detailed geologic maps for the Devonian reef

complexes. Logan and Semeniuk (1976) proposed a radical interpretation for the Devonian reef complexes, suggesting that many of the observed fabrics and geometries were the result of greenschist grade metamorphism. Playford (1980, 1984) refined the existing stratigraphy, paleoecology, paleobathymetry and depositional models for the Canning Basin. In these two publications, Playford was able to disprove the "dynamic metamorphism" hypothesis of Logan and Semenuik (1976) by demonstrating a depositional origin for the reef complexes. Kerans(1985), Kerans et al. (1986), Hurley, (1986), and Wallace et al. (1991) provided detailed characterizations of the stratigraphy, paleogeography, fracture patterns and diagenetic evolution of the Devonian reef complexes.

With the advent of sequence stratigraphy, much of the research of the late 1980's and early 1990's was focused on applying sequence stratigraphic models to the reef complexes (Middleton 1987; Kennard et al. 1992; Holmes and Christie-Blick, 1993; Southgate et al., 1993). The Devonian reef complexes were remapped in detail by Playford and Hocking (1999), and other recent research has focused on: slope processes (George et al. 1995; Ward, 1996; George et al., 1997; George and Chow, 2002); tectonic controls on platform morphology (Ward, 1996; Ward, 1999); refining the stratigraphic framework of the reef complexes (Ward 1999; Playford, 2002 Stephens and Sumner, 2003a); paleoecology (Wood, 1998, 2000; Playford 2002, Stephens and Sumner, 2003b); and the reorganization of the reef complexes following the F/F mass extinction event (George and Chow, 2002; Stephens and Sumner 2003b). The geologic framework established by previous workers in the Canning Basin will be discussed in more detail in the following chapters.

Chapter Two: Evolution and Architecture of a Famennian (Late Devonian) Carbonate Platform, Canning Basin, Western Australia

ABSTRACT

Significant changes in reef-building biota and long-term accommodation patterns are observed in Western Australia's Canning basin across the Late Devonian Frasnian-Famennian (F-F) boundary. Empirical relationships between variations in forcing mechanisms and carbonate platform architecture predict that major changes in facies patterns and stratal architecture should be observed in the Canning Basin's Famennian reef complexes; however, to date major changes in platform architecture have not been recognized in the Famennian and Frasnian models are typically applied. This study integrates measured section and core data with field and digital mapping from the well-exposed Famennian-age Billy Munro Gorge area to investigate how changes in carbonate factory type and decreasing accommodation across the F-F boundary are expressed in the stratal architecture and facies patterns of the Canning Basin's Famennian reef complexes.

The Billy Munro Gorge platform evolved as a high-relief (300-400m), progradational platform (progradation/aggradation ratio of approximately 10), with a subvertical calcimicrobial-constructed margin and an accommodation limited, high-energy grainstone and tepee-pisolite-complex-dominated platform interior. High-frequency cycles in the Famennian typically have supratidal caps

This chapter will be submitted to *Sedimentology*.

with varying degrees of marine-vadose diagenetic modification. Three basic high-frequency cycle types are proposed by this study: (1) fenestral laminite capped; (2) tepee capped; and (3) beachrock capped. This study demonstrates the evolution of a shelf-crest system in the Famennian, with beds expanding basinward and the reef growing in water depths of approximately 5-15 m. The paleobathymetric profile of the Famennian documented by this study represents a departure from the well-documented barrier-reef system of the Frasnian. Digital outcrop models generated by this study capture the facies patterns and stratal architecture of the Famennian and allow for a quantitative comparison of the Frasnian and Famennian of the Canning Basin.

INTRODUCTION

Over the last three decades a considerable amount of research has been devoted to understanding how variations in forcing mechanisms control the development of carbonate platforms. It is generally accepted that carbonate facies patterns and stratigraphic architecture are the product of the complex interaction of internal (e.g., carbonate factory type; Schlager, 2003) and external controls (e.g., relative sea level, climate, ocean conditions and antecedent topography; Kerans and Tinker, 1999; Pomar, 2001). The Late Devonian Frasnian–Famennian (F-F) mass extinction marks the global collapse of the Siluro–Devonian stromatoporoid-coral carbonate factory and the subsequent shift to a microbially dominated carbonate factory in the Famennian. In Western Australia's Canning Basin, changes in reef-building biota, lithofacies and slope architecture across the Frasnian-Famennian boundary have been well documented (Playford, 1980, 1984, 2002; Kerans, 1985; Hurley, 1986; George et al., 1997; Wood, 2000; and Stephens and Sumner, 2003). However, variations in platform facies patterns, cyclicity and stratal architecture

of the Canning Basin's Famennian platforms have not been characterized and it remains unclear how the changes associated the F-F transition are manifested in the Devonian reef complexes.

Based on the well-exposed Famennian section at Billy Munro Gorge, the primary focus of this study is to address how the facies patterns and stratal architecture of the Devonian reef complexes respond to the changes in carbonate factory and accommodation patterns across the F-F boundary. Central to this objective are the following goals: (1) examine the temporal and spatial variability of facies and cyclicity in the Famennian, (2) provide a stratigraphic framework for the Billy Munro Gorge area and document platform evolution, (3) develop a dynamic depositional model for the Famennian reef complexes and evaluate the applicability of current models for the Famennian of the Canning Basin and (4) construct a geocellular model of the Billy Munro Gorge platform from high-resolution LIDAR, measured sections and mapping data.

GEOLOGIC BACKGROUND

Regional Setting

The Canning Basin is Western Australia's largest sedimentary basin covering approximately 430,000 km^2 and recording a 15,000 m vertical section of Ordovician through Cretaceous age strata (Brown et al., 1984). The basin is bounded to the north by the Proterozoic Kimberley block and to the south by the Archaean Pilbara craton. Basin development initiated in the Ordovician with broad intracratonic downwarping, followed by active rifting in the middle Devonian through the early Carboniferous, which is marked by the development of the deeply subsident NW-SE oriented Fitzroy Trough (Figure 2.1a; Drummond et al., 1991). During the Late Devonian, carbonate deposition primarily occurred along the basin's western

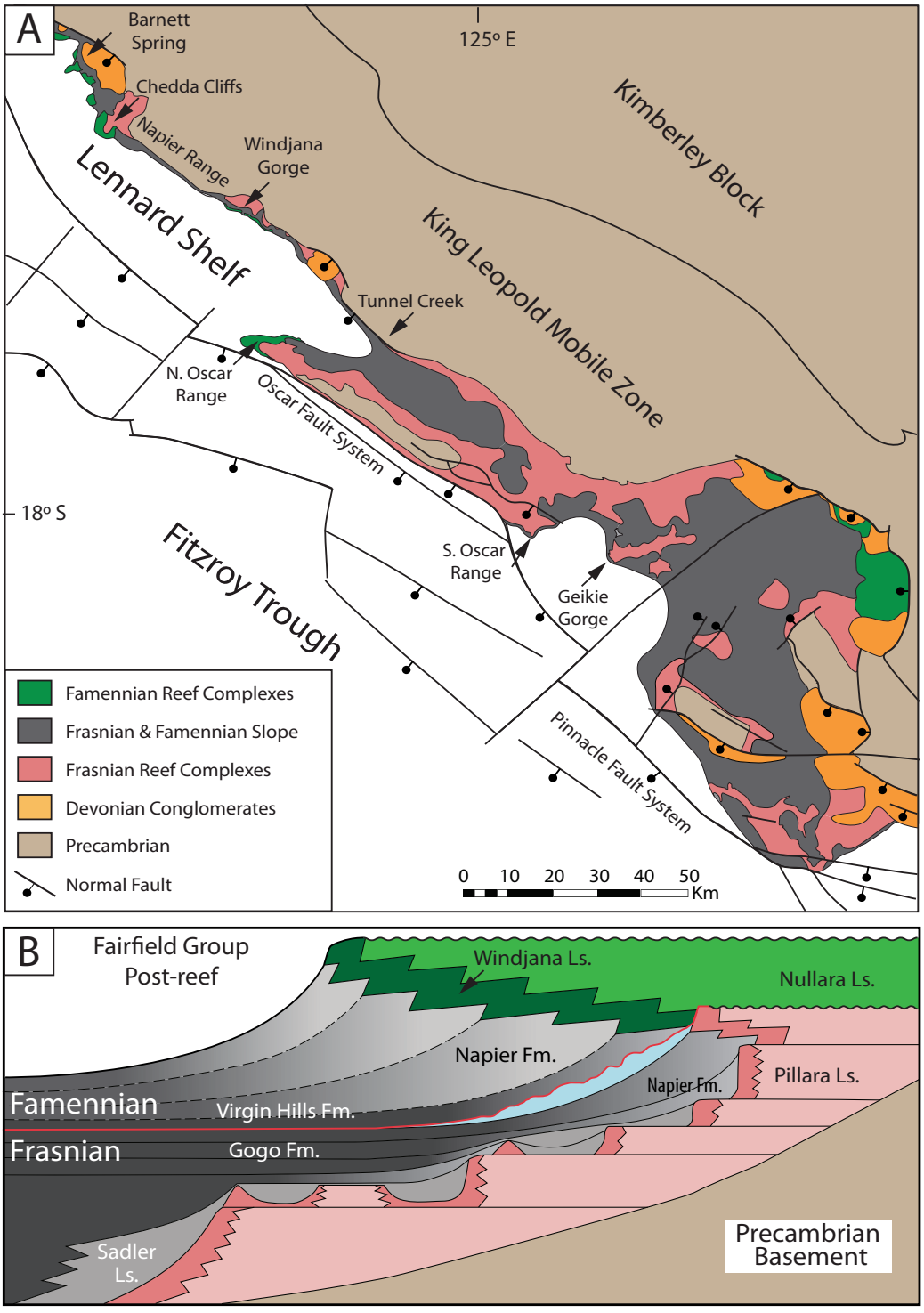

Figure 2.1: Regional geology and stratigraphic setting.

(A) Geology of the Devonian reef complexes, modified after Playford and Hocking 1999. (B) Stratigraphy of the Lennard Shelf. Modified after Playford, 2002.

margin on the shallow Lennard Shelf, with the Devonian reef complexes fringing the mountainous Precambrian Kimberley Block, as well as smaller, isolated, Precambrian emergent uplifts (e.g., Oscar Range; Figure 2.1a). The 10-50 km wide Lennard Shelf is flanked to the northeast by the mountainous Precambrian King Leopold fold-belt of the Kimberley Block and to the southwest by large-scale Late Devonian extensional fault systems (e.g., Oscar Fault and Pinnacle Fault) and the Fitzroy Trough.

Regional uplift in the Late Carboniferous coupled with glaciation in the Early Permian removed many of the younger sediments overlying the Devonian reef complexes (Eyles et al, 2000; Playford, 2002). Following broad, regional Cenozoic uplift, the Devonian reef complexes are today exposed as a rugged 350 km-long northwest- to southeast-trending outcrop belt of flat-topped limestone ranges and much of the original depositional topography of the Devonian reef complexes is relatively undeformed.

Stratigraphy of the Lennard Shelf

Two major reef-building phases are recognized within the Devonian reef complexes as part of a second order sequence: (1) the Givetian-Frasnian Pillara Sequence and (2) the Famennian Nullara Sequence (Figure 2.1b; Playford, 2002 and references therein). The Pillara Sequence developed during a basinwide transgression coincident with peak rifting and is characterized by pinnacle reefs and backstepping high-relief platforms with steep escarpment margins for most of the Frasnian, with progradation in the latest Frasnian (Figure 2.2a). Frasnian platforms were constructed by a consortium of stromatoporoids, corals and calcimicrobes with a narrow (10-50m) and discontinuous reef-rim (Playford, 1980; Kerans 1985; Ward, 1996; Wood, 2000). In many cases the reef is altogether absent

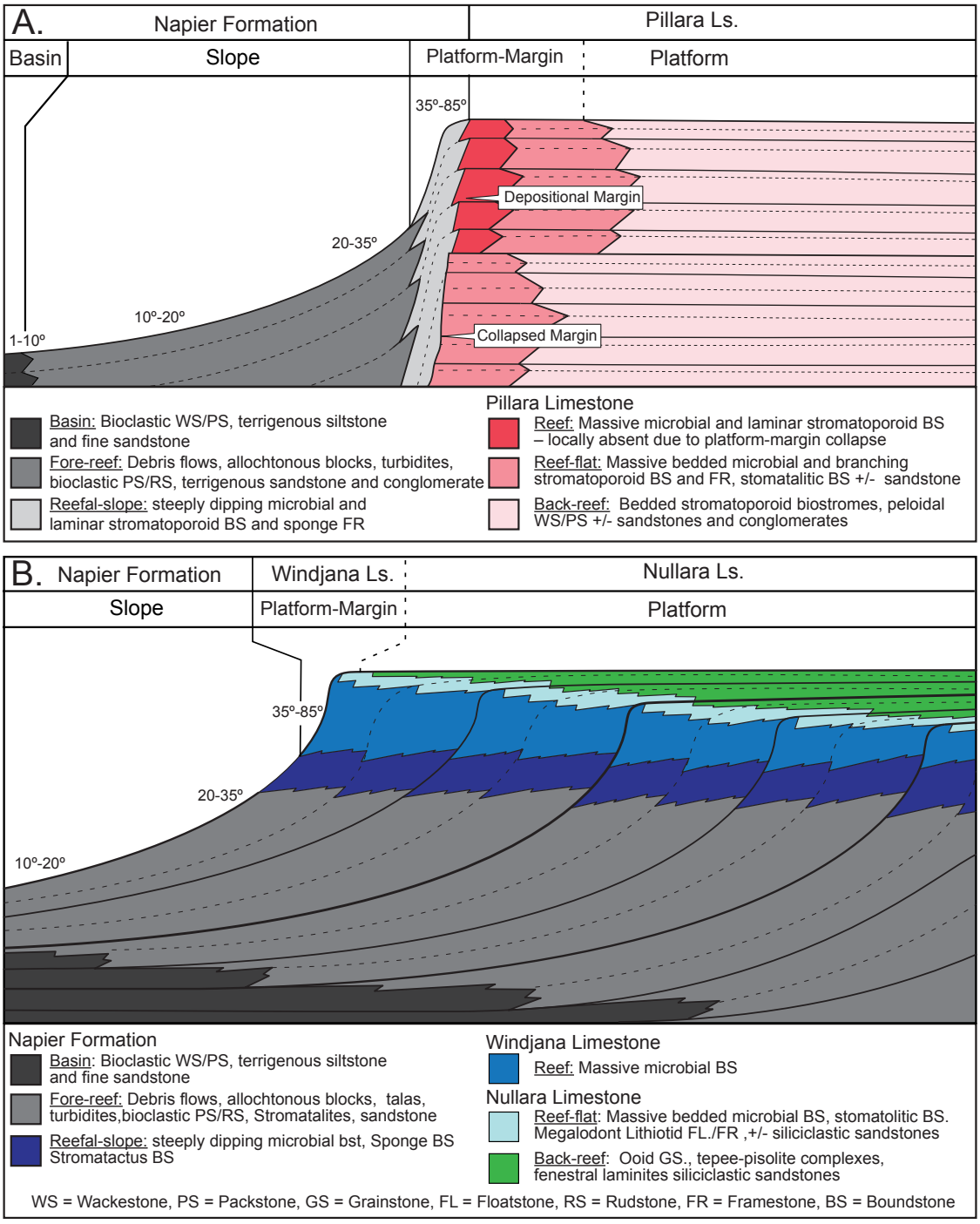

Figure 2.2: Generalized depositional models and lithostratigraphic nomenclature of the Frasnian and Famennian systems.

(A) Frasnian facies tracts and lithostratigraphic nomenclature (modified from Pomar, 2001 after Ward, 1999). (B) Frasnian facies tracts and lithostratigraphic nomenclature (modified from Playford, 1980).

owing to platform margin collapse, juxtaposing reefal-slope and reef-flat strata (Figure 2.2a). The Frasnian reef and reef-flat were deposited in a shallow-water (1-3 m), high-energy setting, creating a paleobathymetric barrier that separated the platform margin from the lower-energy, mud-dominated, subtidal platform interior.

In many cases the Frasnian platforms of the Canning Basin are relatively narrow, with shelf widths of commonly 5 km or less (Figure 2.1a). Narrow shelf-width coupled with proximity to the mountainous Kimberley Block and active basin-bounding faults generated a near constant influx of clastic material. Coarse-grained clastic material frequently bypassed the shelf and platforms often interfingered with conglomerate fans (Playford; Figure 2.1a). Minor progradation occurred in the latest Frasnian, followed by the Frasnian–Famennian (F-F) mass extinction boundary and brief exposure of the reef complexes. The pattern of long-term retrogradation during most of Frasnian, with minor progradation in the latest Frasnian appears to be a global signature, with a similar pattern observed in the Frasnian of the Alberta Basin (Whalen et al., 2000), Kazakhstan (Cook et al., 2002; Zempolich et al., 2002) and China (Chen and Tucker, 2003; Shen and Webb, 2004).

The subsequent prograding Famennian reef complexes of the Nullara Sequence are composed primarily of high-energy grainstones and cyanobacteria (Figure 2.2b; Hurley, 1986; Stephens and Sumner 2003). Famennian platforms have been interpreted as high-relief platforms with microbial activity occurring at considerable depth down the slope (150 m; Playford, 1980). As in the Frasnian, the reef is narrow and extensive early-marine cementation played a fundamental role in the evolution of both the Frasnian and Famennian reef complexes, allowing for the development of a wave-resistant reef rim and steep platform-margin escarpments, as well as brittle material prone to syndepositional fracturing (Playford,

1984, Frost and Kerans, in review a/b).

The Frasnian–Famennian Crisis

The Frasnian–Famennian crisis, one of the five major Phanerozoic extinction events (Sepkoski 1986; McGhee, 1996; Copper, 2002), marks the global collapse of the prolific Siluro-Devonian coral-stromatoporoid tropical reef system. The F-F crisis is generally regarded as a stepwise extinction beginning with the Late Frasnian Kellwasser global anoxic events (Late rhenana and linguiformis conodont zones; Joachimski and Buggisch, 2002; Joachimski et al., 2002) and continuing to end of the Frasnian. Despite the global significance of this event, its cause remains equivocal. Hypotheses range from climate change (Copper, 1986; Joachimiski and Buggisch, 2002), to global anoxia (Buggisch, 1991; Joachimski and Buggisch, 1993), or bolide impact (McGhee, 1996).

In many localities worldwide, reef building ended with the F-F crisis, however in the Canning Basin (Figure 2.1b) and a handful of other localities, reef building continued with the development of microbial reef complexes across the F-F boundary and into the Famennian (Playford, 1980, 2002; Cook et al., 2002; Whalen et al, 2002; Zempolich, 2002; Chen and Tucker, 2004; Shen and Webb, 2004). The F-F boundary in the Canning Basin is characterized by regression in the latest Frasnian, with sea level falling below the terminal Frasnian shelf-edge (Hurley, 1986; Playford 2002). Minor karstification has been reposted in some settings (Playford, 1984; Ward, 1996), possibly enhanced by local tectonic activity (see discussions in Chow et al., 2004 and Playford and Hocking, 2006). Prominent, laterally extensive stromatolite horizons and large-scale stromatolitic bioherms (up to 1 km wide, with up to 50 m of relief) developed in the fore-reef during the F-F interval (Figure 2.1b and Figures 2.3-4; Playford et al., 1976; Playford, 1981;

Hurley, 1986; George, 1999, Webb, 2001).

STUDY AREAS AND METHODS

In order to characterize the stratal architecture, cyclicity and facies patterns of the Canning Basin's Famennian reef complexes, data were collected from the Billy Munro Gorge located in the northern Napier Range (Figures 2.3-4). The Billy Munro Gorge area preserves a complete record across the F-F boundary and the data collected by this study spans the stratigraphic interval from the Late Frasnian through the Late Famennian. Billy Munro Gorge offers a 2.5 km, dip-oriented, cross-sectional exposure of the Famennian backreef and platform-margin. Traditional field data (mapping, measured sections, core description) and digital data (ground-based LIDAR, high resolution satellite imagery) were collected to construct a digital outcrop model (DOM) of the Billy Munro Gorge platform (Figure 2.4). Ancillary Famennian data were collected from the Oscar Range, Limestone Spring and Windjana Gorge (Figures 2.1 and 2.3). Additionally, Frasnian data were collected from Windjana Gorge to serve as a baseline for documenting the variations between the Frasnian and Famennian reef complexes.

Traditional Field Methods

Traditional field data includes 8 measured sections, 450 m of described core and regional field mapping (Figure 2.4a). Measured sections were collected from platform interior to reef facies along Billy Munro Gorge and were plotted on outcrop photographs, along with all key stratigraphic horizons. Where possible, key surfaces identified in individual measured section were "walked out", or were traced on photo mosaics. Hand samples were collected from measured sections and thin sections were prepared to calibrate facies interpretations. An extensive base metal exploration coring program was initiated in the Napier Range in the

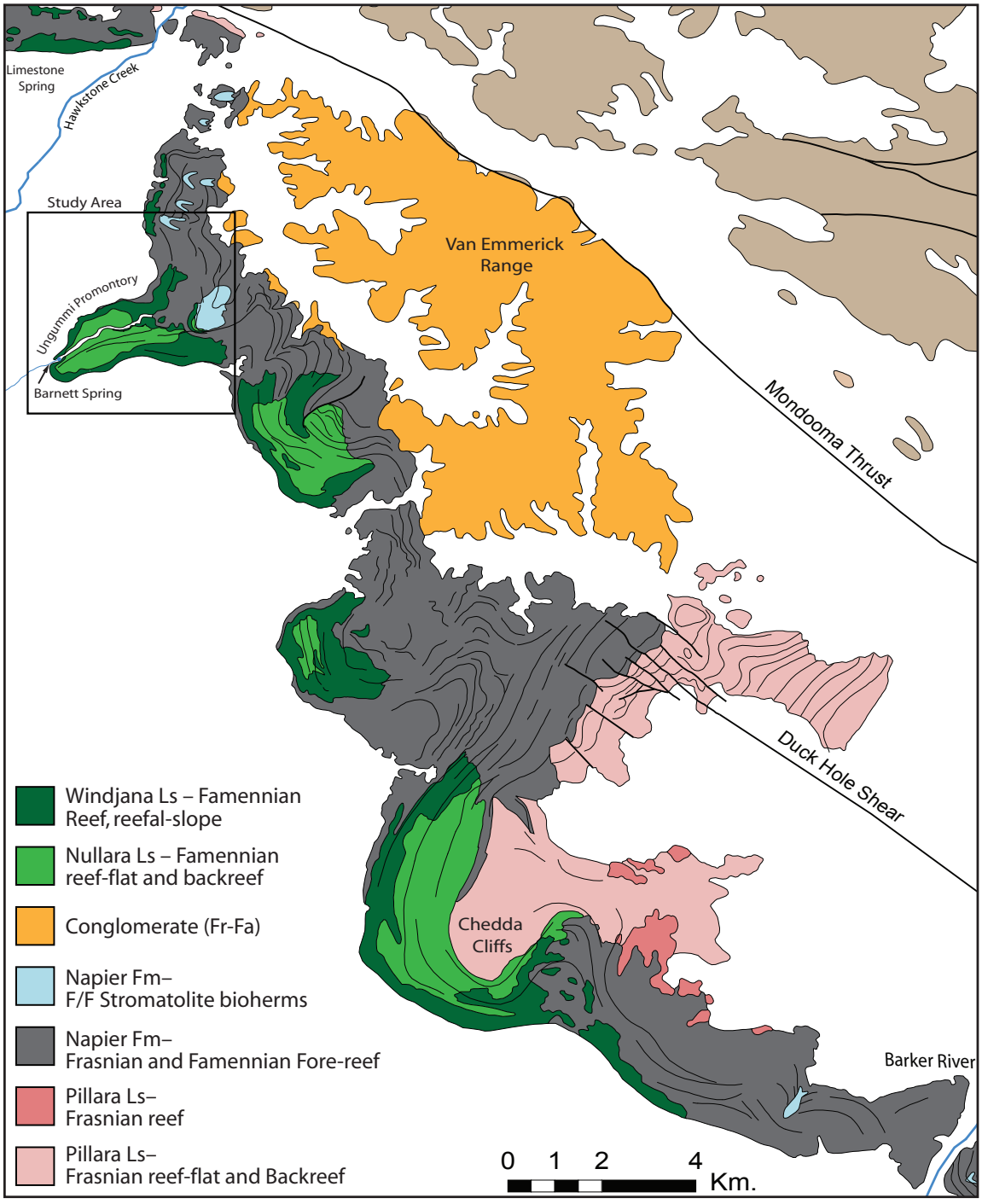

Figure 2.3: Geology of the Northern Napier Range.

Modified after Playford and Hocking 1999.

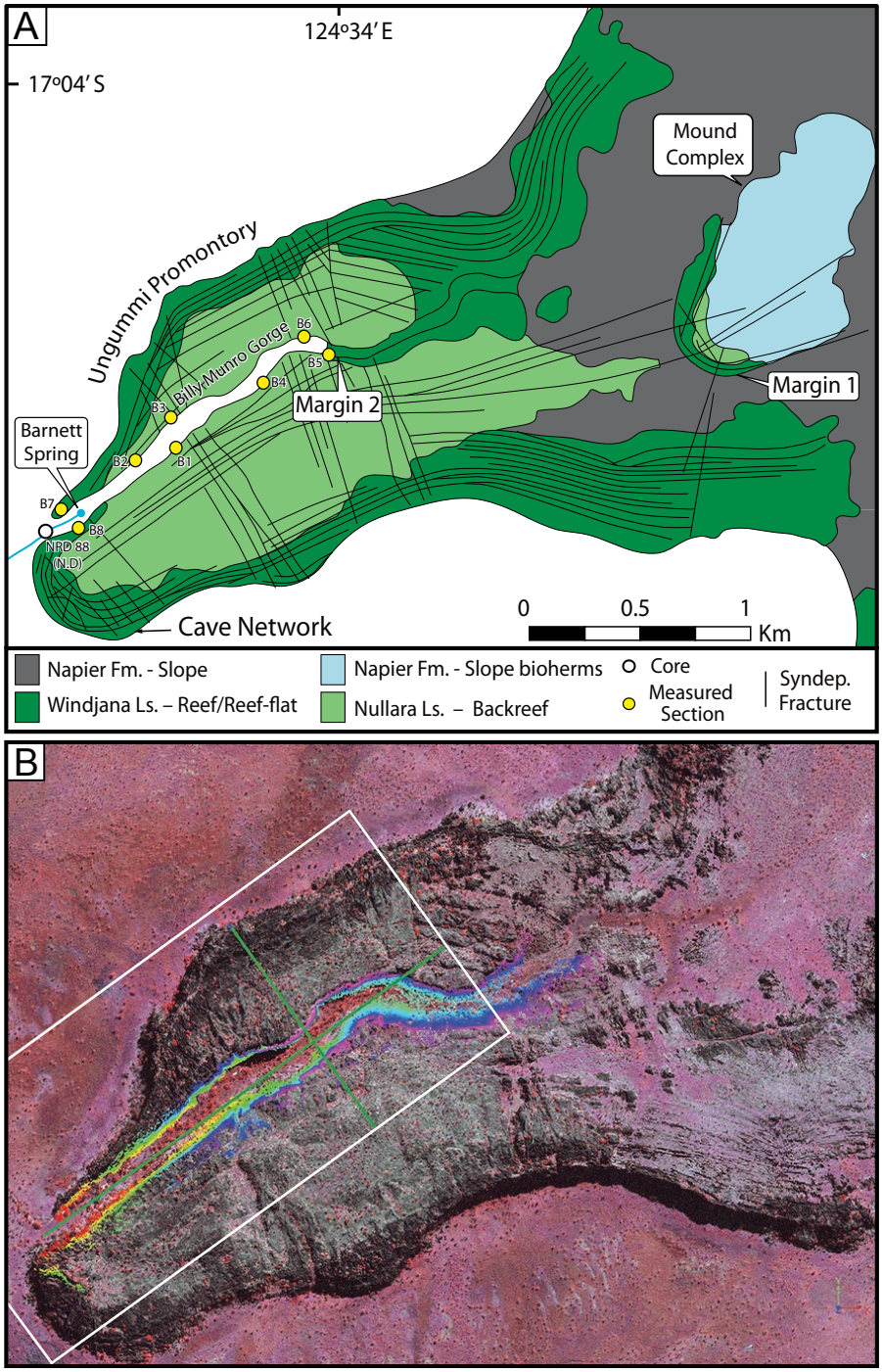

Figure 2.4: Billy Munro Gorge geology and data distribution

(A) Billy Munro Gorge geology and measured section locations, modified after Playford and Hocking (1998), location names after Playford (pers. comm. 2007). (B) Ikonos image of digital data distribution. Rainbow colors represent Lidar data, white rectangle represents gocad model outline.

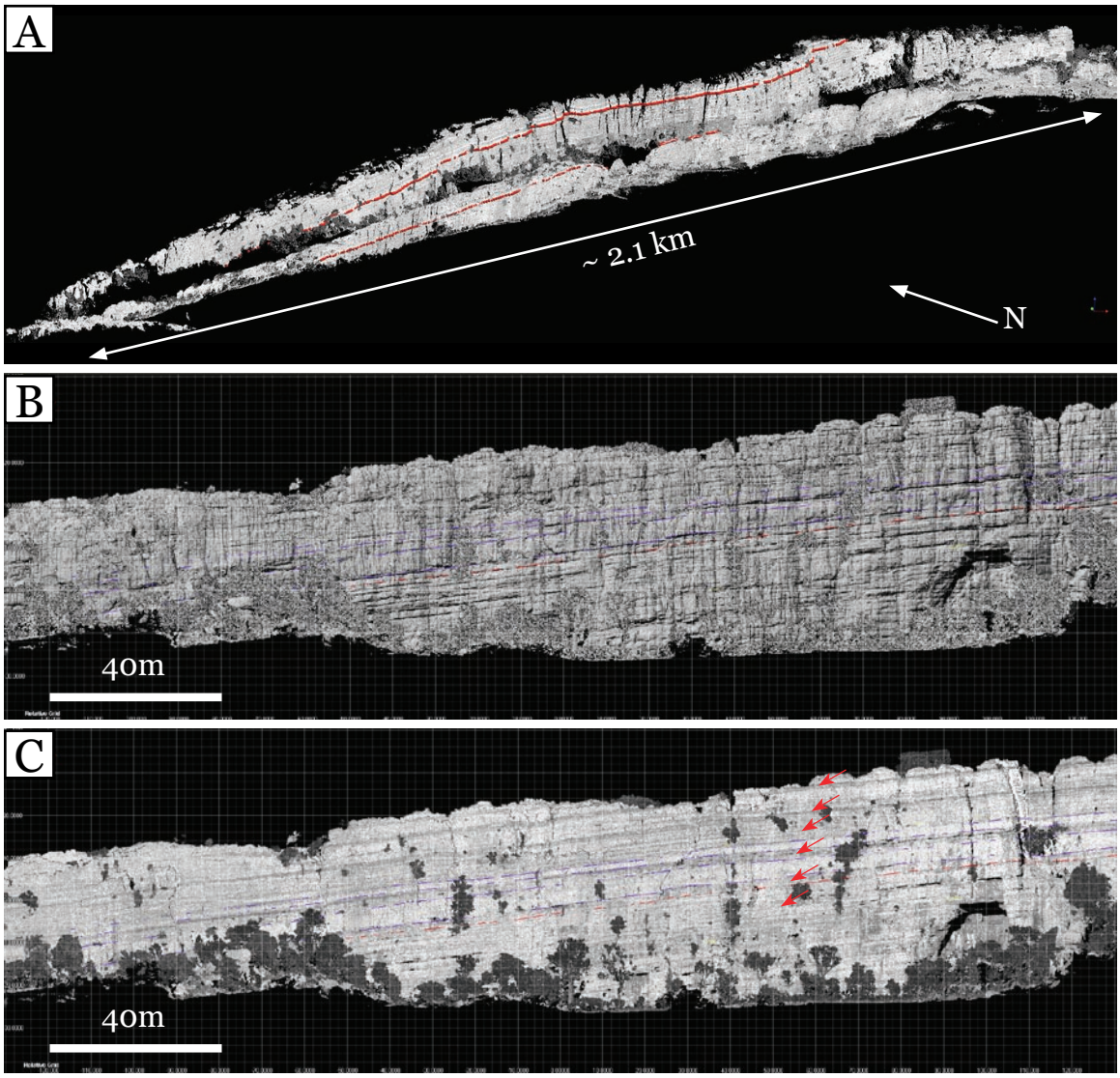

Figure 2.5: LIDAR dataset.

(A) LIDAR pointcloud coverage of Billy Munro Gorge. Red lines represent mapped stratigraphic horizon. (B) Smooth interpolated LIDAR surface, north wall, Billy Munro Gorge. Colored lines represent mapped stratigraphic surfaces. Recessive beds generally correlate to facies with mixed terrigenous content (e.g., fenestral laminites, tepees, beachrock). (C) LIDAR point cloud with intensity values (same view as B). High intensity values (white to light gray) correlate to pure limestone (e.g., ooid grainstone, lithiotid bivalve floatstones), while lower intensity values (medium to dark gray; arrows) generally correlate to facies with mixed terrigenous content (e.g., fenestral laminites, tepees, beachrock). Colored lines represent mapped stratigraphic surfaces.

mid 1970s (Copp, 2000) and a key 450 m core situated near the mouth Billy Munro Gorge was described (NRD-88; Figure 2.4a).

LIDAR Mapping

A three-dimensional digital outcrop model (DOM) was constructed of Billy Munro Gorge from high-resolution ground-based following the methodology of Bellian et al. (2005) and Janson et al., (2007). LIDAR data were collected along the cliff faces of Billy Munroe Gorge at an average point spacing of 3-7 cm (Figure 2.4b) and 164 individual LIDAR scenes covering approximately 2.5km of outcrop were merged and processed following the methods outlined by Bellian et al., (2005). LIDAR data offer several distinct advantages over traditional mapping; (1) LIDAR data are spatially constrained and not subject to the parallax errors which plague photomosaics (Tinker, 1999), (2) object dimensions, spatial distribution and orientations are easily attained and (3) intensity of the returning laser signal provides a qualitative proxy for lithology (Figure 2.5). The DOM provides a high-resolution, spatially constrained template for mapping and serves as the basis for 3D geocellular model construction.

Billy Munro Gorge was mapped at the high-frequency cycle-scale (0.5 – 7 m). High-frequency cycle-scale were first identified in measured section and then mapped laterally with each individual cycle cap mapped directly on the DOM (Figure 2.5). Cycle sets, identified in measured sections, were also mapped on the DOM and were used as guiding surfaces for geocellular model construction. Key geologic features such as individual tepee complexes, laminite caps, or beachrock were mapped directly on the LIDAR pointcloud and given a unique attribute code in the LIDAR interpretation software Polyworks. Measured section paths were digitized on the LIDAR pointcloud as lines and coded for facies at 10 cm spacing

(Figure 2.5). Once the LIDAR interpretation was completed, facies and horizon data were transferred into gOcad and a geocellular model was created following the methodology of Janson et al (2007), which will be discussed in detail in a later section.

FAMENNIAN DEPOSITIONAL FACIES

The Famennian platform interior is characterized as accommodation-limited, consisting of a complex mosaic of high-energy grainstone shoals, tepee-pisolite complexes and fenestral laminites (Hurley, 1986). Microbial, grain-dominated facies replace the mud-dominated facies of the Frasnian platform interior, with a similar shift to grain-dominated facies reflected in the Famennian reef and slope (Kerans 1985). The stratigraphic nomenclature of Playford (1980, 1984) is largely used by this study, however the term facies (i.e., reef facies) is replaced with the term facies tract (i.e, reef facies tract; sensu Kerans and Fitchen, 1995; Tinker, 1998). The term facies tract refers to a genetically linked set of lithofacies that share a common shelf-profile position and reflect deposition in a discrete water depth and energy setting (e.g., reef, reef-flat, or backreef) and is equivalent to the facies belts of Wilson (1975; Tinker, 1998).

Platform Facies Tract

Fenestral laminites

Thin-bedded and laterally continuous fenestral laminites are common features of the Famennian backreef. This facies is composed of coarsely fenestral grainstones and packstones, with common algal binding and a variable component of fine-grained terrigenous material. A broad variety of grain types occur in this facies ranging from peloids, pisoids and ooids to lithoclasts. Microbial binding is prevalent, typically in the form of mats with occasional microdigitate stromatolites

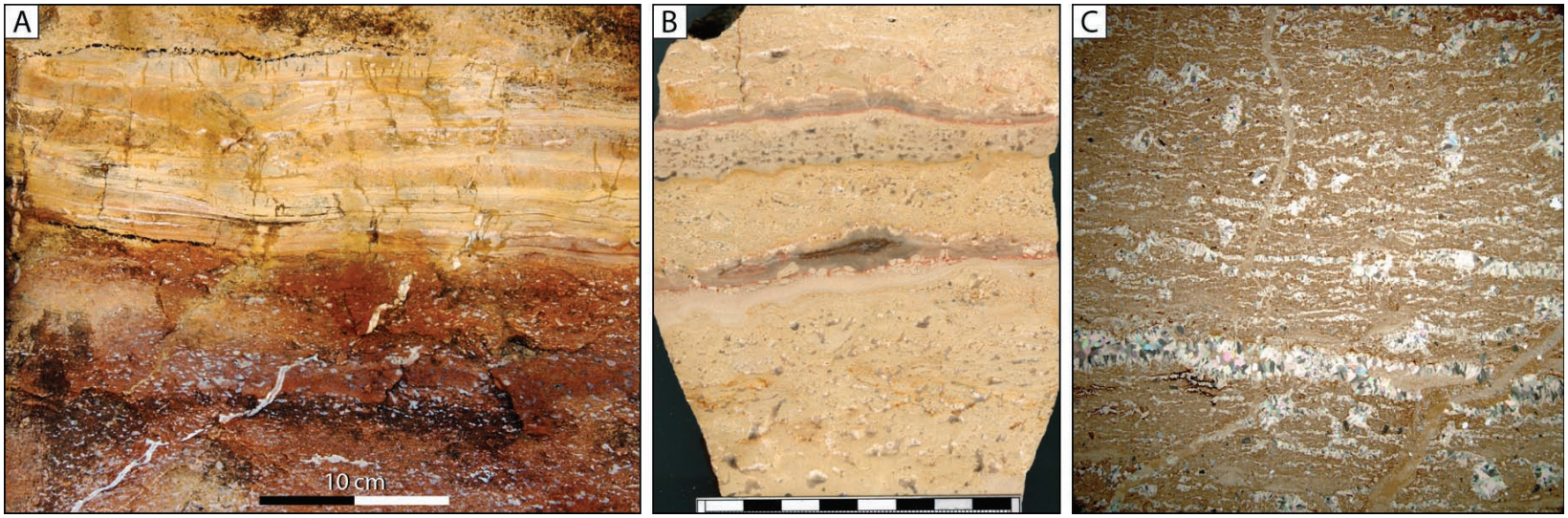

Figure 2.6: Fenestral laminite facies

(A) Laminite cap overlying fenestral grainstone, backreef, Limestone Spring. (B) Sheet cracked, coarse laminite cap, backreef Northern Oscar Range. (C) Laminoid fenestrae and sheet cracks in laminite cap, Billy Munro Gorge. Xpl 0.57 magnification.

(Figure 2.6).

Fenestrae are generally very well developed and irregular, tubular and ammonoid morphologies are common. Vertically elongate tubular fenestrae have been interpreted by previous workers to represent root molds (Read, 1973b; Playford et al., 1989), while laminar fenestrae often coalesce laterally to form sheet cracks (sensu Fischer, 1964). Sheet cracks, which are interpreted to be desiccation features (Fischer 1964; Hardie and Ginsburg, 1977), commonly occur along bedding planes and often in-filled with sediment and pendant cements. This facies has a distinctive weathering pattern, often forming 10–50 cm reddish-brown recessive beds. The terrigenous content of the fenestral laminites attenuates the LIDAR laser signal, giving this facies lower intensity values than pure limestone (Figure 2.5c), The low intensity values of this facies coupled with its recessive nature give this facies a unique character in the DOM, aiding correlation of these beds between measured sections.

Tepee complexes

Tepee complexes are perhaps one of the most striking facies of the Famennian platform interior. These antiformal compressional structures have been described from a number of settings in the geologic record (Asseretto and Kendall, 1977; Fischer, 1964; Hanford et al., 1984; Kendall and Warren, 1987; Dunn, 1992; Kerans and Harris, 1993). In the Famennian backreef, tepee complexes occur in disrupted layers sheet-cracked, fenestral laminite and coated-grain grainstone. Sheet cracked fenestral laminite beds can be traced into tepee beds, with tepees initiating from sheet cracks in some cases (Figure 2.7).

In Billy Munro Gorge tepees occur either as isolated 0.25-1.50 m tall individual features distributed along specific stratigraphic horizons, or as stacked

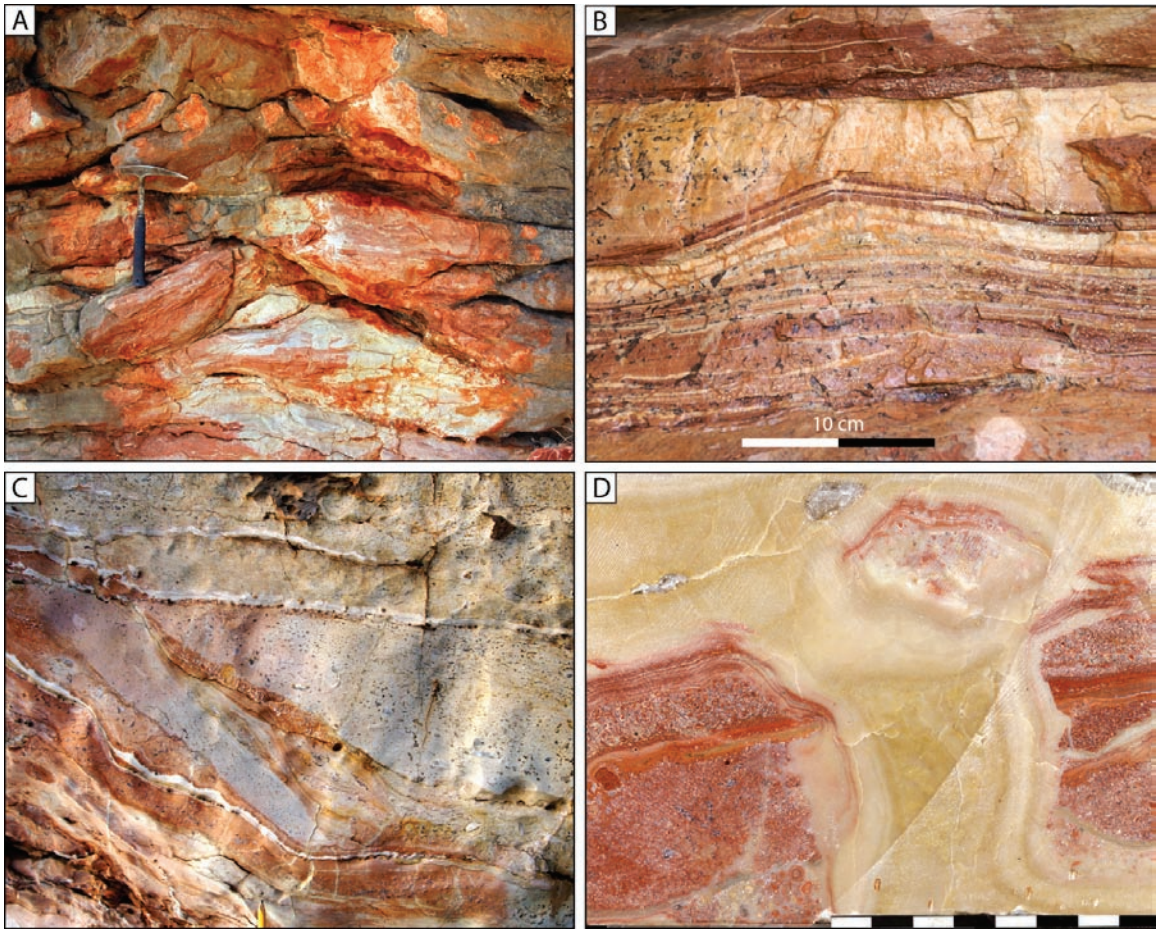

Figure 2.7: Tepee structures

(A) Stacked small-scale tepees, with at least four discrete tepee horizons, Famennian backreef, Billy Munro Gorge. (B) Small-scale nascent tepee in fenestral laminite facies, Famennian backreef, Billy Munro Gorge. (C) Disrupted fenestral laminites along tepee flank, latest Frasnian backreef, Geikie Gorge. note rotated sheet cracks with geopetal fill. Pencil for scale at base. (D) Tepee core with radiaxial fiberous marine cement fill, Famennian backreef, Billy Munro Gorge. Scale gradations are in cm.

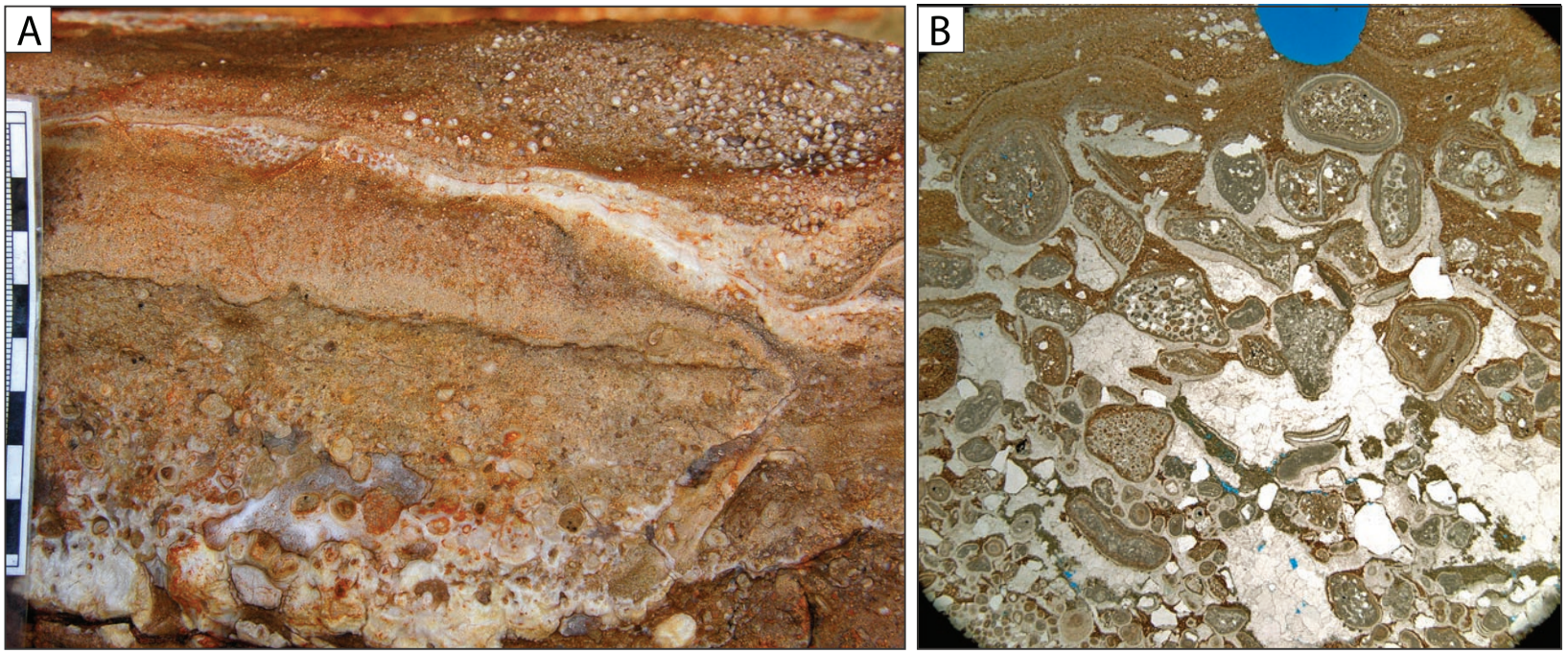

Figure 2.8: Coated-grain peloid microbial packstone-rudstone.

(A) Coated-grain packstone-rudstone with pendant cements, Famennian backreef, Oscar Range. (B) Capped oncoids, Famennian backreef, Billy Munro Gorge.

composite tepee-pisolite complexes up to 13.5 m tall. In composite tepee zones, individual tepees tend to stack vertically over one another across high-frequency cycles, suggesting that once tepees develop, they seed continued growth of tepees in subsequent younger layers (Figure 2.7a).

It is generally accepted that tepees are products of marine-vadose diagenesis that form due to compressional stress generated by displacive crystallization in early-lithified sediment crusts or hardgrounds (Kendall and Warren, 1987). Tepee generation requires repeated cycles of inundation and exposure and is best developed on local paleo-topograhy such as emergent shoal crests, or barrier beach complexes (Egenhoff et al., 1999; Kerans and Tinker, 1999 Barnaby and Ward. 2007) and the basinward extent tepee belts can be used as a paleo-strandline or sea level indicator (Esteban and Pray, 1977; Kerans and Tinker, 1999).

As a tepee develops its characteristic chevron morphology, void space forms under the buckled slabs in the tepee core; this space is subsequently infilled with sediment and cement. Famennian tepee fills observed in the Billy Munro Gorge area include: marine cement, grainstone, fossils, microbialite or in some cases siliciclastic sand. Extensive marine cementation in tepee cores is generally not common, with the exception of when tepees develop near the platform margin or syndepositional fractures (Figure 2.7d). Dunn (1992) has argued that the compression required for tepee growth occurs to a large degree from intergranular crystal growth, rather than solely from the elaborate cement mosaics often observed in tepee cores (Asseretto and Folk, 1980) and that in many cases these cements are secondary ornamentation (Figure 2.7d).

Chow and George (2004) proposed that several examples of tepee features were agglutinated microbial mounds, not marine-vadose compressional features and proposed that based on morphology many of the tepee features observed in

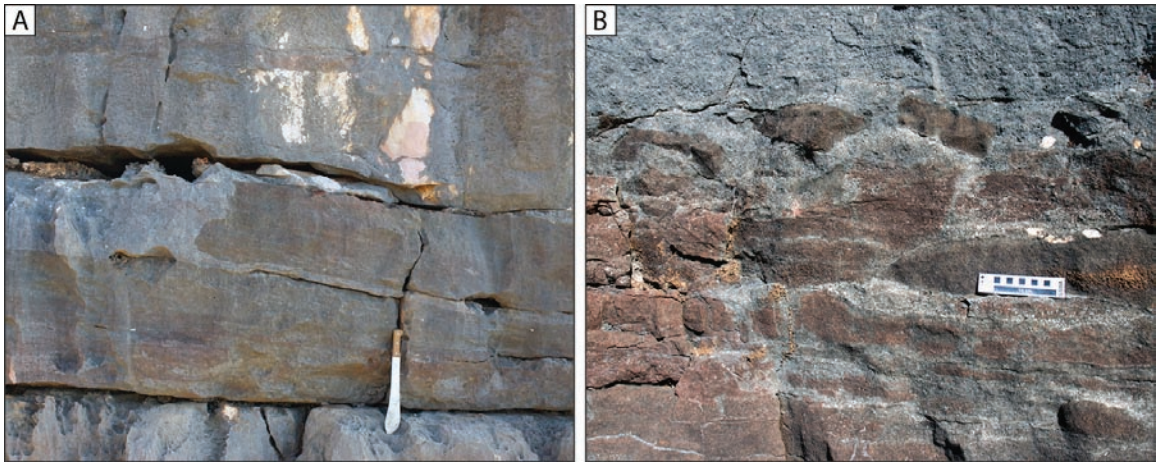

Figure 2.9: Beachrock.

(A) Cuesta morphology in beachrock, Billy Munro Gorge. (B) Reworked beachrock slabs, Billy Munro Gorge.

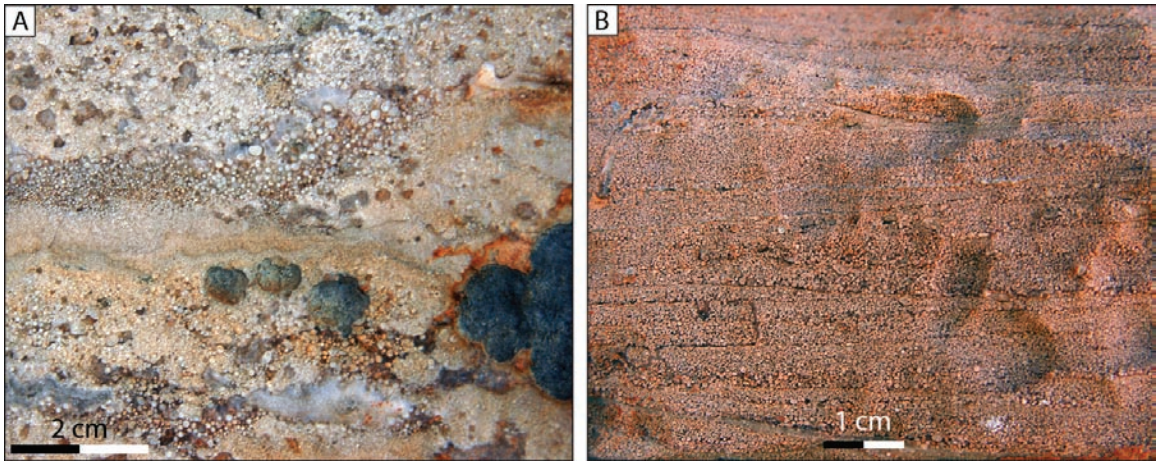

Figure 2.10: Ooid grainstone.

(A) Bubble fenestral ooid grainstone-boundstone, Northern Oscar Range. (B) Cross laminated ooid grainstone, Billy Munro Gorge.

the Famennian were microbial mounds. The basis for Chow and George's (2004) interpretation came from the close association of tepee features with microbial fabrics, the lack of cement in many tepee cores and "thickened" tepee cores. This interpretation will be addressed in detail in a later section.

Coated-grain floatstone-rudstone

The coated-grain floatstone-rudstone is one of the most prevalent facies in the Famennian backreef (Kerans, 1985) and occurs in close association with tepee complexes. This facies contains a broad range of nonskeletal allochems ranging from pisiods, peliods, ooids, grapestone, oncoids and lithoclasts, with a variable siliciclastic component (< 35%). Microbial binding is prevalent and occurs primarily in the form of ferruginous, laminated, micritic crusts (Kerans, 1985), small-scale digitate stromatolites, grainy oncoids and oncoids with growth caps (Figure 2.8). This facies is often coarsely fenestral, with abundant bubble fenestrae and sheet cracks. Skeletal material is generally uncommon, with rare gastropod and bivalve fragments. Grains are often iron stained and meniscus and pendant cements are often observed in this facies suggesting intermittent vadose conditions (Figure 2.8b).

The coated-grain floatstone-rudstone interfingers down dip with ooid grainstones and laterally with tepee complexes. Two depositional settings are represented by this facies: (1) in the absence of tepees, this facies is interpreted to represent stabilized sand flats (Kerans, 1985) in a back shoal setting (Harris, 1979); and (2) when tepees are present, this facies association is interpreted to be analogous to the shelf-crest tepee pisolite complexes of the Permian Yates-Tansil Formation of West Texas (Dunham, 1969; Esteban and Pray, 1977; Kerans and Harris, 1993).

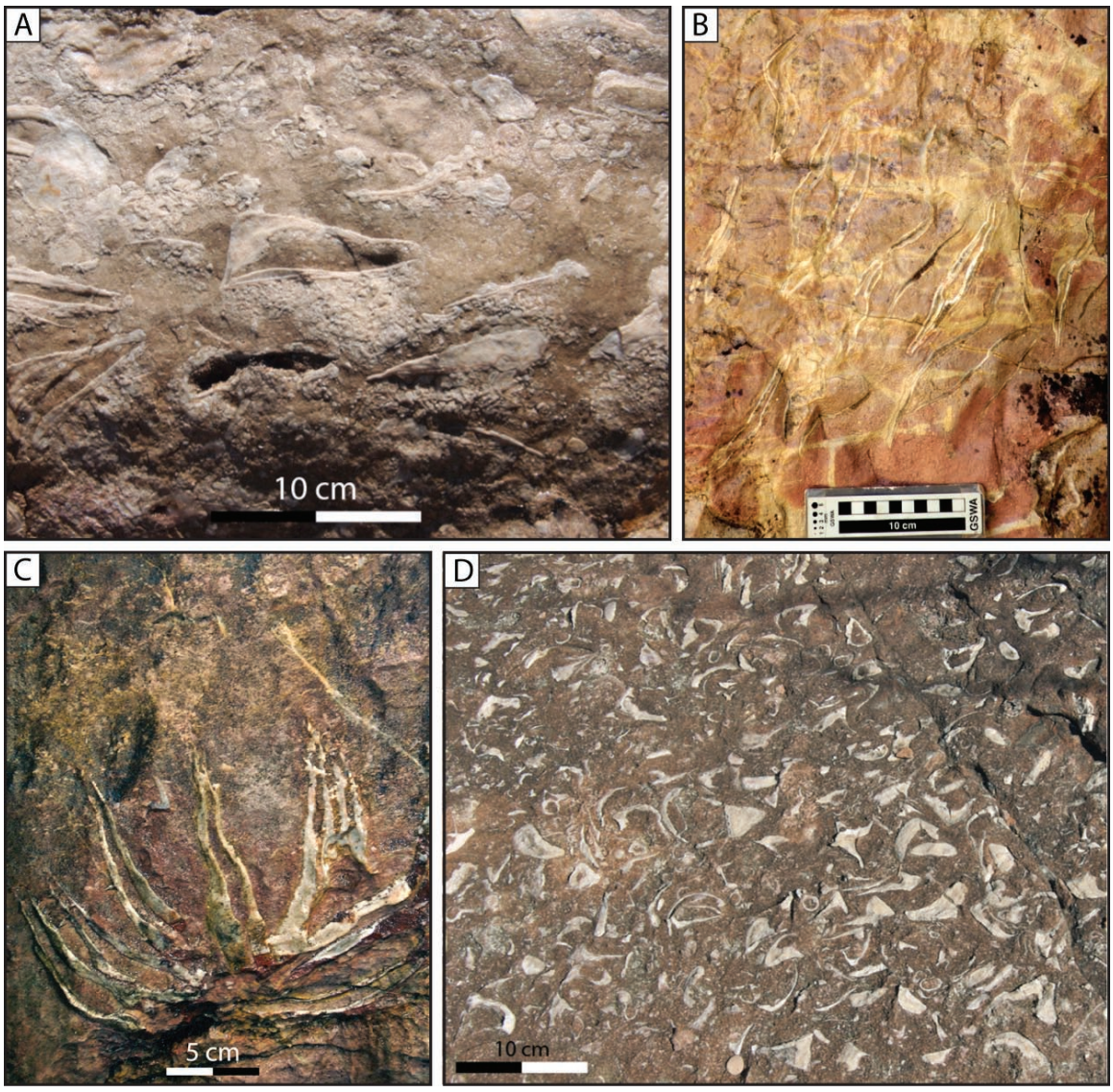

Figure 2.11: Lithiotid-megalodont floatstone-bafflestone facies.

(A) Lithiotid megalodont ooid floatstone, backreef, Billy Munro Gorge. (B) Lithiotid bivalves in growth position. Lithiotid bafflestone with ooid grainstone matrix, near platform-margin, Billy Munro Gorge. (C) Lithiotid bivalves in colonial growth arrangement. Lithiotid bafflestone with ooid grainstone matrix, near platform-margin, Billy Munro Gorge. (D) Megalodont floatstone with sandy matrix. Reef-flat Billy Munro Gorge.

Beachrock

Beachrock is an important facies in Billy Munro Gorge and has not been previously recognized in the Canning Basin. The beachrock facies consists of early-lithified, low-angle, basinward dipping slabs of ooid grainstone and v amounts of siliciclastic sandstone (<25%). In some cases the classic "cuesta" morphology (Ginsburg, 1953) associated with the landward truncation of beachrock slabs is observed (Figure 2.9a). Individual beachrock horizons can be traced landward into tepee-pisolite horizons and down dip into bioclastic ooid-grainstones and megalodont floatstones where reworked beachrock slabs are common (Figure 2.9b). In modern settings, beachrock represents in-situ lithification of foreshore sediments at or above the intertidal zone as a function of marine vadose diagenesis associated with tidal wetting and drying cycles (Donaldson and Ricketts, 1979; Ginsburg 1953). While volumetrically insignificant in the Famennian, beachrock is an important facies given its utility as a reliable strandline indicator and serves as datum for paleobathymetric interpretations.

Ooid grainstone

Two types of ooid grainstone (GS) are common in the Famennian backreef (Kerans, 1985; Figure 2.10): (1) bubble-fenestral, ooid grainstone-boundstone and (2) cross-stratified, bioclastic, ooid grainstone. Microbial activity is prevalent in the bubble-fenestral, ooid grainstone and is generally manifested as grainy thrombolites (Stephens and Sumner, 2003). Bubble fenestrae are believed to represent either gas bubbles from soft-body decay (Shinn, 1968), keystone vugs developed from the displacement of interstitial gases associated with tidal flooding (Kerans, 1985; Demicco and Hardie; 1994; Figure 2.10a), or microbial stabilization (Chow and George 2004). Isopacous fibrous marine cements are common (Hurley, 1986)

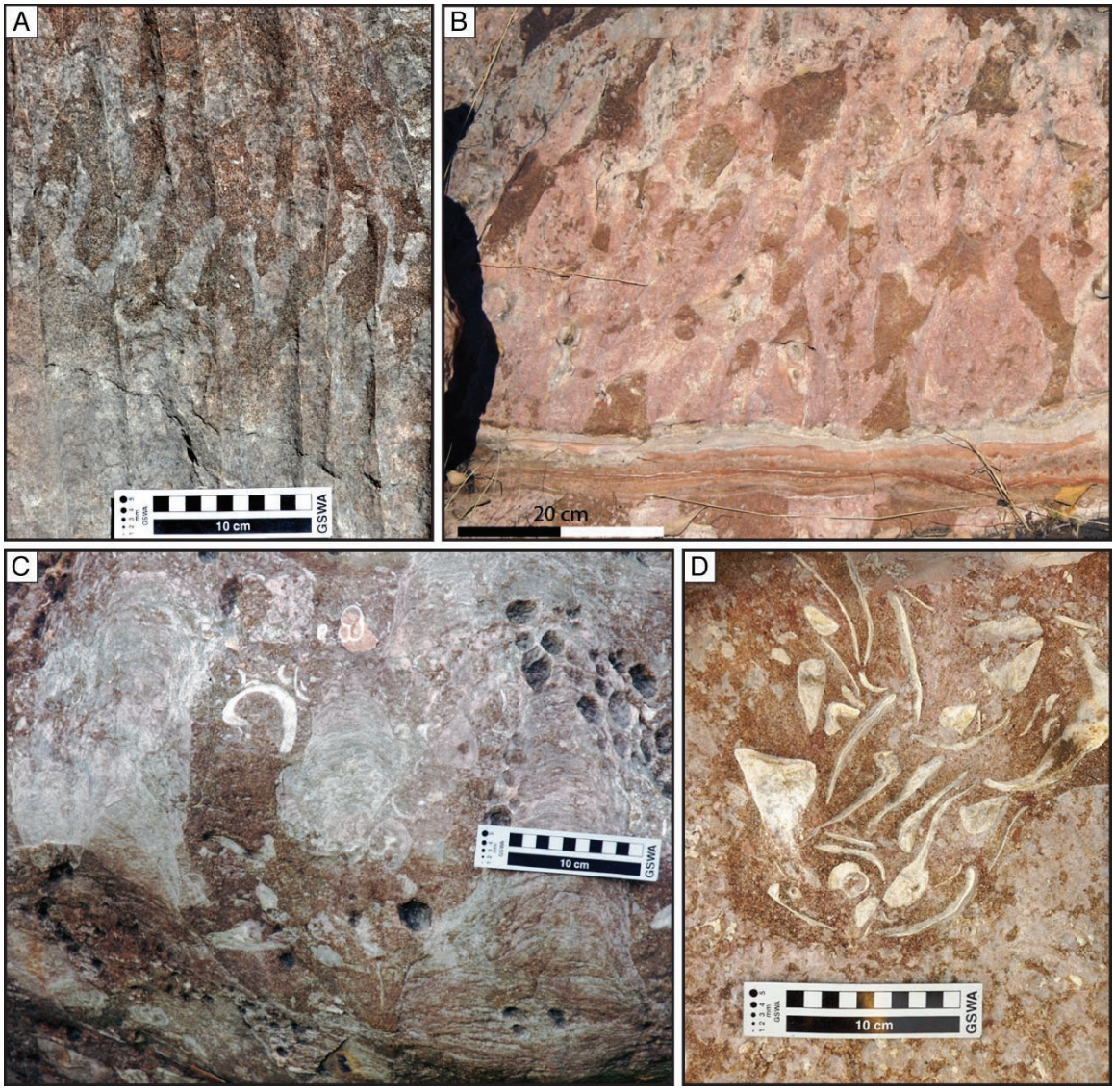

Figure 2.12: Stromatolitic/Thrombolitic Boundstone.

(A) Digitate stromatolites with coarse siliciclastic sandstone lining growth porosity, note tube-like morphology of coarse sand pockets (B) Coalesced stromatolite/thrombolites growths, with coarse siliciclastic sandstone lining growth porosity forming gymnosolen (sand tubes). (D) laminated club-shaped stromatolites in megalodont floatstone with coarse siliciclastic sandstone matrix. (D) Skeletal material and coarse siliciclastic sandstone lining thrombolites growth porosity. Note partially eroded contact of thrombolite (arrow).

and in some cases meniscus cements are well developed in the bubble-fenestral grainstone. Bioclast content is variable in the Famennian ooid grainstones and increases with proximity to the platform-margin. Famennian grainstones represent peritidal deposition in either, active ooid shoals (cross-stratified grainstone), or back-shoal sand flats (bubble-fenestral grainstone). Bubble-fenestral grainstones transitions updip into the coated-grain floatstone-rudstone and downdip into the cross-stratified, bioclastic ooid grainstones. While best developed in the Famennian, ooid grainstones also occur in the latest Frasnian prograding sequence around the Margaret River Embayment in the Southern Oscar Range (Hurley, 1986) and Geikie Gorge (Figure 2.1; Wallace et al., 1991).

Lithiotid, ooid floatstone–framestone

Skeletal material is generally scarce in the Famennian backreef, with the exception of lithiotid, ooid floatstone–framestone beds (Figure 2.11). This facies is composed of lithiotid bivalves in a matrix of ooid grainstone, with bivalves preserved either in growth position as upright colonial "blossoms" (Frasier et al., 2004; Figure 2.11b/c) or as reworked as disaggregated debris. The lithiotid bivalve beds range in thickness from 2-5 m and are laterally continuous (>2 km). Lithiotid, ooid floatstone–framestone horizons are temporally restricted and occur as discrete stratigraphic intervals that represent platform-wide flooding and open-marine, subtidal conditions across the platform top. Moreover, given the stratigraphic restriction and lateral continuity of these beds, the lithiotid ooid floatstone–framestone are used as datums for stratigraphic correlation.

Platform-margin Facies Tract

For this discussion we use the term platform-margin is used to refer to the reef-flat, reef and reefal-slope facies of Playford (1980, 1984; Figure 2.2).

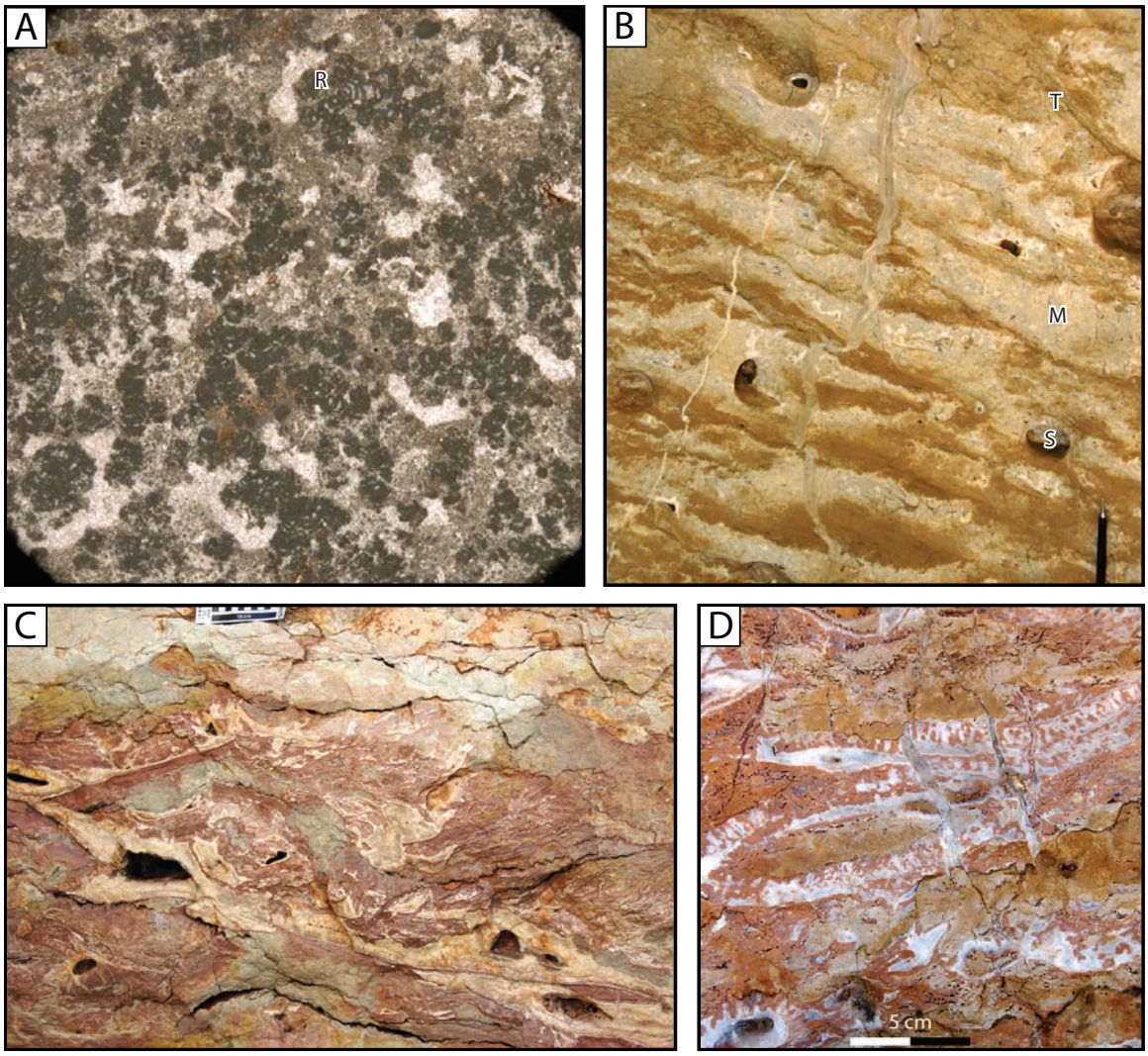

Figure 2.13: Famennian reef facies.

(A) Fenestral, recalcis boundstone from the base of section B-4, reef, Billy Munro Gorge. (B) URS boundstone lenses (M) in terregenous, peloidal maxtrix (T). Vugs are formed by dissolution of sponges (S). Reefal-slope, Windjana Gorge. (C) Stromatactus in microbial boundstone, reefal-slope, Billy Munro Gorge. (D) Receptaculitid bafflestone and URS boundstone in reefal-slope, Windjana Gorge.

Figure 2.14: Famennian platform-margin

Oblique airphoto of the Famennian platform-margin escarpment with in-situ fore-reef slope beds and fore-reef – escarpment contact (arrows), southern margin, Billy Munro Gorge (see Fig. 13c). Cliff height is approximately 70 m tall.

Megalodont floatstone

Megalodont floatstone is composed of thick-walled megalodont bivalves and lithiotid bivalves in a variable matrix of ooid grainstone, lithoclasts and coarse-grained terrigenous material (up to 50%; Figure 2.11d). This facies is typically poorly sorted, skeletal material is generally disaggregated and reworked stromatolite/thrombolites heads are common near the base of these beds. Cross-stratification is common and large reworked beachrock blocks and tepee slabs are observed, suggesting deposition is a high-energy setting. Lithiotid bivalves become more abundant in this facies towards the platform-margin, with an increasing number preserved in individual and colonial upright growth positions (e.g., Frasier et al., 2004; Figure 2.11 b/c).

Stromatolitic boundstone

Stromatolitic boundstone is common in the Famennian platform-margin and is characterized by abundant digitate to club-shaped stromatolites and thrombolites (Figure 2.12). The matrix material in this facies ranges from ooid grainstone to coarse siliciclastic sandstone, with abundant skeletal material such as disaggregated megalodont and lithiotid bivalves (Figure 2.12). One of the characteristic features of the facies is the development of pockets of coarse matrix material, that when viewed in cross-section appear as irregular vertical tubes (Kerans, 1985), often referred to as "sand tubes" (George and Powell, 1997). These features are common in the rock record and have traditionally been interpreted to represent the coalescence of columnar stromatolites/thrombolites to form a vertical network of growth porosity (Cosseti and Grotzinger, 2004; Goldhammer et al., 1993; Demicco and Hardie, 1994; Kerans, 1985; Playford, 2002; Stephens and Sumner, 2003); while George and Powell (1997) suggested a karst origin for the development of

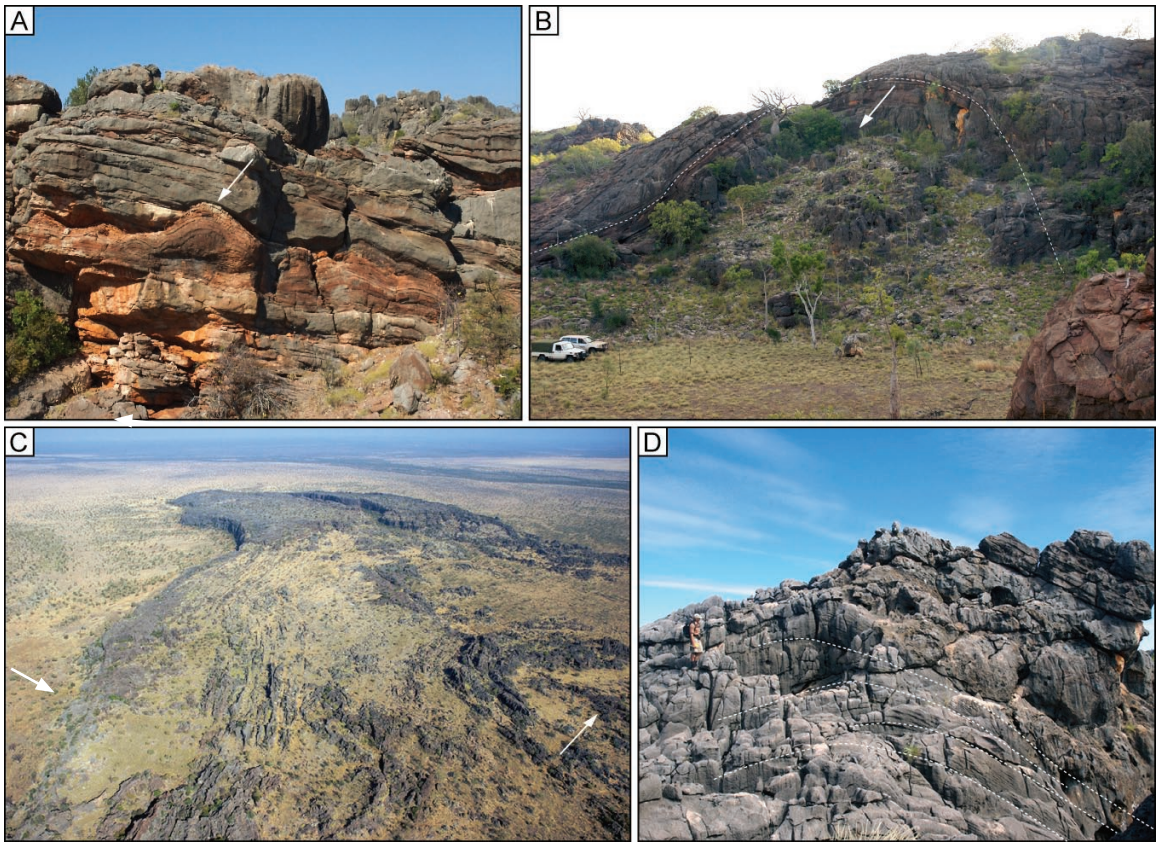

Figure 2.15: F–F interval deep-water mound complexes.

(A) Stromatolite horizons in fore-reef strata, Napier range. Stromatolite interval is approximately 5-7 m thick. (B) Large antiformal Late Frasnian sponge-coral bioherm complex (trucks for scale), fore-reef, Dingo Gap. (C) Stromatolite mound complex, Billy Munro Gorge (arrows point to location of figs. 2.14 and 2.16. Billy Munro Gorge stromatolite mound complex. (D) Large antiformal stromatolitic mound complex, Billy Munro Gorge.

these features in the Canning basin. The boundary between matrix and stromatolite is diffuse and feathered, with matrix material intercalated within the stromatolite structure (Figure 2.12) and evidence for a karst origin for the sand tubes has not been observed by this study. Scalloped submarine erosion surfaces on individual stromatolite/thrombolites are common suggesting a high-energy setting and it has been proposed that wave-surge was largely responsible keeping the stromatolite porosity network open (Kerans, 1985; Playford, 2002). The stromatolitic boundstone facies typically occurs from the landward boundary of the reef-flat to the platform edge, with robust morphologies occurring in the high-energy settings of the reef-flat and increasingly delicate and diffuse morphologies towards the platform-margin (Stephens and Sumner, 2003).

Reef and reefal-slope boundstones

Two primary types of reef boundstone are common in the Canning Basin's Famennian reef complexes (Kerans, 1985; Stephens and Sumner, 2003): (1) fenestral, *Renalcis* boundstone (Figure 2.13a); and (2) laminar, *Uralinella-Renalcis-Sphaerocodium* (URS) boundstone (Figure 2.13b). These boundstones occur in the steep reef scarps of the Famennian and helped construct wave-resistant high-relief platform-margins in the Famennian (Playford, 1984; Figure 2.14). In the reefal-slope below the platform-margin escarpment (Figure 2.2), steeply dipping (35°-65°) beds of stromatactis-rich microbial boundstone (Figure 2.13c) and sponge/receptaculitid framestone are abundant (Figure 2.13c), occurring with intercalated platform-derived debris. Based on observations from Windjana Gorge and the NRD-88 core, microbial binding appears to be significant down to water depths of at least 150-200 m and perhaps as deep as 300 m (Kerans, 1985; Stephens and Sumner, 2003).

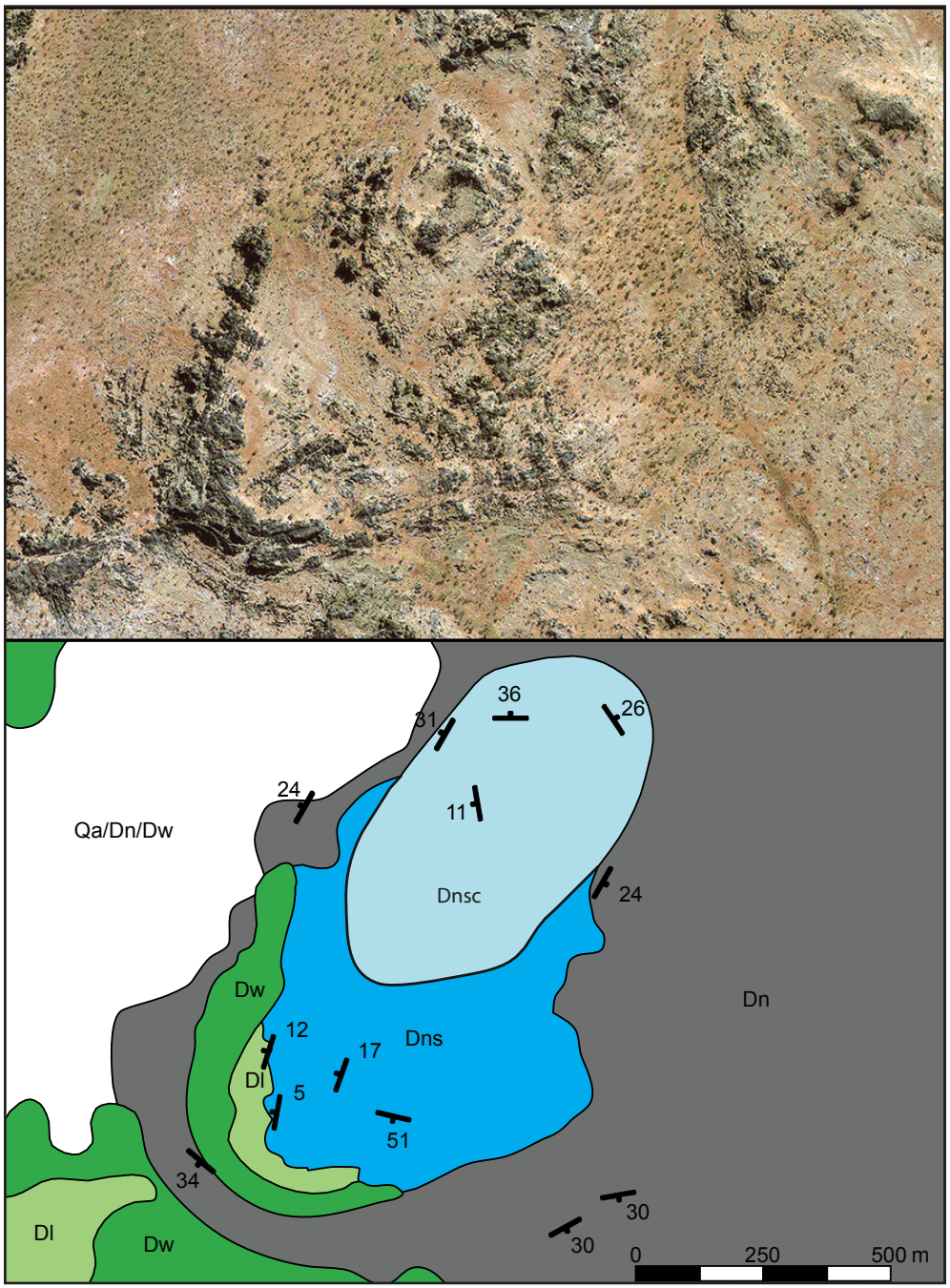

Figure 2.16: Billy Munro Gorge stromatolite mound complex.

The bioherm complex is a composite structure that consists two primary features: (1) an oblong mound core (Dnsc), and (2) a dip-elongate, southwest-plunging antiformal mound complex (Dns; Fig. 2.15d) composed of numerous smaller mounds. The mound complex is surrounded by fore-reef strata, and disconformably overlain by Famennian (Dl) platform and reef (Dw).

Fore-reef Facies Tract

The Famennian fore-reef slope strata are generally grain-dominated, with facies that range from talus deposits, sediment gravity flows, rolled blocks lithoclasts megabreccias, platform derived grainstones and nodular packstones. With the exception of the F-F boundary bioherm complexes, these facies were not studied in detail in this study and readers are referred to investigations by Playford (1980), Kerans (1985), George and others (1997) and Playton (in prep) for detailed descriptions of these facies.

Sponge-stromatolite bioherm complexes

Sponge, stromatolite bioherm complex development was widespread throughout the fore-reef of the Canning Basin during the F-F transition (Playford et al., 1976; Playford 1981; Hurley, 1986, George et al., 1997; George, 1999). Bioherm morphology and scale are highly variable, ranging from individual, bed-bounded, stromatolite horizons intercalated in fore-reef strata (Figure 2.15a), to large sponge-coral microbial bioherms (George et al., 1997; Figure 2.15b), or large-scale bioherm complexes nucleated on drowned Frasnian reef topography (e.g., the Elimberrie bioherms; Playford, 1981; Hurley, 1986). Bioherm development has been documented to occur in water depth down to at least 45m (Playford and Cockbain, 1969).

A large (1.2 x 0.74 km), antiformal, dip-elongate bioherm complex is preserved in the Billy Munro Gorge area (Figure 2.15c, 2.16). This composite bioherm structure consists of numerous smaller mounds and two primary features are differentiated: (1) an oblong mound core (Figure 2.15d) composed primarily of stromatolites and receptaculitids (Figure 2.16; Dnsc) with flanks dipping steeply away from a central high and (2) a dip elongate, southwest-plunging antiformal

mound complex (Figure 2.15; Dns) composed of numerous smaller mounds containing primarily stromatolites, with varying quantities of receptaculitids, *Renalcis*, *Sphaerocodium* and laminar stromatoporoids. The mound complex developed either on topography created by a clastic fan associated with the Van Emmerick conglomerate (Figure 2.3), or a drowned Frasnian reef spine. Given the presence of laminar stromatoporoid reef fabrics, a common constituent of Frasnian reef strata, it seems likely that the bioherm complex developed on relict Frasnian topography in a similar fashion to the Elimberrie Bioherms (Hurley, 1986). This feature is believed to be latest Frasnian to early Famennian in age, assuming age-equivalency to the other large stromatolite complexes described elsewhere along the Lennard Shelf, e.g., Preema Bioherms (Playford pers. comm., 2004), Elimberrie Bioherms and the Naralara stromatolite horizon (George, 1999; Playford et al., 1976; Kerans, 1985).

FAMENNIAN CYCLICITY

Frasnian cyclicity has been well documented for the Lennard Shelf (Brownlaw et al., 1996; Hocking and Playford 2002; Kerans 1985; Playford et al., 1989; Read 1973a/b) and cyclicity in the Famennian backreef is apparent (Hocking pers. Comm., 2004; Figures 2.5 and 2.17). Famennian high-frequency cycles typically have a grainstone base which grades up into fenestral laminites, tepee-pisolite zones, or beachrock (Figure 2.17). HFC thickness ranges from 0.3–7.3 m, with an average thickness of roughly 1.5 m (Table 2.1). High-frequency cycles observed by this study are either capped by: supratidal (laminites) caps; or marine-vadose diagenetically modified (tepees, beachrock) caps (Figure 2.18). Based on mapping and measured section data from Famennian backreef strata in the Oscar Range, Limestone Spring and Billy Munro Gorge, three basic high-frequency cycle types

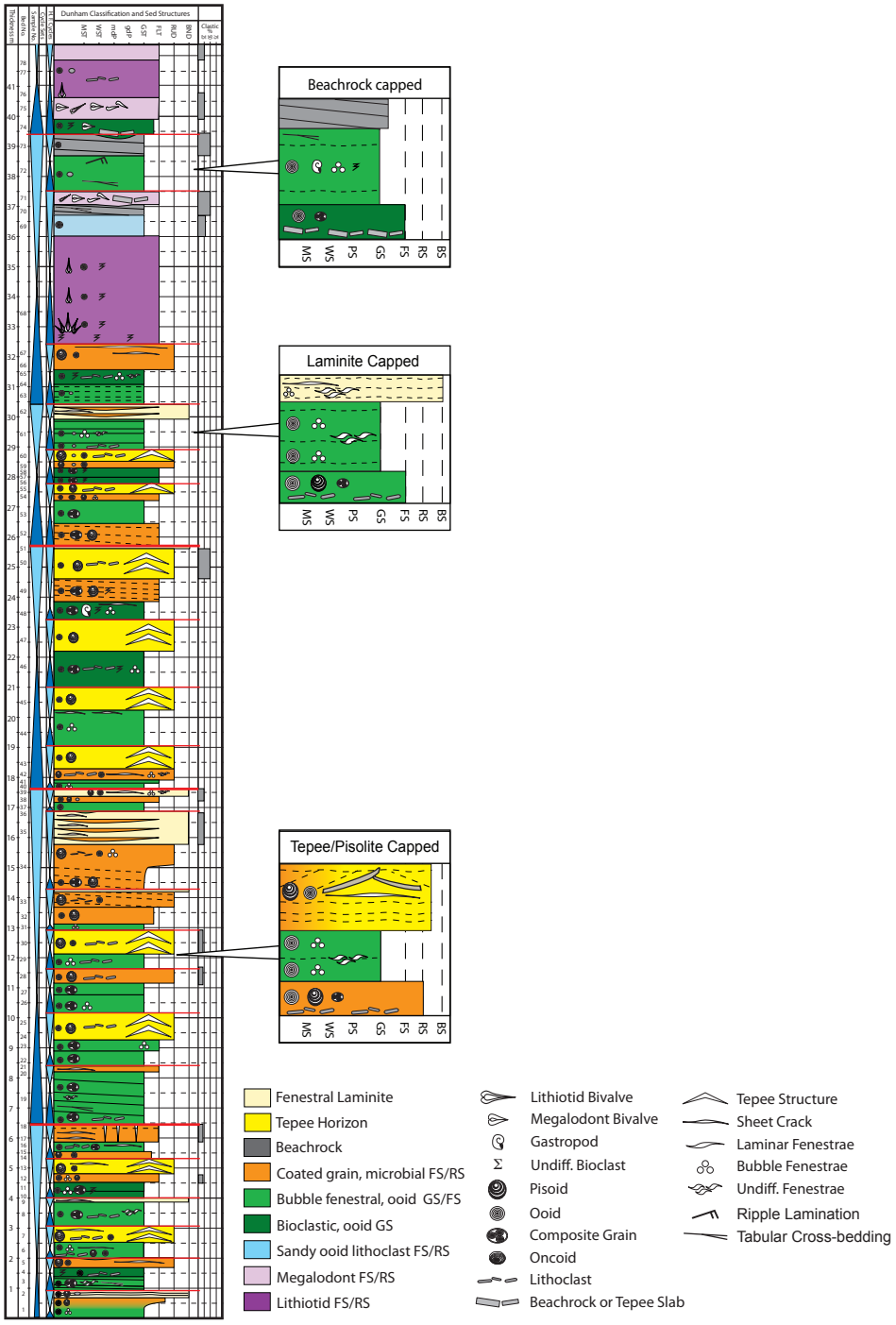

Figure 2.17: 1-D stacking patterns, and idealized cycle types

Measured Section B-2, Billy Munro Gorge. See fig. 2.20 for location. Three primary cycle types are recognized (1) Laminite capped, (2) tepee capped, and (3) beachrock capped.

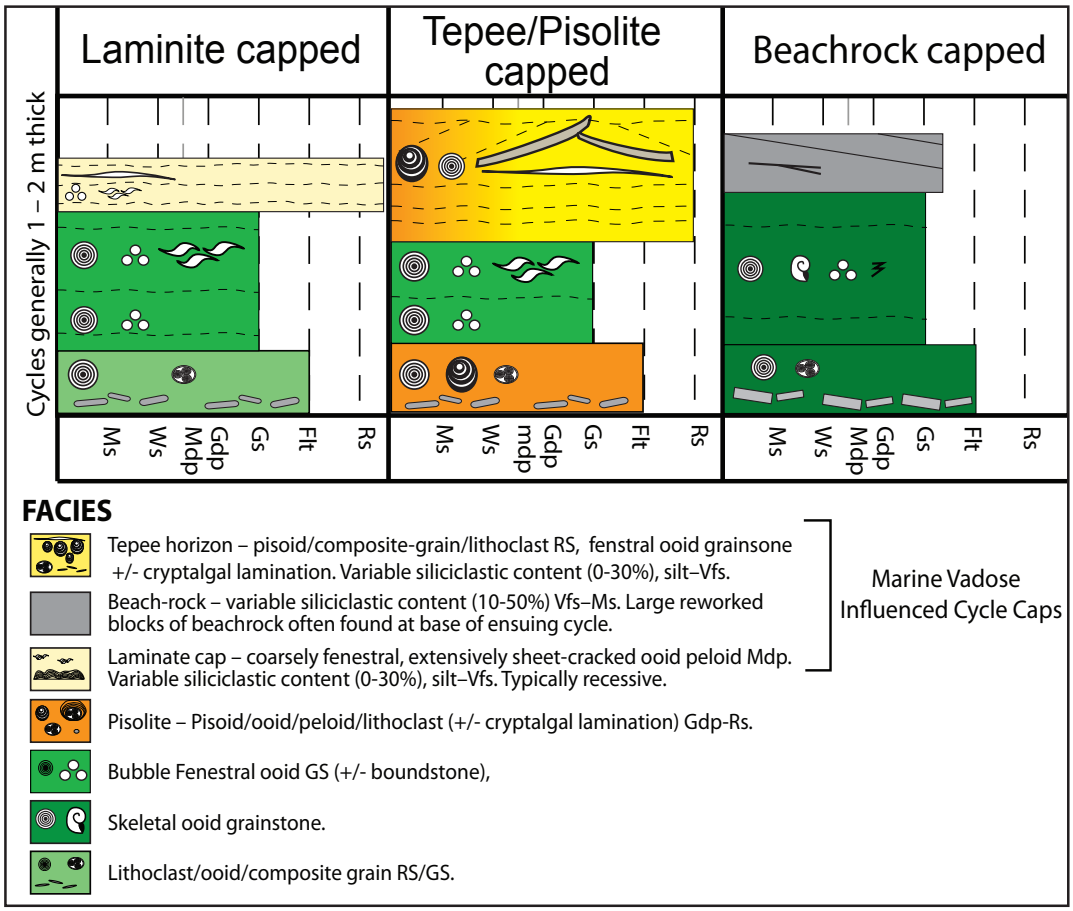

Figure 2.18: Idealized Famennian backreef cycles.

Three primary cycle types are recognized (1) Laminite capped, (2) tepee capped, and (3) beachrock capped.

Frasnian Cyclicity			
Author	Average Thickness	Min. Thickness	Max. Thickness
Playford et al., 1989	5.00	1.30	12.60
Brownlaw, 2000	3.51	0.36	21.70
Hocking, Unpublished	4.22	1.25	11.00
This Study	2.58	0.53	6.73
Famennian Cyclicity			
Author	Average Thickness	Min. Thickness	Max. Thickness
Hocking, Unpublished	4.2	1.3	11.0
This Study	1.50	0.27	7.30

Table 2.1: Frasnian and Famennian cycle data

are proposed: (1) fenestral laminate capped cycles; (2) tepee-pisolite capped cycles; and (3) beachrock capped cycles (Figure 2.18).

The idealized high-frequency cycles proposed by this study represent a departure from those described in the Frasnian, where subtidal to intertidal cycles dominate (e.g., subaqueous cycles of Hocking and Playford, 2002; Brownlaw, 1996) and supratidal caps are less common (Read, 1973 a/b). Moreover, marine-vadose caps are rare throughout most of the Frasnian and appear to be restricted to the latest Frasnian of Geikie Gorge and the Southern Oscar Range (this study; Hurley, 1986). Famennian cycles on the other hand, suggest that extremely shallow water conditions prevailed across the platform top and tepee, beachrock and fenestral laminite capped cycles are indicative of the persistence of intermittent subaerial exposure (e.g., pendant cements in Figure 2.8). Average high-frequency cycle thickness decreases from the Frasnian into the Famennian (Table 2.1) indicating limited accommodation in the Famennian.

FAMENNIAN FACIES PATTERNS AND STRATAL ARCHITECTURE

Mapping, measured section and core data collected by this study show that the Billy Munro Gorge platform developed as a high-relief (300-400 m tall) pro-gradational platform with a progradation to aggradation (P/A) ratio of 9.6 (Figure 2.19). Tepee complexes, coated-grain floatstone-rudstones and fenestral laminites dominate the platform-interior, while ooid grainstones, skeletal floatstones and beachrock comprise the outer-shelf (Figure 2.19). High-frequency cycle mapping demonstrates that the cycle types proposed in the previous section occur as lateral equivalents to one another. Individual tepee complexes can be traced landward into tidal flats and basinward into beachrock zones along the same stratigraphic horizon (Figure 2.20), with cycle thickness expanding dramatically towards the

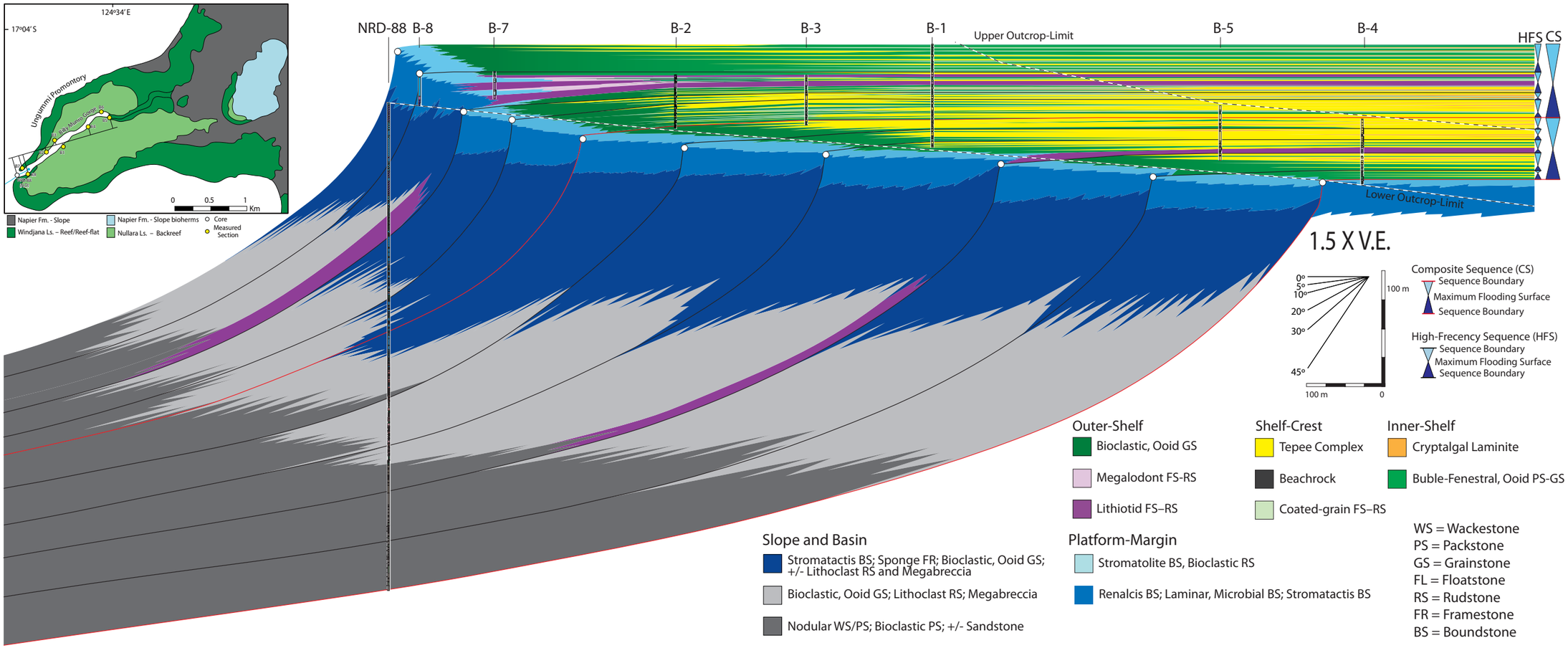

Figure 2.19: Stratigraphic architecture of the Billy Munro Gorge Area.

2D cross-section created from projected measured section and core data, 1.5 times vertical exaggeration, The upper lithiotid floatstone bed provides a regional datum and high-frequency cycle tops serve as guiding surfaces.

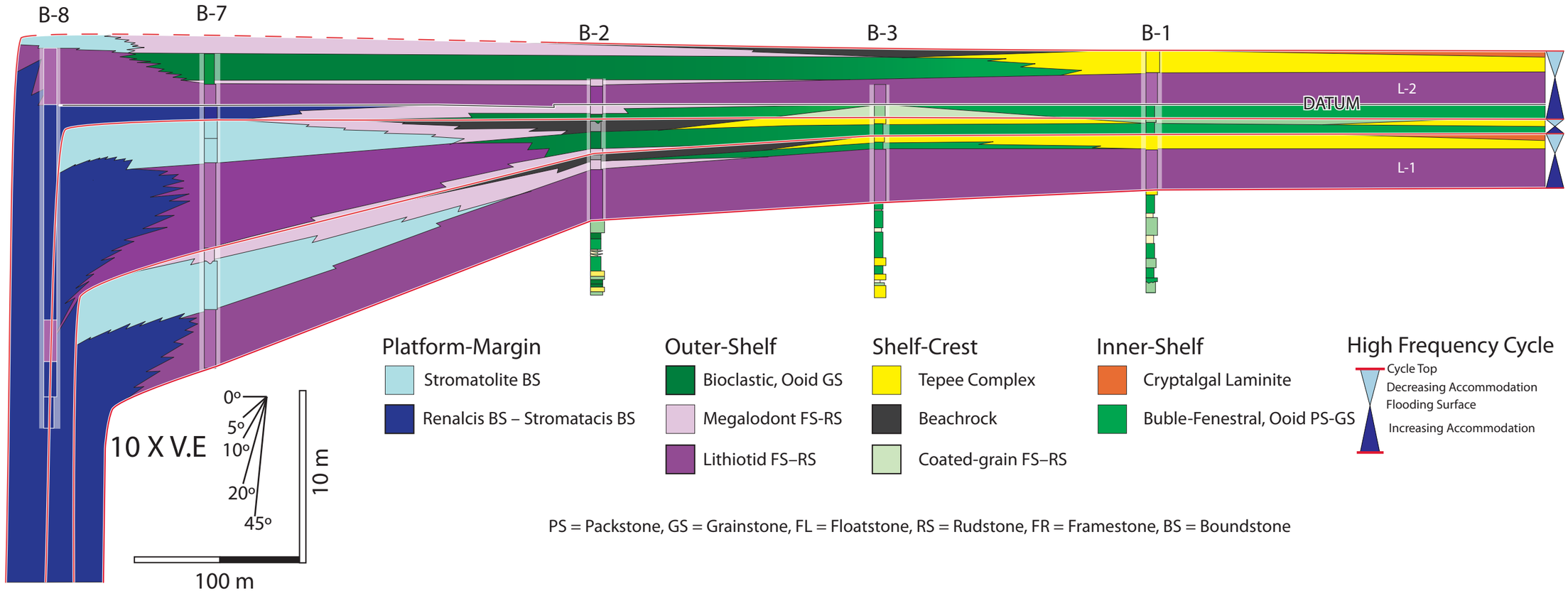

Figure 2.20: Architecture of the platform-margin and shelf crest.

Detailed cross-section of the platform margin and outer-shelf constructed from measured sections. L-2 lithiotid floatstone bed provides datum, with high-frequency cycle tops serving as guiding surfaces (10X vertical exaggeration), see Figure 2.19 for location. Fenestral laminites, tepee complexes and beachrock occur as lateral equivalents of one another, with progressively deeper water facies encountered towards the platform margin.

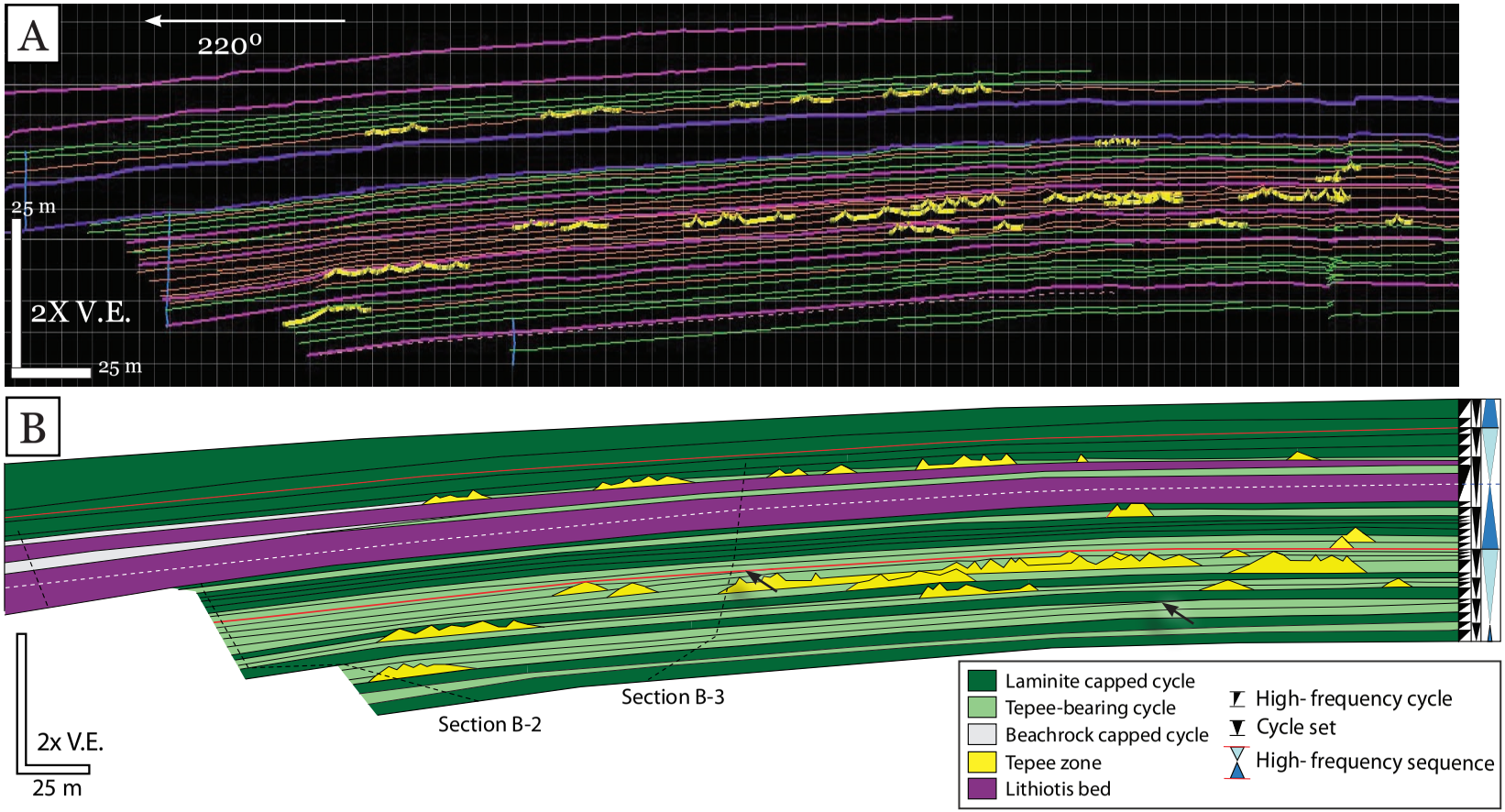

Figure 2.21: LIDAR cycle and tepee complex mapping.

Individual high-frequency cycle caps and tepee features from LIDAR mapping of the north wall of Billy Munro Gorge. This cross section represents a small portion of the total area mapped with lidar, and tepee-`bearing cycles refer to high-frequency cycles that either have tepees updip or on the other canyon wall. Cycle set tops are picked on the basis of stratal truncation (arrows), or at the boundary between major grainstone flooding surfaces, and tepee-bearing cycles.

platform-margin (two to six fold increase; Figure 2.20). Depositional dips range between 2° – 5° between the downdip limit of beachrock zones and tepee complexes and the reef facies, placing the platform-margin break at least 5-15 m below the shelf crest (Figures 2.20-2.21). Moreover as stratigraphic surfaces are traced downdip from the seaward edge of tepee complexes or beachrock zones, progressively deeper water facies are encountered, passing from cross-stratified and bioclastic grainstones, into megalodont floatstones and lithiotid bafflestones, into the boundstones of the platform-margin facies tract (Figures 2.19-2.21).

Marine-vadose influenced facies such as tepee complexes and beachrock form in a very narrow bathymetric window and the lateral relationship between these facies and the depositional environments that they represent have several implications for Famennian stratal architecture. Beachrock is formed in the foreshore environment and provides a pining point for mean sea-level. The observation that tepee complexes occur updip from beachrock zones, suggests that these features developed in a supratidal, back-beach setting.

The distribution and lateral extent of tepee complexes is highly variable and LIDAR mapping shows that individual tepees and tepee complexes extend along the same stratigraphic interval for several hundred meters (Figure 2.21), and the width of the tepee belt is controlled largely by stratigraphic position. During highstand conditions tepee complexes are areally extensive across the platform top, extending out towards the platform-margin and the width of the outer shelf decreases (50–150m; Figures 2.19). As accommodation decreases tepee complexes begin to stack vertically in the platform-interior and individual grainstone beds and tepee horizons can be traced updip in to composite tepee zones. Composite tepee zones can reach thicknesses of up to 13.5m (e.g., section B-4 Appendix A; Figure 2.19) and are interpreted to represent the amalgamation of several high-frequency

cycles associated with periods of minimum accommodation across the platform top. Cycle set and high-frequency sequence boundaries (sensu Tinker 1998) are picked at the contact between erosionally truncated composite tepee zones and the most landward incursion of ooid grainstone beds (Figures 2.19 and 2.21).

During high-frequency flooding events, the tepee belt becomes areally restricted and retreats landward, replaced by shoals and sand-flats (Figures 2.19, 2.20 and 2.22). During transgression the platform margin continues to prograde, albeit at a reduced rate, causing the width of the outer-shelf to expand dramatically (up to 700m) as tepee complexes retrograde. A similar phenomenon has been described in the Permian (Guadalupian) Seven Rivers and Yates Formations of New Mexico and Texas (Tinker, 1998; and Kerans and Tinker 1999). Tepees are only completely absent during the platform-wide flooding events when lithiotid bivalve biostromes cover the platform top (Figures 2.19) and these events are interpreted as composite sequence flooding events.

In other systems, where tepees are common such as the Late Permian of Texas (Dunham, 1969; Esteban and Pray, 1977; Tinker, 1998; Kerans and Tinker 1999; Barnaby and Ward, 2007) and the Middle Triassic of Italy (Eggenhoff, 1999; Emmerich et al., 2005), these features are interpreted to represent emergent, positive topographic relief associated with shorelines or island complexes. The lateral association of tepees and beachrock coupled with the basinward expansion of high-frequency cycles documented by this study suggests that the same is true in the Famennian of the Canning Basin and that the tepee-beachrock association represents a barrier beach complex, or shelf crest system. Tepee complexes are interpreted to represent an intermittently sub-aerially exposed paleobathymetric high, while beachrock is indicative of a foreshore beach system which transitions downdip into bioclastic grainstones and megalodont-lithiotid floatstones that

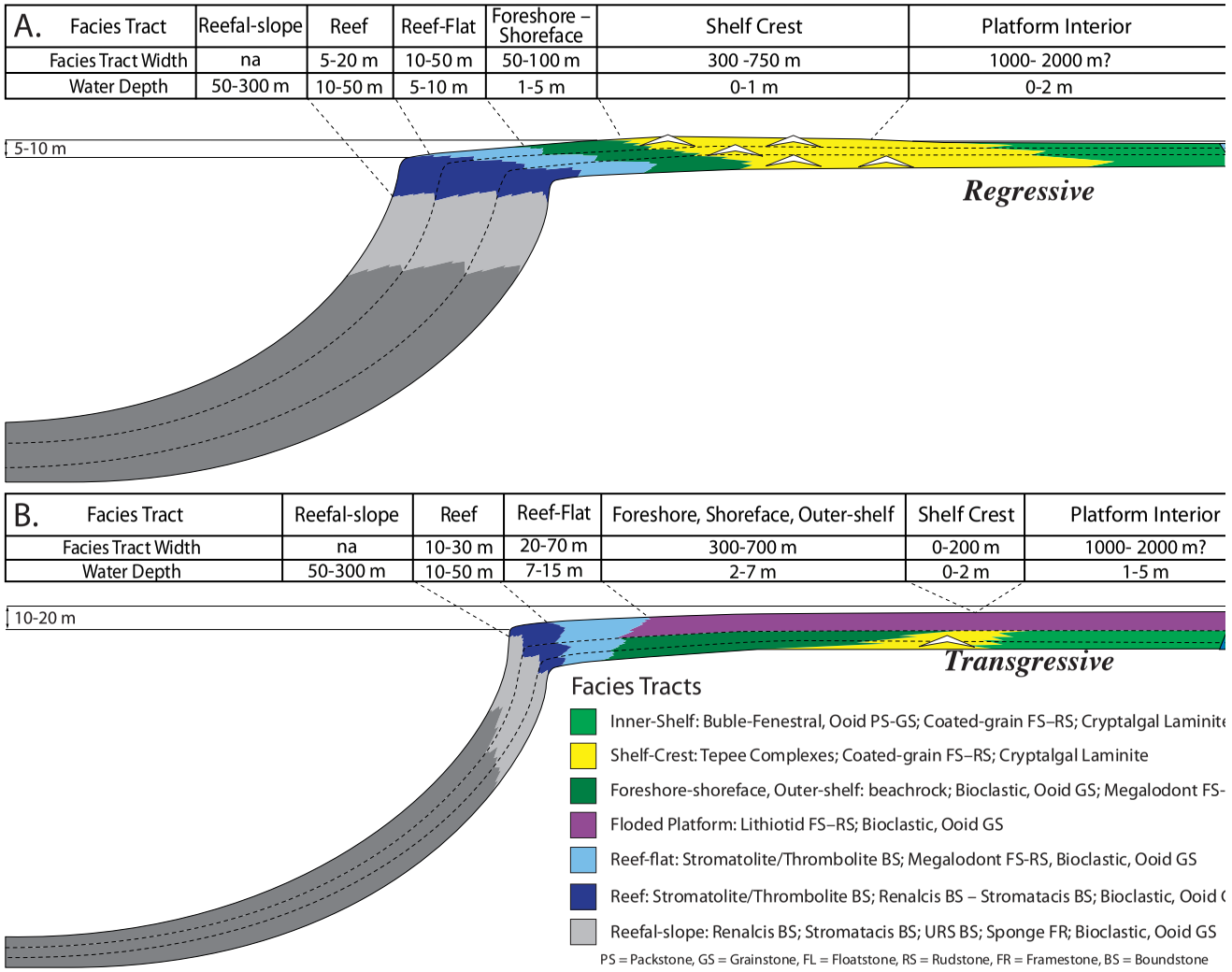

Figure 2.22: Proposed high-frequency sequence stratal architecture and depositional model for the Famennian system at Billy Munro Gorge.

reflect deposition in an upper-shoreface setting. Landward tepee complexes transition into sand-flats and tidal-flats (Figure 2.19, 2.20 and 2.22). The Famennian shares other similarities to the Late Permian and Middle Triassic in the respect that the Famennian reef grows in deeper water (5-15 m; Figures 2.19 and 2.20) resembling the marginal-mound geometry proposed by Dunham (1972) for the Capitan Formation.

GEOCELLULAR MODELLING

A 3D geocellular model of the Billy Munro Gorge platform was constructed from outcrop data following the methods outlined by Janson et al. (2007; Fig 2.23): (1) digitize stratigraphic surfaces on LIDAR pointcloud in Polyworks; (2) digitization of measured section paths on LIDAR pointcloud in Polyworks; (3) create 3D stratigraphic surfaces in gOcad; (4) create a stratigraphic grid in gOcad from multiple guiding surfaces; (5) populate digitized measured sections with coded facies data and calculate vertical facies proportions in gOcad; and (6) extrapolate facies based on outcrop conditioning data, measured sections, and controlling surfaces.

Measured section paths were digitized on the LIDAR pointcloud as polylines and subsequently coded with facies attribute data at 10 cm intervals (Figure 2.23a/b). Strata along Billy Munro Gorge were mapped at the high-frequency cycle scale (0.5 – 7 m); cycles were first identified in measured sections and then mapped laterally with each individual cycle cap mapped directly on the LIDAR pointcloud (Figures 2.3, 2.21 and 2.23c). Cycle sets identified in measured sections, were also mapped on the pointcloud and were used as conditioning data to generate 3D guiding-surfaces for stratigraphic grid construction (Fig 2.23d).

3D surfaces were generated from outcrop conditioning data using a kriging algorithm in gOcad. Once all 3D stratigraphic guiding surfaces were created, a

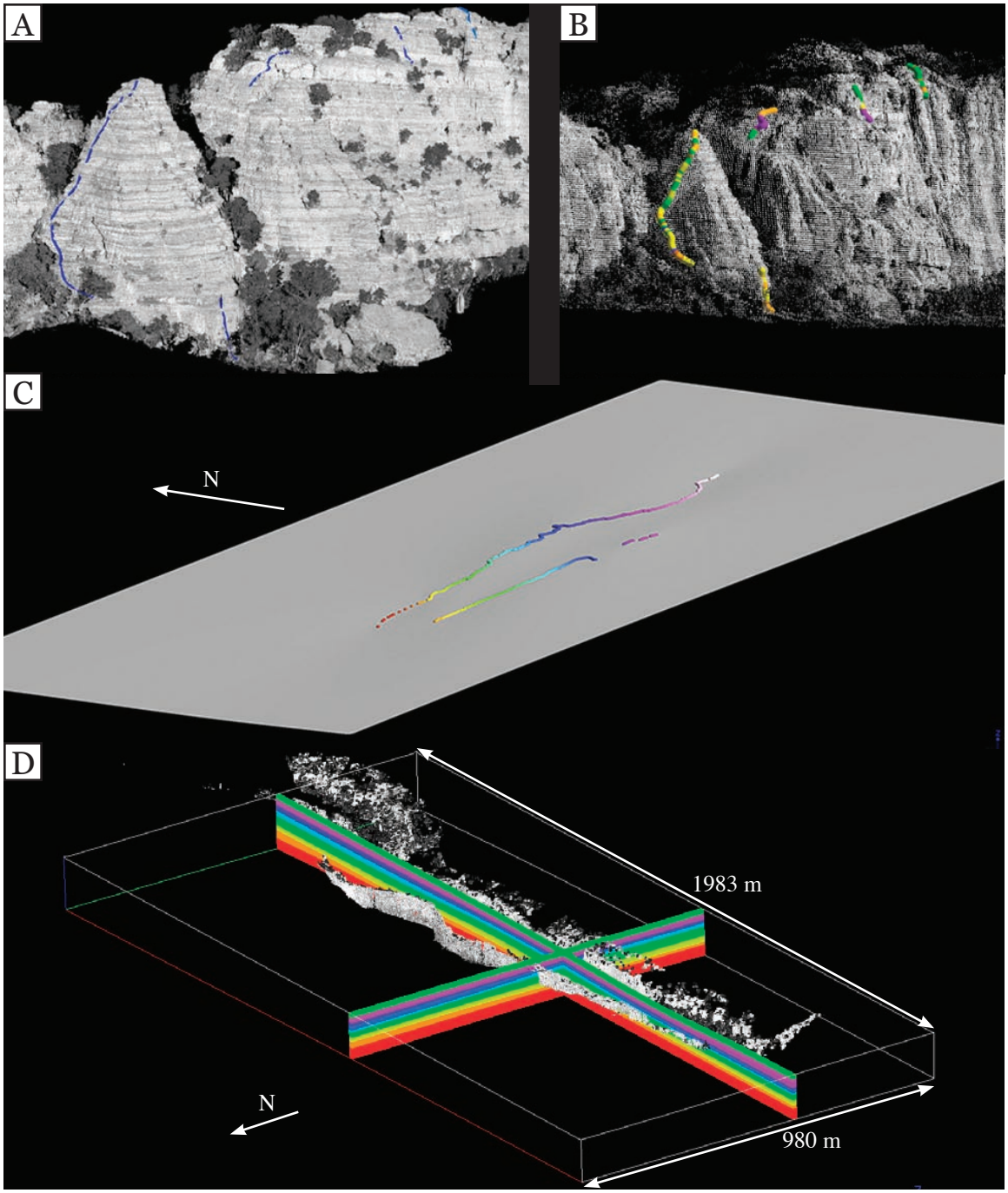

Figure 2.23: Geocellular model construction.

(A) Measured section track (section B1; blue line) on lidar point cloud. (B) Facies coded measured sections and intensity on decimated point-cloud in gocad. (C) 3D surface created from outcrop conditioning data (L-1 bed; Figure 2.20) . (D) Slices through the 3D stratigraphic grid, each color represents a different horizon.

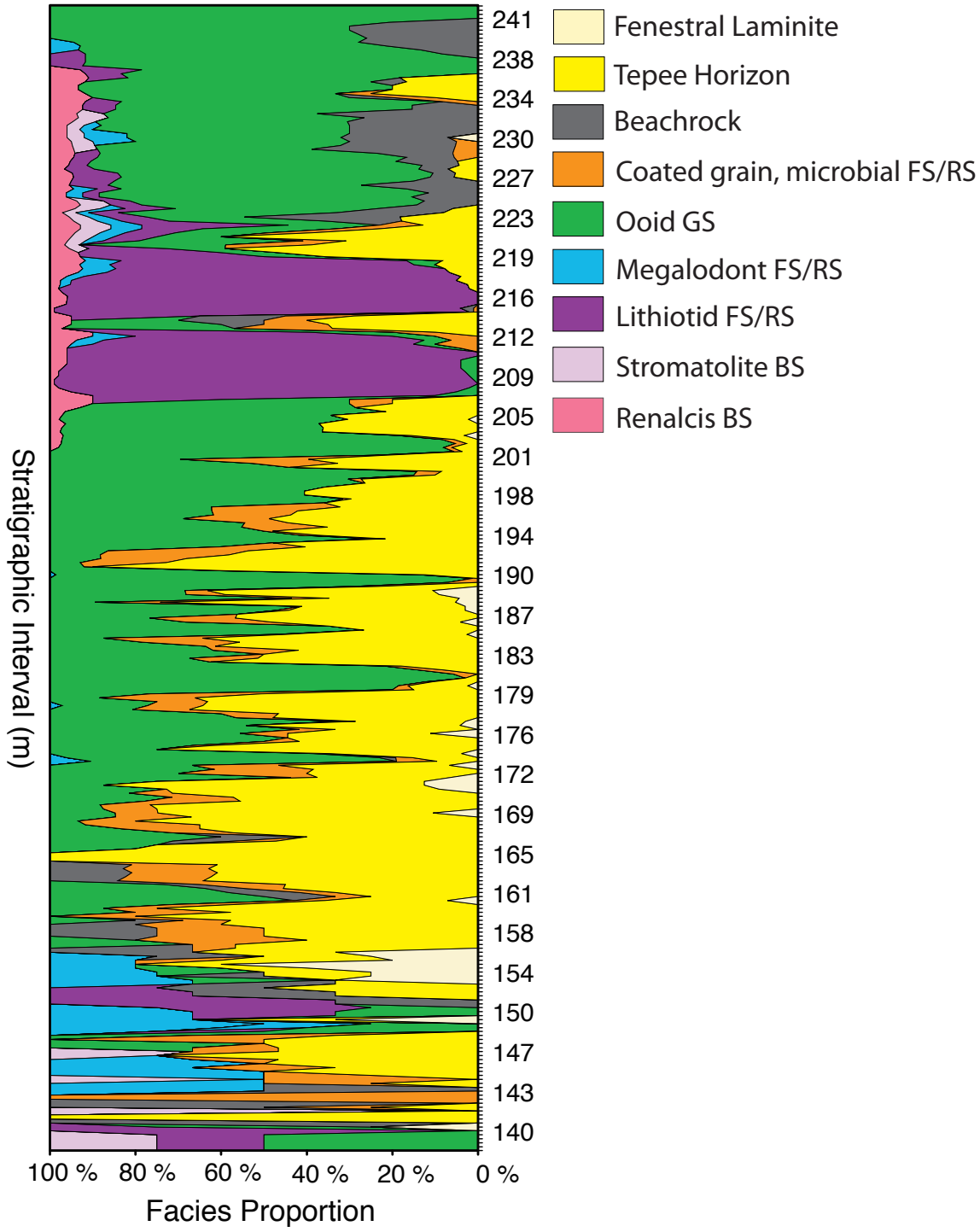

Figure 2.24: Vertical facies proportions.

Facies proportions calculated in gOcad from measured sections. Due outcrop exposure platform-margin only sampled from 200–240m

stratigraphic grid was constructed with 0.5 m thick cells with a horizontal dimension of 10 m. The final stratigraphic grid was roughly 1950 m long, 950 m wide and contained 297 layers with a total of over 5.6 million cells. All digitally mapped geologic features (e.g., individual tepee complexes, laminite caps, beachrock) were given a facies attribute code and assigned to the stratigraphic grid as conditioning data (Figure 2.21). Facies-attribute-coded measured section paths were imported into gOcad and were used to constrain the vertical facies proportions of the model (Figure 2.24).

In order to distribute facies throughout the 3D stratigraphic grid a stochastic indicator sequential Gaussian simulation (SGS) algorithm was used (Janson et al., 2007). Variograms were calculated for each facies from outcrop conditioning data, and differences in range, sill, and orientation are observed between individual facies (Table 2.2). In order to produce geologically realistic results, facies interpolation was conducted separately within "regions" created for the backreef, outer-shelf and reef facies tracts of each individual cycle set horizons (Figure 2.25). This strategy produced acceptable results, however the geometry of each region is based on the interpreted facies tract dimensions (Figure 2.25a-c) and vertical boundary artifacts occur between regions (Figure 2.25e). Due to a lack of constraining data, the reefal-slope and fore-reef strata were not included in the model.

The 3D geocellular model created by this study produces a reasonable rendition of the facies heterogeneity and the stratal geometry of the Famennian Billy Munro Gorge platform (Figure 2.25). The model is most reliable in the upper layers where all facies tracts are exposed, as opposed to the lower portions of the model where the platform margin and outer-shelf plunge into the subsurface. Model results can be validated by "painting" the interpolated facies attribute onto the LIDAR point cloud (Figure 2.25d), which allows for modeled facies distributions

Facies	Sill	Range 1 (m)	Range 2 (m)	Azimuth
Laminite Cap	0.12	500	500	N.A.
Tepee Zone	0.24	175	125	45°
Coated.Grain FS/RS	0.10	150	150	N.A.
Beachrock	0.10	150	50	Variable
Ooid GS	0.29	150	150	N.A.
Lithiotid FS	0.28	500	500	N.A
Megalodont FS	0.10	150	50	Variable
Stormatalite BS	0.10	150	50	Variable
Renalcis BS	0.10	150	50	Variable

Table 2.2: Variogram data for the Billy Munro Gorge Geocellular Model.

The sill is the variance at which the model becomes stationary and range is the distance at which the model reaches the sill (Janson et al., 2007). Azimuth refers to the orientation of range 1. Variable azimuth reflects a variogram that was allowed to follow the trend of the platform margin.

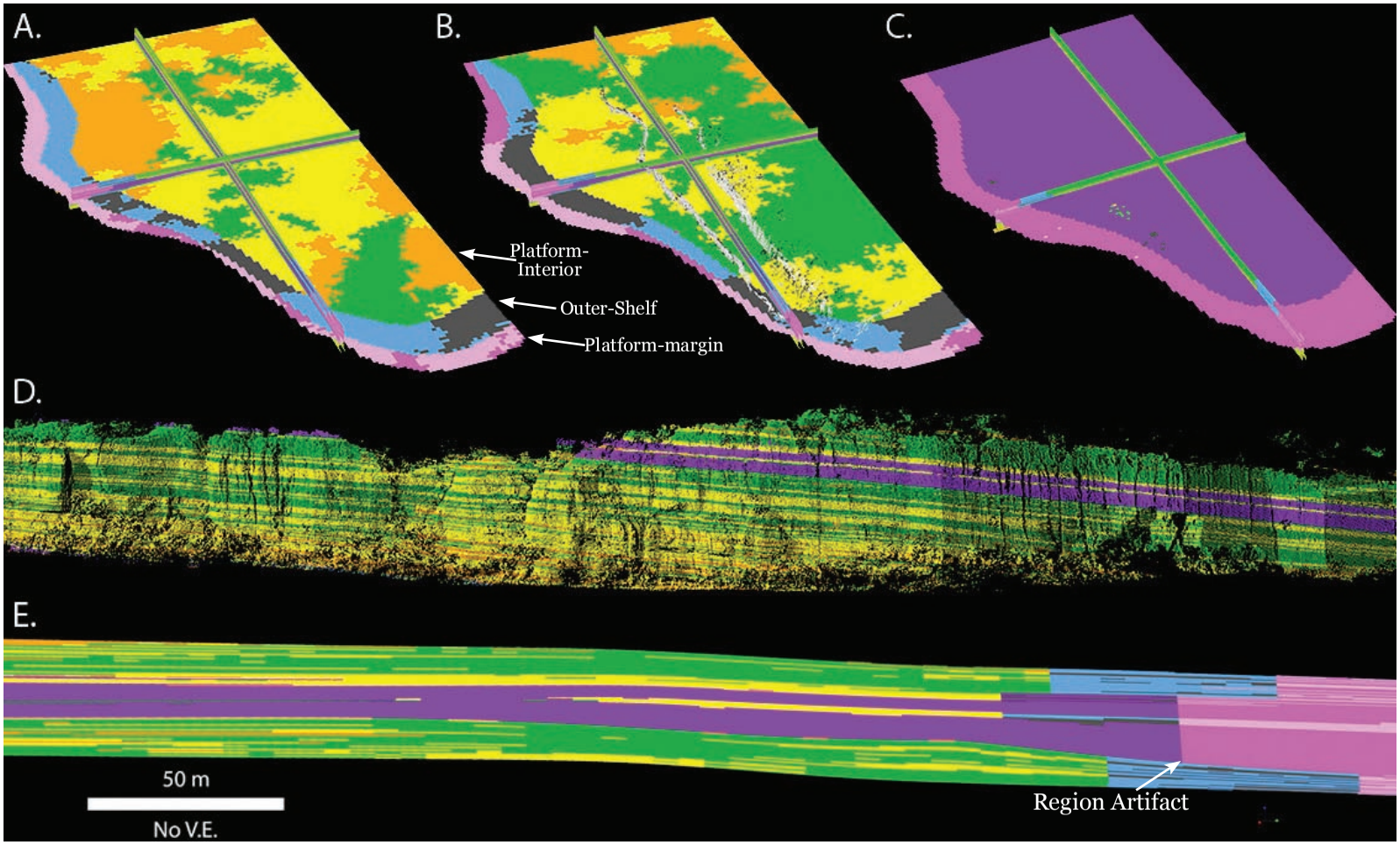

Figure 2.25: DOM results for Billy Munro Gorge.

(A) Tepee dominated horizon. (B) Mixed tepee and grainstone horizon. (C) Flooded platform, dominated by lithiotid biostromes. (D) Facies model results “painted” to Lidar data.Wall is oriented oblique to strike. (E) Dip-oriented cross section, showing expansion of beds towards the margin. See Figure 2.24 for facies key.

to be checked against mapped distributions.

BILLY MUNRO GORGE PLATFORM EVOLUTION

The Billy Munro Gorge platform developed as a progradational, narrow (3.5 x 1km) promontory with a steep microbial escarpment margin (Figure 2.19; Plate 1). This morphology is proposed to be the result of three distinct phases of Famennian stages evolution (Figure 2.26). (1) The development of a large, antiformal, deep-water stromatolite bioherm complex similar in scale and distribution to the Elimberrie Bioherms (Playford, 1981; Hurley, 1986) on drowned Frasnian topography during the F-F crisis (stages 1-3; Figure 2.26). (2) Platform nucleation and shoal-water carbonate development on the positive antecedent topography created by the marginal-slope mound complex (stage 4; Figure 2.26). (3) Rapid progradation along antecedent topographic highs and the development of an extensive network of syndepositional neptunian dikes (stages 5-6; Figure 2.27).

Famennian platform and reef sediments unconformably overlie the mound complex along its western margin marking the nucleation of the Billy Munro Gorge platform. During the Famennian, the Billy Munro Gorge platform prograded roughly 3km from the mound complexes to its western terminus (Figures 2.26-2.27). The slender promontory of Billy Munro Gorge suggests that the platform followed a narrow topographic high. The antecedent topography that controlled Billy Munro Gorge morphology is not exposed and the exact morphology of the antecedent topographic control is unclear. However, given the size of the mound complex and the proximity of other large mounds, it seems logical that the morphology of the Billy Munro Gorge platform was controlled by the down dip continuation of this mound complex or perhaps another isolated mound complex (Figure 2.26-2.27).

One feature of the Billy Munro Gorge platform that helps shed light on

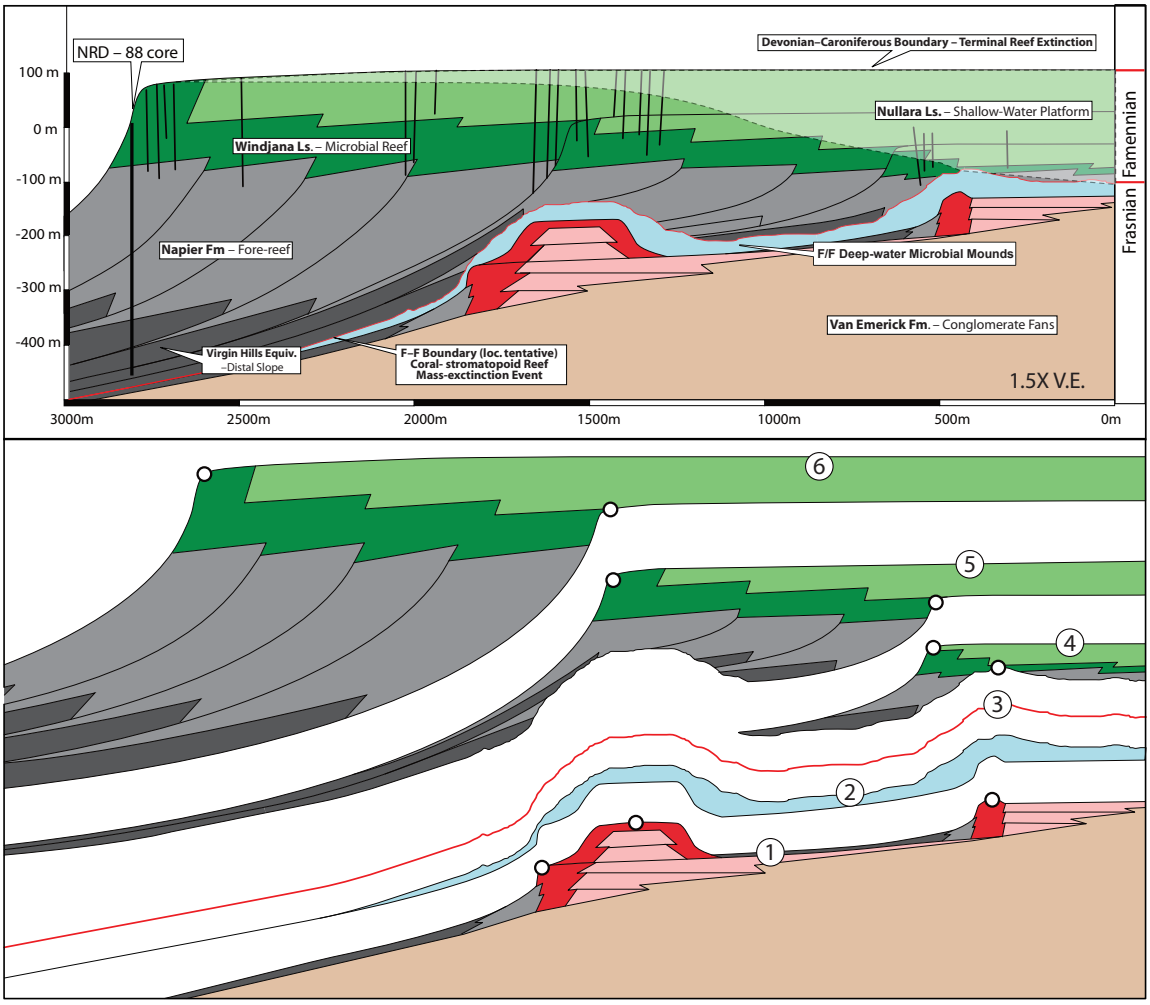

Figure 2.26: Proposed evolution of the Billy Munro Gorge platform.

Three distinct phases of evolution are proposed for the Billy Munro Gorge platform: (1) the development of a deep water stromatolite mound complex on drowned Frasnian topography during the F/F crisis (stages 1-3); (2) development of shallow water Famennian carbonates on mound complex topography (stage 4); and (3) progradation of shallow water Famennian carbonates along the mound complex crest (stages 5-6).

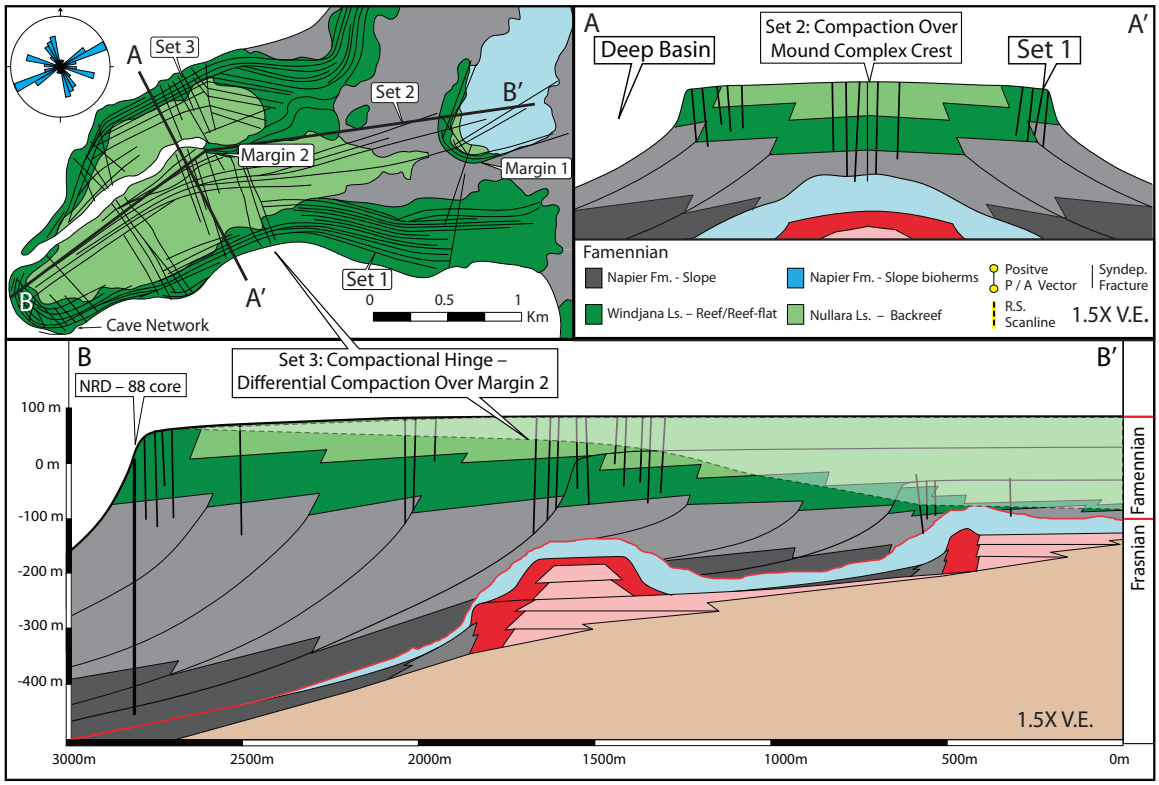

Figure 2.27: Antecedent topography controlled syndepositional fracture patterns

The antecedent topography that controls the Billy Munro Gorge platform's morphology is manifested in syndepositional fracture patterns. Three sets of fractures are recognized; set 1, margin parallel fractures, set 2, fractures oriented parallel to the long axis of the platform, and set 3, fractures oriented perpendicular to the long axis of the platform. Set 2 fractures are believed to represent differential compaction over the mound complex, while set 3 fractures represents compactional hinge development over an older platform-margin (margin 2).

platform morphology is the distribution and orientation of a series of well-developed opening-mode syndepositional fractures (Figure 2.27). The geometries of these fractures can be used to delineate the dimensions of the underlying antecedent topography. Syndepositional fractures 0.5-2 km long and striking parallel to the length of the platform define the crest of the underlying antiformal structure. These fractures were generated by differential compaction of early-lithified platform sediments over the rigid crest of the underlying antiformal bioherms and platform-margins (e.g., compactional hinge of Hunt and Fitchen 1999; Frost and Kerans, in review).

DISCUSSION

Models of Famennian Reef Architecture and Comparison to Other Settings

Depositional models for the Frasnian typically show the classic morphology of a barrier reef-rimmed carbonate platform, with reef and reef-flat building up to near sea-level creating a paleobathymetric barrier with a protected, subtidal lagoon developed in the backreef (Fig 2.28; Playford, 1980, 84; Playford et al., 1989; George and Powell, 1997; Wood 2000). Famennian facies patterns have been recognized by previous workers to reflect sedimentation in high-energy, accommodation-limited conditions (Kerans, 1985; Hurley, 1986; Playford et al., 1989; Stephens and Sumner, 2003). However, aside from accounting for changes in platform-margin trajectory, models for the Frasnian and Famennian systems generally show no difference in overall stratal architecture, despite markedly different biota, facies distributions and accommodation patterns. To date, a unique depositional model for the Famennian has not been presented and the Frasnian barrier-reef model is typically applied (e.g., George and Powell, 1997; Wood 2000).

Based on measured sections and mapping, this study demonstrates that tepee horizons are stratigraphically significant features and the that movement of the tepee belt represents systematic changes in accommodation. The lateral association of tepees and beachrock coupled with the basinward expansion of high-frequency cycles suggests that a shelf-crest existed in the Famennian. None of the tepee-shaped microbial mound features described by Chow and George (2004) were encountered by this study. While it is clear that microbial activity played a major role in the Famennian reef complexes, no evidence was found to support a microbial origin for any of the tepee features described by this study. Instead the tepee features encountered in the Barnett Spring area have a clear-cut marine-vadose origin (e.g., abundant sheet-cracks, pisoids, pendant and meniscus cements; Figures 2.7 and 2.8) and occur as the lateral equivalent to other supratidal facies over short distances (e.g., tepees and beachrock; Figures 2.19–2.21). Moreover, the appearance of marine-vadose tepee features in prograding, Late Frasnian backreef strata (e.g., Geikie Gorge; Figure 2.7c), rather than being restricted exclusively to the Famennian, indicates that tepee formation is intimately linked to decreasing accommodation rather than faunal drivers associated with the F-F mass-extinction as suggested by Chow and George (2004).

To date there has been a degree of confusion on whether the Famennian platform-margin consisted of a rollover margin with no scarp (e.g. Webb, 2001), or whether a platform-margin scarp existed (Playford 1984). The data presented by this study demonstrate that the Famennian reef complexes of the Canning Basin developed as high-relief, reef-rimmed platforms and a subvertical reef scarp did indeed exist for much of the Famennian in the Billy Munro Gorge platform (Figures 2.11b, 2.12c and 2.19). However, while reef-rimmed, the Famennian reef complexes do not develop a shallow barrier-reef; instead the Famennian reef appears to have

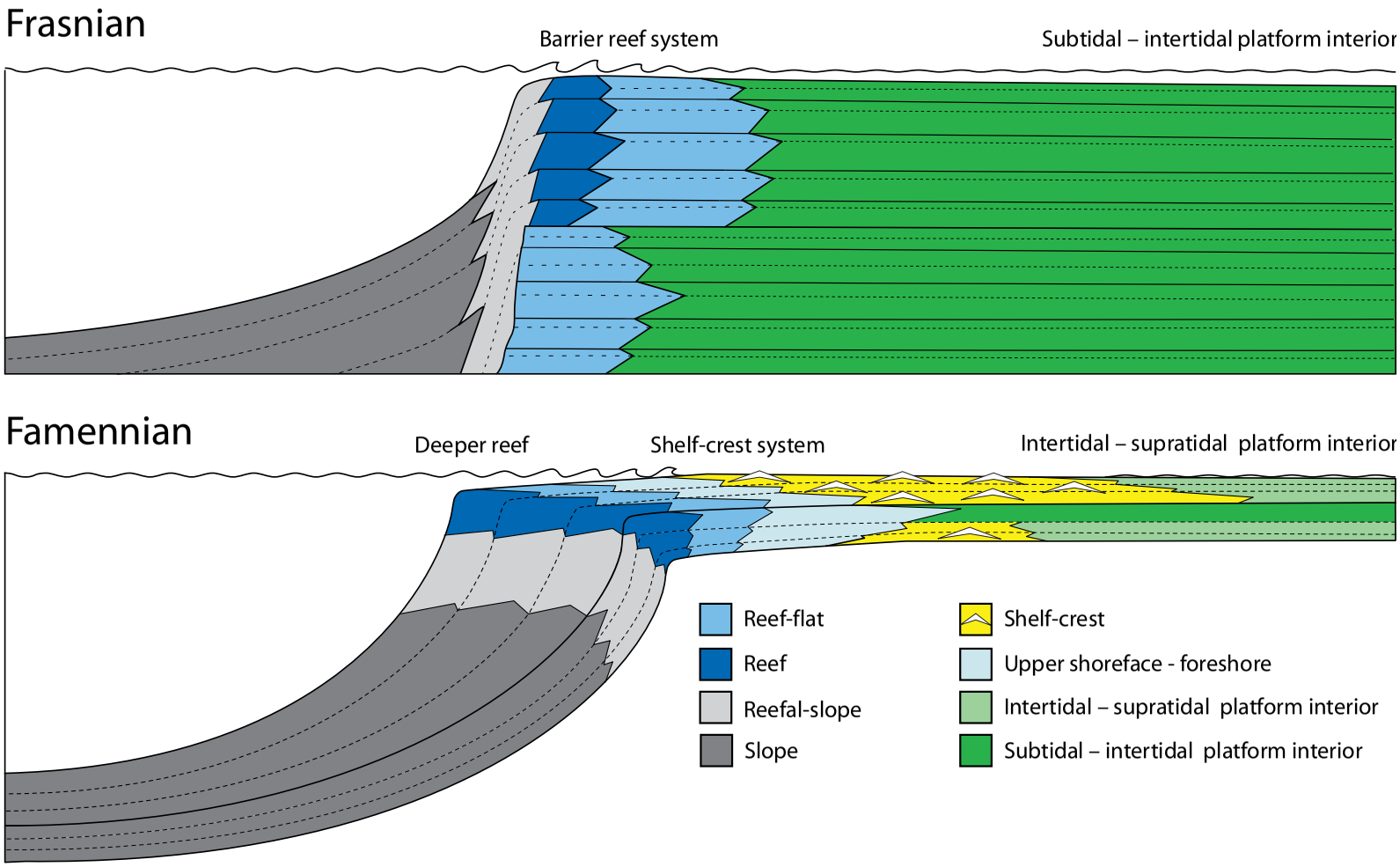

Figure 2.28: Variations in stratal architecture across the Frasnian-Famennian boundary.

The barrier-reef and protected, subtidal, platform interior of the Frasnian are replaced by a deeper reef, a shelf-crest and a high-energy platform-interior in the Famennian.

developed in deeper water (5-15 m; Figures 2.19, 2.20 and 2.28). Several factor are likely to have contributed to the change in reef geometry across the F-F boundary: (1) changes in the vertical growth-rates between the Frasnian stromatoporoid-coral-microbial carbonate factory and the microbial factory of the Famennian, (2) decreased light dependence of the Famennian microbial community and (3) a change in sediment type, size, production rates and dispersal patterns associated with the faunal turnover at the F-F boundary.

Rotation due to differential compaction has been invoked to explain the marginal mound geometry and basinward bed expansion observed in the late Permian Yates formation (Hunt et al., 2002). However, while early-compaction has been proposed as a driver for syndepositional fracture patterns in the Canning Basin (Frost and Kerans in review a/b; Playford, 1984), the observed progressive deepening of facies towards the platform argues against differential compaction as the sole driver responsible for generating the Famennian paleobathymetric profile.

The paleobathymetric model presented here has implications for the long standing debate of whether or not the "sand tube" facies of the Famennian platform-margin represents paleokarst (George and Powell, 1997). If the reef did indeed grow in deeper water (5-15m) as suggested by this study, then it seems unlikely that the platform margin would be karsted without significant karstification of the shelf crest and backreef. No significant penetrative karst surfaces are observed in the Famennian backreef despite well developed sand tubes at the platform margin, suggesting instead a syndepositional origin for this facies (Kerans, 1985; Playford, 2002; Stephens and Sumner, 2003).

The Famennian system as described by this study has several similarities to other well-documented shelf crest systems such as the Late Permian, Yates–Tansil

system (Tinker, 1998; Osleger and Tinker, 1999) and the Middle Triassic Latemar platform (Eggenhoff, 1999; Emmerich et al., 2005) including: (1) a microbial reef factory, (2) a reef system that developed in deeper water than the platform interior; (3) a high-relief, reef-rimmed platform-margin (4) moderately progradational (P/A > 20; Kerans and Tinker, 1999) to aggradational platform-margin trajectory and (5) facies patterns indicative of shallow-water conditions in the backreef.

The development of marine-vadose modified facies require repeated cycles of inundation and exposure as well as a relatively stable shoreline (Kerans and Tinker, 1999). The prevalence of tepees, fenestral laminites and beachrock in the Famennian succession indicates that limited accommodation conditions prevailed and suggests that decreasing long-term accommodation was largely responsible for the development of the shelf-crest system. However, it is unclear what role the deep microbial reef system and the lack of a barrier-reef plays in shelf crest development. Kerans and Tinker (1999) have documented that where tepee complexes are best developed in the Yates-Tansil system, the reef grows at shallower water depths (30 m) and when the tepee belt is absent, the reef grows in deeper water (80 m). These authors interpreted this relationship to highlight the shelf-crest's role as a topographic barrier, protecting the reef from highly saline platform-interior brines and in its absence the reef responded to unfavorable salinity conditions by growing in deeper water. In small platforms were evaporitic brines are absent, such as Billy Munro Gorge and the Latemar, this control on reef depth would not be a factor. Instead, it is possible that the lack of a barrier reef allowed for increased wave-energy across the platform top, altering sediment dispersal patterns and leading to increased landward transport of sediment, perhaps facilitating the development of a barrier island complex and shelf crest.

CONCLUSIONS

This study documents the evolution of platform architecture and facies patterns across the Frasnian-Famennian boundary in the Canning Basin. The Famennian facies models presented here represent a fundamental departure from those observed in the Frasnian. A positive topographic barrier or shelf crest system, characterized by tepee complexes, fenestral laminites and beachrock developed in the Famennian platform interior, flanked by a deeper water microbial reef, rather than the shallow barrier reef system observed in the Frasnian. The interpretations presented here for the Famennian are constrained by digital outcrop mapping and are captured in three-dimensional geocellular models. While a single definitive cause for the development of the Famennian paleobathymetric profile can not be isolated, this study proposes that the Famennian reef geometry was driven by the faunal turnover associated with the F-F boundary; while the development of the shelf-crest was controlled dominantly by decreasing long-term in accommodation space throughout the Famennian. The models for Famennian facies patterns and stratal architecture presented by this study are markedly different than those observed in the Frasnian; however they are not unique in the geologic record and instead these patterns appear to be characteristic of high-relief microbial systems that developed in limited accommodation conditions throughout the geologic record.

Chapter Three: Controls on Syndepositional Fracture Patterns, Devonian Reef Complexes, Canning Basin, Western Australia

ABSTRACT

Syndepositional deformation in carbonate platforms is often acknowledged to be stratigraphically controlled; however, it remains unclear how variations in stratigraphic architecture affect syndepositional fracture patterns. This study integrates outcrop and remote-sensing data from the Canning Basin's Devonian reef complexes to test the hypothesis that syndepositional fracture attributes (orientation, intensity, and spatial arrangement) are a function of depositional facies, position along a carbonate platform, and platform-margin trajectory.

Three basic control types are proposed for the generation of syndepositional fractures: gravitational instability and compaction (Type I), differential compaction over antecedent topography (Type II), and active structural deformation (Type III). Strong variations in syndepositional fracture intensity, extension, and spatial arrangement are observed with changes in lithofacies. Evidence of temporal evolution of the mechanical properties of the Devonian reef complexes is presented, with early-lithified strata effectively behaving as a single mechanical unit during syndepositional fracture development, while secondary fractures are strongly affected by bed-scale mechanical heterogeneity introduced by progressive diagenesis. Syndepositional fracture intensity is shown to vary systematically with changes in platform-margin trajectory; with high fracture intensities observed in

This chapter is in review in the *Journal of Structural Geology*.

strongly progradational platforms and decreased fracture development in aggradational and retrogradational platforms.

INTRODUCTION

Large, syndepositional, opening-mode fractures, often referred to as neptunian dikes, represent an important style of early deformation in many carbonate platforms throughout the geologic record. Fracture development in carbonates has traditionally been attributed to stress associated with regional tectonic deformation and attributed fracture characteristics (e.g., spacing, orientation, and termination) to variations in bed-scale mechanical properties (Narr and Suppe, 1991; Bai and Pollard, 2000; Underwood et al., 2003; Shackleton et al., 2005). Large-scale syndepositional fractures present a paradox because these features often develop in the absence of coeval regional structural controls and crosscut numerous small mechanical layers, implying that the mechanical units that control these features occur at scales (50–150 m) not typically addressed by mechanical stratigraphy.

Previous studies have focused on various aspects of syndepositional deformation in carbonate platforms, including syndepositional faulting in backreef strata of strongly prograding platforms (Hunt and Fitchen, 1999; Hunt et al., 2002; Kosa et al., 2005), the relationship between syndepositional fractures and karst development (Baceta et al., 2007; Guidry et al., 2007), and syndepositional fracturing as a function of active tectonic deformation (Miller et al., 2007). Although many workers have acknowledged a stratigraphic control on syndepositional fractures, to date no relationships between long-term variations in stratigraphic architecture and syndepositional fracture patterns have been reported.

This study addresses utilizes outcrop- and remote-sensing-scale fracture attribute data collected from a broad spectrum of platform types (prograding,

aggrading, and retrograding) in the Canning Basin's Devonian reef complexes to address the following questions: (1) Does a systematic relationship exist between syndepositional fractures patterns and stratigraphic architecture—quantified here by progradation to aggradation (P/A) ratio? (2) Can tectonic and stratigraphic controls on syndepositional fracturing be separated? (3) How do depositional facies influence syndepositional fracturing? (4) At what scale do the mechanical units occur in early fracture systems? And (5) do these mechanical units vary temporally with continued diagenesis?

GEOLOGIC SETTING

Regional Setting

The Canning Basin is Western Australia's largest sedimentary basin covering approximately 430,000 km^2 and containing over 15,000 m of Ordovician- through Cretaceous-age strata (Brown et al., 1984). The Canning Basin is bounded to the east by the Proterozoic Kimberley Block and to the west by the Achaean Pilbara craton (Figure 3.1-3.2). The northeastern portion of the Canning Basin can be subdivided into a number of prominent structural elements (Figure 3.1a): the Lennard Shelf, the Fitzroy Trough, and the Broome Arch. Basin development initiated in the Ordovician with broad intracratonic downwarping, followed by active rifting in the Middle Devonian through the early Carboniferous, marked by the development of the deeply subsident NW-SE-oriented Fitzroy Trough (Figure 1c). During the Late Devonian, carbonate deposition primarily occurred along the eastern margin of the Canning Basin on the shallow Lennard Shelf, with the Devonian reef complexes fringing the mountainous Precambrian Kimberley Block, as well as smaller, isolated, emergent Precambrian topography (e.g., Oscar Range; Figure 3.2a). The 10-50-km-wide shallow Lennard Shelf is flanked to the northeast by the

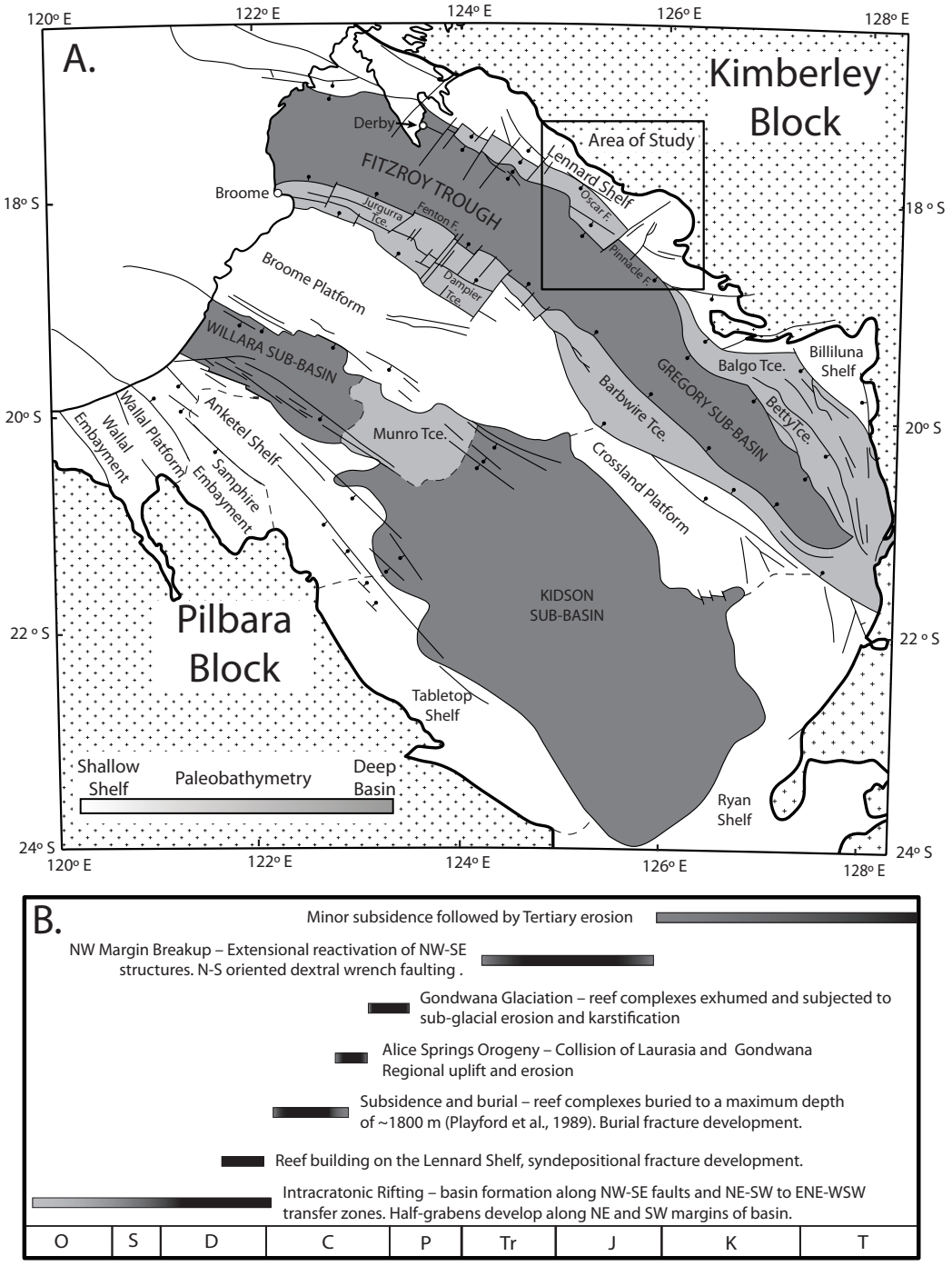

Figure 3.1: Study area location and geology.

(A) Regional setting and structural elements of the Canning Basin, modified from Shaw (1994). (B) Timing of major events impacting the Devonian reef complexes (modified from Brown et al., 1984; Craig et al., 1984; Drummond et al., 1988; Playford et al. 1989; and Eyles et al., 2001).

mountainous Precambrian King Leopold foldbelt of the Kimberley Block and to the southwest by large-scale Late Devonian extensional fault systems (e.g., Oscar Fault and Pinnacle Fault) and the Fitzroy Trough.

Maximum burial of the Devonian of approximately 1800 m occurred in the early to middle Carboniferous (Playford et al., 1989). Regional uplift associated with the Alice Springs Orogeny in the late Carboniferous coupled with glaciation in the late Carboniferous to Early Permian removed many of the younger sediments overlying the Devonian reef complexes (Figure 3.1b; Eyles et al., 2001; Playford, 2002). Permian glacial sediments of the Grant Group subsequently buried the reef complexes. After broad, regional, Cenozoic uplift, the Devonian reef complexes are now represented as a rugged 350-km-long, northwest-to-southeast-trending outcrop belt of flat-topped limestone ranges.

Stratigraphy of the Devonian Reef Complexes

Two major reef-building sequences are recognized within the Devonian reef complexes, (1) the Givetian-Frasnian Pillara Sequence and (2) the Famennian Nullara Sequence (Figure 3.2b; Playford, 2002, and references therein). The Pillara Sequence developed during basinwide transgression coincident with peak rifting and is characterized by long-term backstepping with the development of pinnacle reefs and high-relief platforms with steep escarpment margins. Platforms of the Pillara sequence were constructed by a consortium of stromatoporoids, corals, and calcimicrobes. Minor progradation occurred in the latest Frasnian, followed by the Frasnian-Famennian (F-F) mass extinction event and brief exposure of the reef complexes. Subsequent prograding Famennian reef complexes of the Nullara Sequence are composed primarily of high-energy grainstones and cyanobateria. Extensive early marine cementation played a fundamental role in the evolution of

both the Frasnian and Famennian reef complexes, allowing for the development of stout, wave-resistant reef rims and steep platform-margin escarpments. Early lithification also created brittle facies that were prone to syndepositional fracturing (Playford, 1984; Kerans, 1986).

Much of the original depositional topography of the Devonian reef complexes is relatively undeformed, with syndepositional fractures well exposed along the dip-oriented polished walls of present-day river gorges and along the top of most of the limestone ranges. Differential weathering and vegetation accentuate the fracture planes, creating linear depressions that are easily resolvable from satellite imagery (Figure 3.3).

SYNDEPOSITIONAL FRACTURES

Background and Terminology

Syndepositional fractures are common in many carbonate systems throughout the geologic record (Playford, 1984; Smart et al., 1988; Hunt and Fitchen, 1999; Cozzi, 2000; Kosa et al., 2003; De La Porta et al., 2004; Collins et al., 2006; Guidry et al., 2007) and are a hallmark of early-lithified and brittle platform-margin facies of steep reef-rimmed carbonate platforms. The Canning Basin contains one of the best preserved syndepositional fracture sets, and these features have been the focus of a considerable amount of research by a number of workers (Playford, 1980, 1984; Hurley, 1986; Kerans et al., 1986; Playford et al., 1989; Dörling et al., 1996; Ward 1996; Miller et al., 2007).

Three primary fracture populations are recognized by this study in the Canning Basin: (1) Neptunian Dikes, well-documented large-aperture (10 cm–20 m) fractures filled with late Devonian marine sediment and or marine cement (3.4-5); (2) syndepositional veins, smaller aperture (1 mm–25 cm) fractures infilled

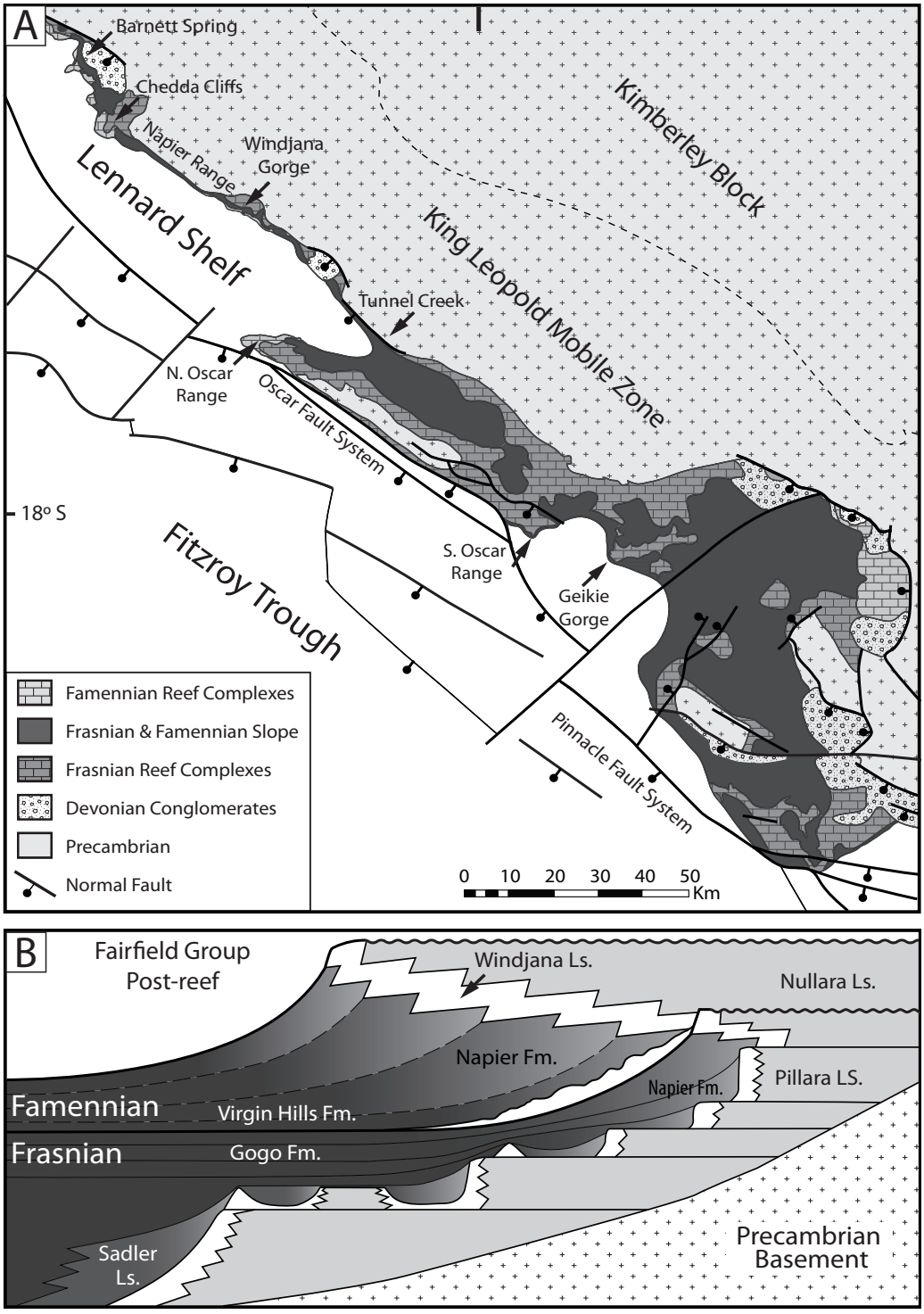

Figure 3.2: Geology of the Devonian reef complexes.

(A) Geology of the Lennard Shelf, modified after Playford and Hocking (1999).
(B) Stratigraphy of the Devonian reef complexes, modified after Playford (2002).

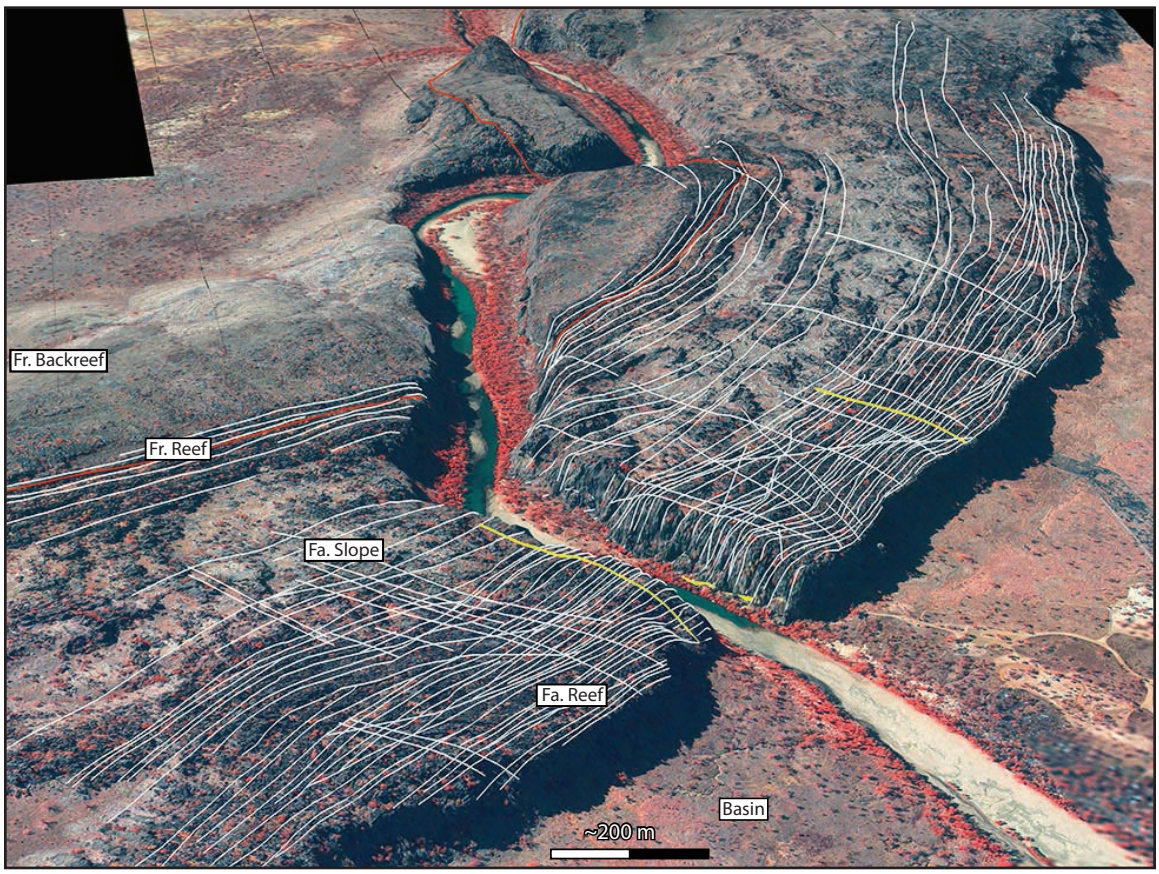

Figure 3.3: Syndepositional fractures at Windjana Gorge.

Cliff face is approximately 80–90 m tall. Image constructed from false-color Ikonos satellite imagery, high-resolution ground-based lidar, and 90-m SRTM data

with Late Devonian marine cement, but in most cases lacking platform-top derived sediment (Figure 3.5): and (3) secondary (postdepositional) fractures, small (0.215–5 mm) aperture fractures that are filled with blocky, equant, calcite spar (Figure 3.5), which are thought to be related to burial in the Carboniferous and Permian (Figure 3.1, Hurley, 1886). The two syndepositional fracture populations of the Canning Basin are genetically related, so these fractures will be referred to collectively simply as syndepositional fractures.

Occurrence and Timing

Syndepositional fractures are common throughout the Devonian reef complexes; however, they are most abundant in the early-lithified facies of the upper slope, platform margin, and reef flat (Playford, 1984). Syndepositional fractures in the Canning Basin are dominantly opening mode (tensile); however, a minor component of normal offset is observed in tectonically active areas (e.g., Tunnel Creek; Ward, 1996; Miller et al., 2007) and strongly prograding backreef strata (e.g., Billy Munro Gorge; Frost and Kerans, in review) Fractures typically crosscut bedding and reach vertical heights exceeding 90 m (outcrop limit), while kinematic apertures up to 20 m and fracture trace lengths of 5 km have been reported (Figures 3.3-4; Hurley, 1986; Kerans et al., 1986; Playford et al., 1989).

Fracture fills are highly variable (Figure 3.5) and include marine cement; microbial communities; platform-top-derived detritus including bioclastic wacke/packstones, oolitic grainstones, and siliciclastic sandstones; breccia; and large marine-cement-coated grains known as “spar balls” (sensu Playford 1984; Figure 3.5G). Fracture timing has been established as syndepositional by (1) recognition of Late Devonian marine cement, coeval platform-derived sediment, encrusting marine microbial colonies and benthic organisms (Playford et al., 1989) lining

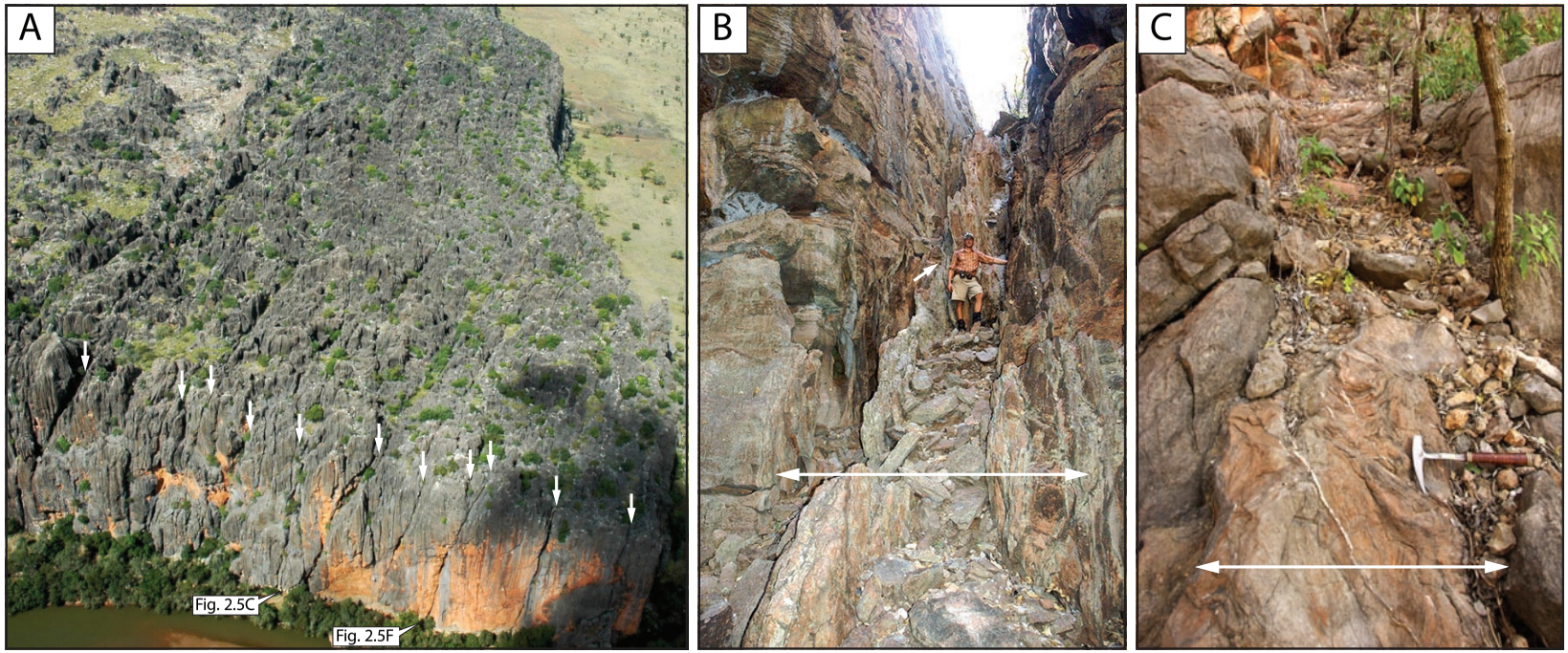

Figure 3.4: Outcrop-scale syndepositional fractures.

(A) Oblique aerial photo of large syndepositional fractures (white arrows) in prograding Famennian reef, Windjana Gorge. Cliff face is 90 to 100 m tall. Despite modern solution enhancement, a syndepositional origin is clear from fracture fill (see Figures 3.5C and 2.5F). (B) Large syndepositional fracture, Famennian backreef, Billy Munro Gorge. Fracture is approximately 2 m wide and cuts through at least 65 m of backreef strata with no vertical offset. Large modern cave network has formed below field of view. (C) Sandstone-filled syndepositional fracture, Famennian fore-reef slope, Windjana Gorge. Fracture is approximately 1 m wide and cuts through at least 90 m of fore-reef strata with no vertical offset. Sand is horizontally laminated, implying infill from above; small crosscutting, marine-cement-lined fractures confirm syndepositional origin.

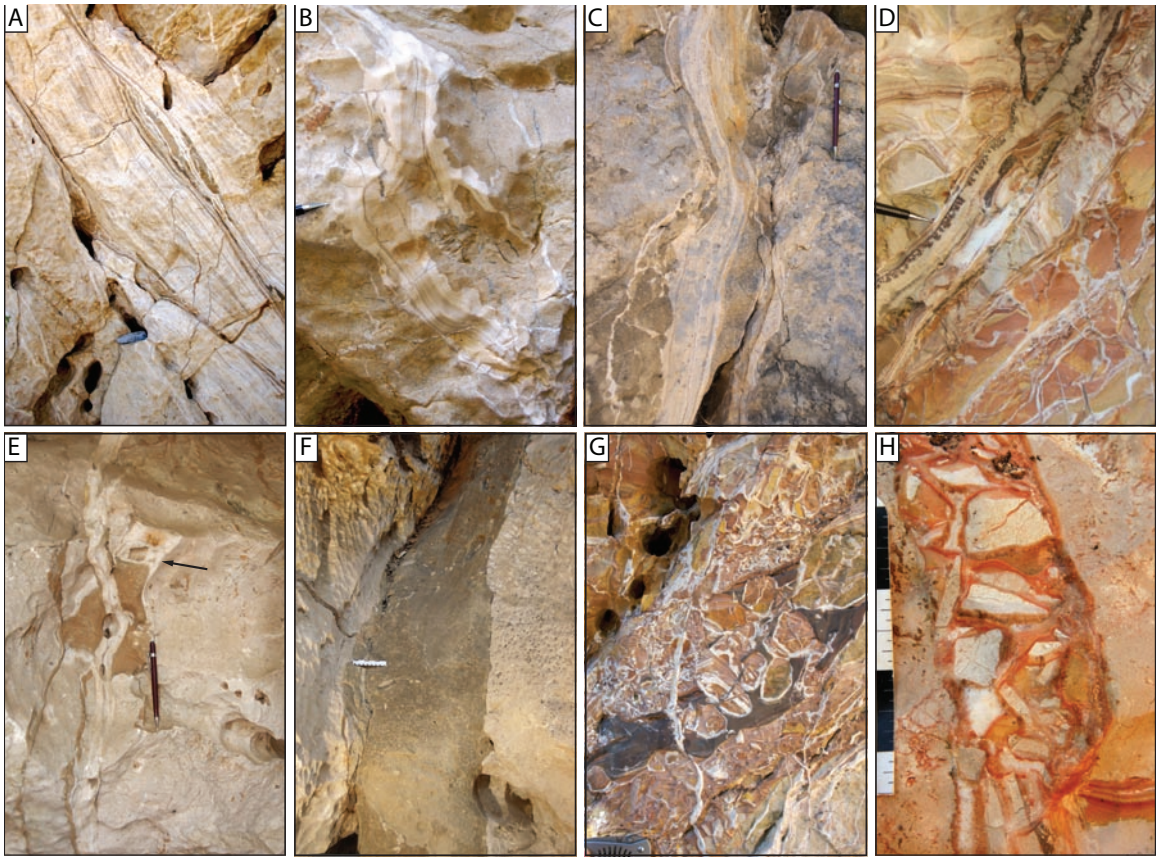

Figure 3.5: Syndepositional fracture fills.

(A) Marine cement with multiple crack-seal events, Frasnian fore-reef slope, Geikie Gorge. (B) Marine cement, with equant-spar-filled, crosscutting, secondary fractures, Famennian deep reef, Windjana Gorge. (C) Marine cement with sandstone, Famennian deep reef, Windjana Gorge. (D) Microbialite and marine cement. *Frutexities* (dark pendant microbial growths at pen) encrust fracture wall prior to cement infill. Frasnian backreef, Tunnel Creek. (E) Sandstone and marine cement. Note ammonoid (arrow) in sandstone fill. Marine cement-lined fracture crosscuts sandstone. Famennian, reef, Windjana Gorge. (F) Sandstone and wall-rock breccia. Sandstone has same composition as 3E. Famennian reef, Windjana Gorge. (G) "Spar balls," marine cement, and sandstone, along minor normal fault. Frasnian backreef, Tunnel Creek. (H) Breccia fill, Frasnian backreef, Geikie Gorge.

fracture walls (Figure 3.5D) and (2) by crosscutting relationships with stylolites and later fractures. Secondary fractures are differentiated on the basis of their clear blocky spar burial-phase cements (Hurley, 1989; Wallace 1989) and coeval crosscutting relationships with stylolites. Secondary fractures are strongly influenced by meter-scale bedding, and they have trace heights rarely more than a few centimeters and apertures less than 2.5 mm in width.

Controls on Syndepositional Fracture Development

The two fundamental requirements for syndepositional fracturing are an early-lithified, brittle medium and stress. Early-lithified carbonate strata are common in the geologic record, and a broad number of mechanisms have been proposed for generating the stress required of syndepositional fracturing. On the basis of previous studies and observations presented here, we propose a three-part classification of syndepositional fracture controls (Figure 3.6; Frost and Kerans, in review): (1) Gravitational instability and substrate compaction (Type I), (2) differential compaction over rigid antecedent topography (Type II), and (3) active structural deformation (Type III). Each control type represents a unique end-member with distinct fracture patterns (Kosa et al., 2003); however, any given fracture set can be the product of one or all of these drivers.

Type I fractures are generated by extensional stress associated with (1) oversteepening and defacement of the active platform-margin escarpment (Ward, 1996) and (2) down-to-the-basin tilting related to early compaction of basinal sediments and bedding-plane slippage in ductile slope strata (Playford et al., 1989; Hunt and Fitchen 1999). In high-relief carbonate platforms, the subvertical escarpment of the platform-margin is unconfined on the open ocean side, and as a result the minimum effective stress axis runs parallel to the platform-margin trend

(Daugherty et al., 1986; Whitaker and Smart, 1997). This “free air” surface facilitates the development of margin-parallel opening-mode fracture networks. As the height an d angle of the escarpment increase from reef growth or headward slope erosion (Schlager and Camber, 1986), the platform margin becomes increasingly unstable and prone to increased fracturing and gravitational collapse (Playton, in prep.). Gravitational instability of the escarpment is most effective at producing fractures in the platform margin, and fracture intensity decreases into the platform interior in the absence of any other drivers. Stress associated with compaction of basinal strata (Kosa et al., 2003) and slippage along bedding planes (Playford, 1984; Hurley, 1986) also produce syndepositional fractures that run dominantly parallel to the platform margin. These mechanisms are most effective in prograding platforms, where brittle early-lithified sediments build over more compactable strata. Once fractures are initialed in the reef facies, these features remain active as zones of weakness, propagating upward into overlying backreef strata as inherited fractures (sensu Kosa and Hunt, 2005). Small-scale faults (>0.5m offset) become more common in the most progradational platforms (e.g., Billy Munro Gorge); however, the degree of compactionally controlled faulting proposed by Kosa and Hunt (2005) in the Permian Capitan Formation of Texas is not observed.

Type II syndepositional fractures are generated by differential compaction and flexure of early-cemented strata over rigid antecedent topography such as older platform escarpments (Hunt and Fitchen, 1999; Ruscudeli and Di Simone, 2007), fore-reef bioherm complexes, and drowned reef spines (Frost and Kerans, in prep.) or crystalline basement topography (Hurley, 1986). Type II fractures typically occur in discrete swarms focused over the crest of the underlying topographic element.

Type III fractures are generated by stress associated with syndepositional

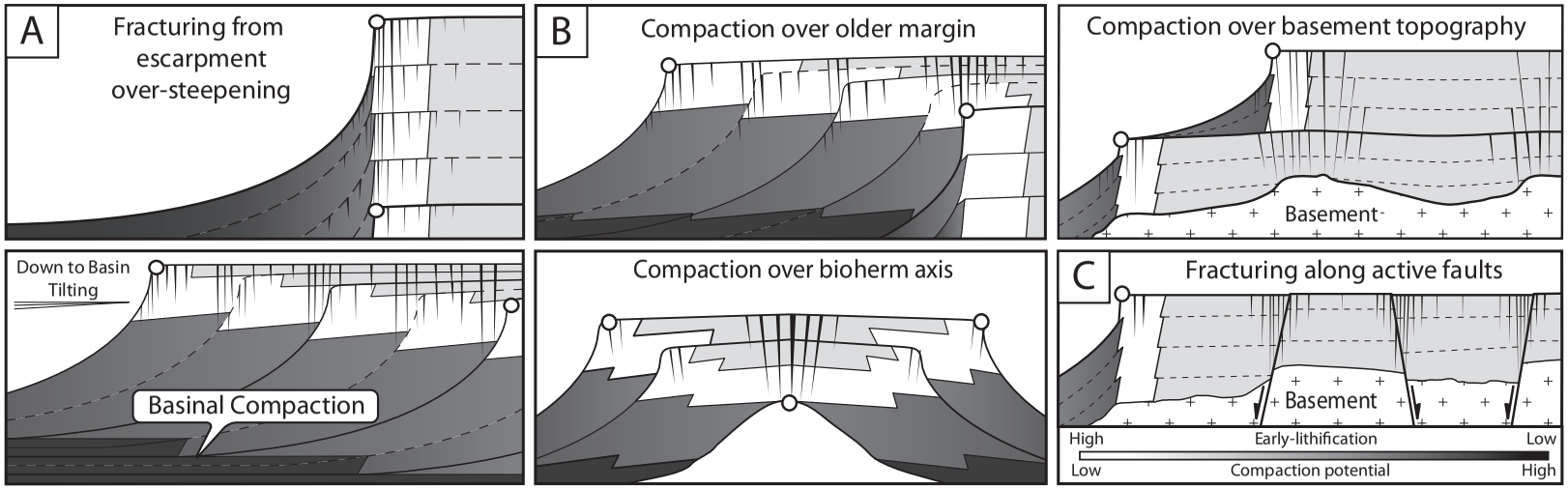

Figure 3.6: Proposed syndepositional fracture mechanisms.

(A) Type I, gravitational processes. (B) Type II, antecedent topography. (C) Type III, active regional tectonic deformation. Compiled from Hurley (1986), Playford (1984), Ward (1996), Hunt and Fitchen (1999), and Kosa et al. (2003).

tectonics and are orientated parallel to the active deformation feature or regional stress field (Hurley, 1986; Cozzi, 2000; Miller et al., 2007); a component of vertical displacement is often observed. Type III fractures require an extrinsic mechanism such as active regional structural deformation, while Type I and Type II fractures are formed by passive deformation mechanisms and are intrinsic to the stratigraphic architecture of many carbonate systems.

METHODS

In order to characterize the distribution of syndepositional fractures within stratigraphic framework of the Devonian reef complexes, four study areas with well-exposed fractures and well-defined stratigraphy were selected along the Napier and Oscar Ranges (Figures 3.7-10). To test the hypothesis that syndepositional fracture characteristics (e.g., intensity and orientation) are related to stratigraphic architecture, fracture attribute data were collected at two scales of observation: (1) remote-sensing-scale lineaments with apertures of 0.5 m and larger, and (2) outcrop scale, all fractures with apertures 0.2 mm and larger.

Large-scale fracture populations were examined across the platform on high-resolution (~1-m-pixel) IKONOS satellite imagery. Syndepositional fractures are well exposed along the top of most of the limestone ranges, with fractures often differentially weathering to form vegetation-lined corridors easily resolvable from satellite imagery (Figure 3.3). Fracture traces were mapped at regional (1:24,000 and 1:10,0000) and local scales (1:3,309; Ikonos resolution limit). Orientation and spacing were measured for approximately 1,500 fractures (b > 0.5 m) in 11 one-dimensional scanlines using ArcGIS (Figures 3.7-10; Table 3.1). Because many syndepositional fractures are solution enhanced along a modern karst plane, no attempt at characterizing apertures was made. Remote-sensing interpretations were

calibrated to ground-based scanlines, field mapping, and published data (Hurley, 1986) in order to ensure that only syndepositional fractures were recorded.

Outcrop fracture data were collected along the polished canyon walls of Windjana Gorge in the Napier Range (Figure 3.2-3.3). Fracture attributes such as orientation, extension, fracture intensity, scaling, and spatial arrangement were analyzed along 12 one-dimensional scanlines using the methodology of Ortega et al. (2006). Syndepositional fractures were differentiated from secondary fractures on the basis of fill and crosscutting relationships, and the fracture attributes from each population are reported separately (Table 3.2). In order to characterize vertical fracture relationships (i.e., crosscutting, orientation, and termination), syndepositional fracture planes were interpreted on a high-resolution (3-5cm) ground-based lidar point cloud and tied to outcrop scanlines. We used Normalized Correlation Count (NCC; Gomez, 2007; Marrett et al., in press), a recently developed analytical technique, to determine the spatial arrangement of fractures.

Fracture intensity (FI; Ladeira and Price, 1981) was used to compare syndepositional fracturing at different localities, given its relative ease of acquisition at both scales of observation. FI values vary by nearly three orders of magnitude between the remote sensing scale (low FI) and outcrop (high FI) owing to disparate resolutions of the two methods. Fracture aperture populations in each of the ground-based scanlines follow power-law scaling, allowing for large-scale apertures to be characterized from a smaller subset (Marrett et al., 1999). To facilitate direct comparison between the two scales of observation, normalized fracture intensity (FIn; Ortega et al., 2006) was calculated for apertures 0.5 m and larger (FIn0.5; the smallest detectable aperture by remote sensing) for each ground-based scanline. Results from Windjana Gorge demonstrate that FIn calculated from ground-based scanlines accurately predicts FI calculated from remote sensing data (e.g., 9559

Scanline	Locality	Method	Control	Progradation (m)	Aggradation (m)	P/A Ratio	Fracture Intensity (fractures/m)		Average Spacing (m)	
							Reef	Platform	Reef	Platform
Famennian Platforms										
BMG_L	Billy Munro (Long axis)	RS	I, II	1759	160	11.0	0.119	0.058	8.4	17.4
BMG_S	Billy Munro (Short axis)	RS	I, II	685	160	4.3	0.089	0.038	11.2	26.2
MMG	Mick Malcom Gap	RS	I	1450	160	9.1	0.109	0.053	9.1	18.9
Chd	Chedda Cliffs	RS	I	1729	200[1]	8.6	0.109	ND	9.2	ND
NO_Mrwn	N Oscars (MRWN)	RS	I	1511	168[3]	9.0	0.112	0.048	8.9	20.8
NO_SM	N Oscars (SWM)	RS	I, III	550	168[3]	3.3	0.084	ND	11.9	ND
W_Fa-1	Windjana Gorge	RS	I	704	169[#]	4.1	0.088	ND	11.4	ND
9559	Windjana Gorge	G	I	613	148[#]	4.1	0.087[$]	ND	11.5	ND
Famennian Platforms										
W_Fr-7	Windjana Gorge	RS	I	167[3]	233[3]	0.7	0.072	ND	13.9	ND
9434 / 9460	Windjana Gorge	G	I	–82	74	-1.1	0.051[$]	0.029[$]	16.4	34.5
SO_Fr-6	S Oscars (Fr6)	RS	III, II, I	–1326[2]	547[2]	-2.4	0.054	0.043	18.4	23.3
SO_Fr-7	S Oscars (Fr7)	RS	III, II, I	328[2]	256[2]	1.3	0.075	0.054	13.4	18.5
TC-1	Tunnel Creek	G	III, II	–100[4]	50[4]	-2.0	ND	0.074[$]	ND	13.5

$ Normalized fracture intensity for fractures greater than 0.50 m. [1] Chow et al., 2004; [2]Hurley, 1986; [3]Playford and Hocking, 1999; [4]Ward 1996.

Table 3.1: Fracture attributes and stratigraphic architecture data.

Fracture intensity and average spacing for ground-based scanlines have been normalized to the minimum detectable aperture from remote sensing data (0.5m).

and W_Fa–1; Table 3.1). Due to incomplete mechanical boundary preservation from modern erosion, FI was not normalized for mechanical unit thickness (sensu Narr and Suppe, 1991).

Progradation to aggradation (P/A) ratio quantifies platform-margin trajectory and serves as a proxy for stratigraphic architecture (Tinker 1998; Kerans and Tinker, 1999; De La Porta et al., 2004). P/A ratio was calculated from field mapping (this study), satellite imagery, or published data (Table 3.1). In the absence of a platform section, the mean thickness of time-equivalent sections was applied. Owing to differential stratigraphic preservation, aggradation values do not necessarily reflect total thickness and are best thought of as minimum values. Absolute rates are not calculated for this study because of limited chronostratigraphic data, and P/A ratios reported here represent long-term trends.

LARGE-SCALE SYNDEPOSITIONAL FRACTURE PATTERNS

Southern Oscar Range

The Frasnian outcrops of the southwest Oscar Range provide an excellent example of a well-developed syndepositional fracture network in a retrograding and aggrading platform (Hurley, 1986; Figure 3.7; Table 3.1). Two primary sets of syndepositional fractures in the Southern Oscar Range are set 1, weakly developed margin-parallel fractures that mimic the morphology of the platform and set 2, fractures with an average trend of 308°, which run subparallel to regional syndepositional structural features (e.g., Djowi Fault, Oscar Fault) and dominantly follow the regional structural trend of the Oscar Range (315°). Set 2 syndepositional fractures intersect the southern margin of the Oscar Range at high angles and do not appear to be influenced by gravitational processes at the platform margin. Owing to extensive early-marine cementation, platform strata generally

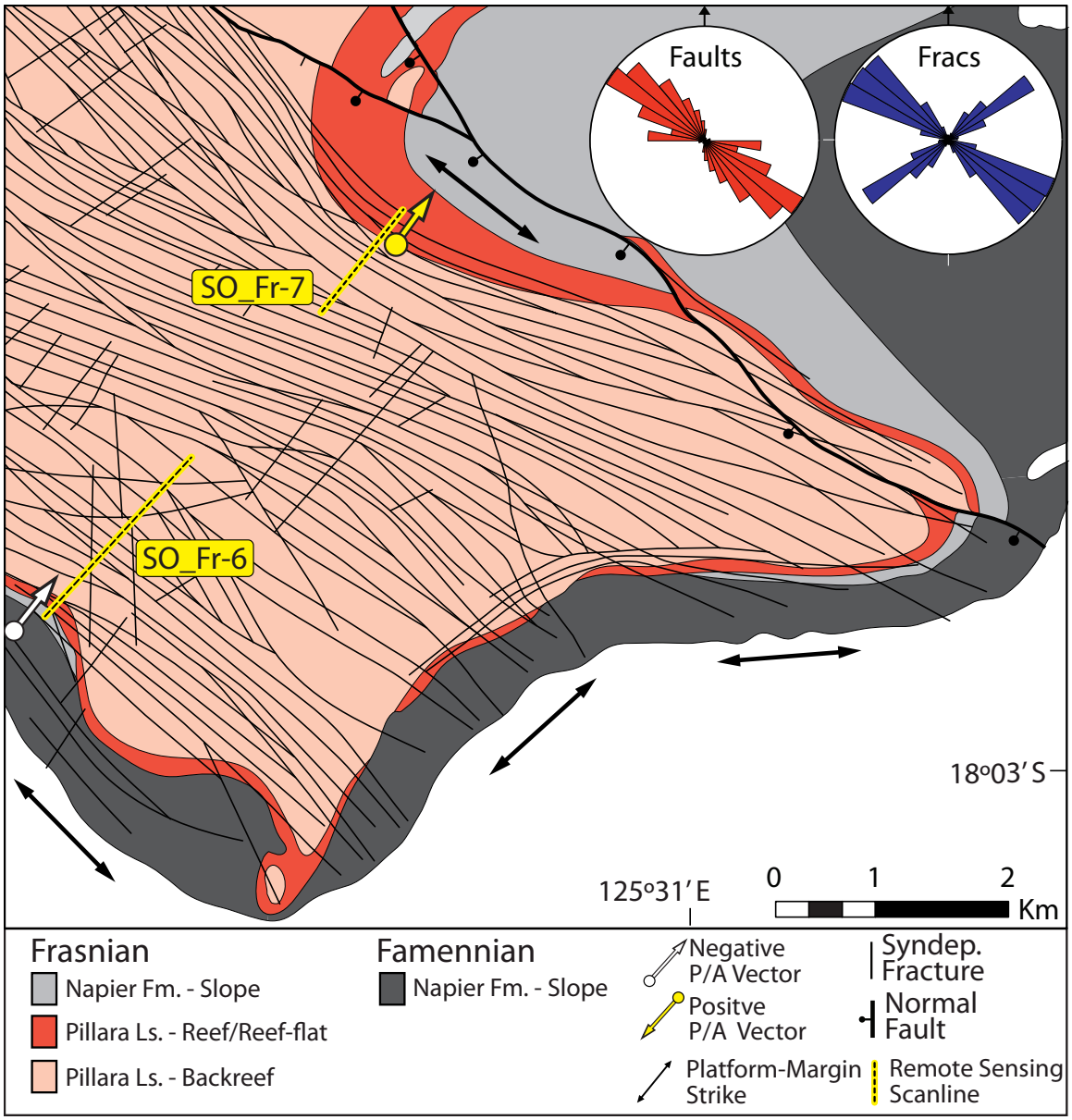

Figure 3.7: Simplified fracture patterns of the Southern Oscar Range.

Geology modified from Playford and Hocking (1999) after Hurley (1986). Syndepositional fractures dominantly follow regional structural (Devonian) elements and often intersect the southeast margin at high angles. Margin parallel fractures are weakly developed and localized along SE margin.

have a lower early-compaction compaction potential when compared with basin and fore-reef sediments (up to 70%; Playford 1984; Playford and Wallace 2001); the classic model of syndepositional fracturing related to gravitational instability (Playford, 1984) subsequently does not fully account for the large number of fractures observed in the backreef of the Oscar Range. Hurley (1986) proposed that set 2 fractures are generated by Devonian fault movement (Type III) and differential compaction over the Precambrian basement topography (Type II).

Northern Oscar Range

In the Northern Oscar Range, syndepositional fracture networks are well exposed in a series of prograding Famennian reef complexes (Figure 3.8). Along the strongly progradational northern margin, syndepositional fractures are well developed (Table 3.1) and run parallel to the platform margin (90°), not the regional tectonic grain of the Oscar Range (310°; Playford and Hocking, 1999). Hurley (1986) reported apertures as wide as 10 m and syndepositional extension of approximately 7% (scanline NO_Mrwn; Figure 3.8) in this setting. This margin-parallel syndepositional fracture population is interpreted to be gravitationally controlled (Type I), with compaction of fore-reef and basinal sediments and fore-reef bedding-plane slippage proposed as the dominant controls on fracture development (Hurley 1986).

Syndepositional fractures are also well developed in the prograding Famennian reef complexes of the fault-bounded southern margin of the northern Oscar Range (Figure 3.8; Table 3.1). Fractures are margin parallel (310°); however, given the close proximity to the major basin-bounding Oscar fault network and that the southern margin of the Oscar Range follows the overall trend of regional structure (310°), syndepositional fractures in this setting are most likely controlled

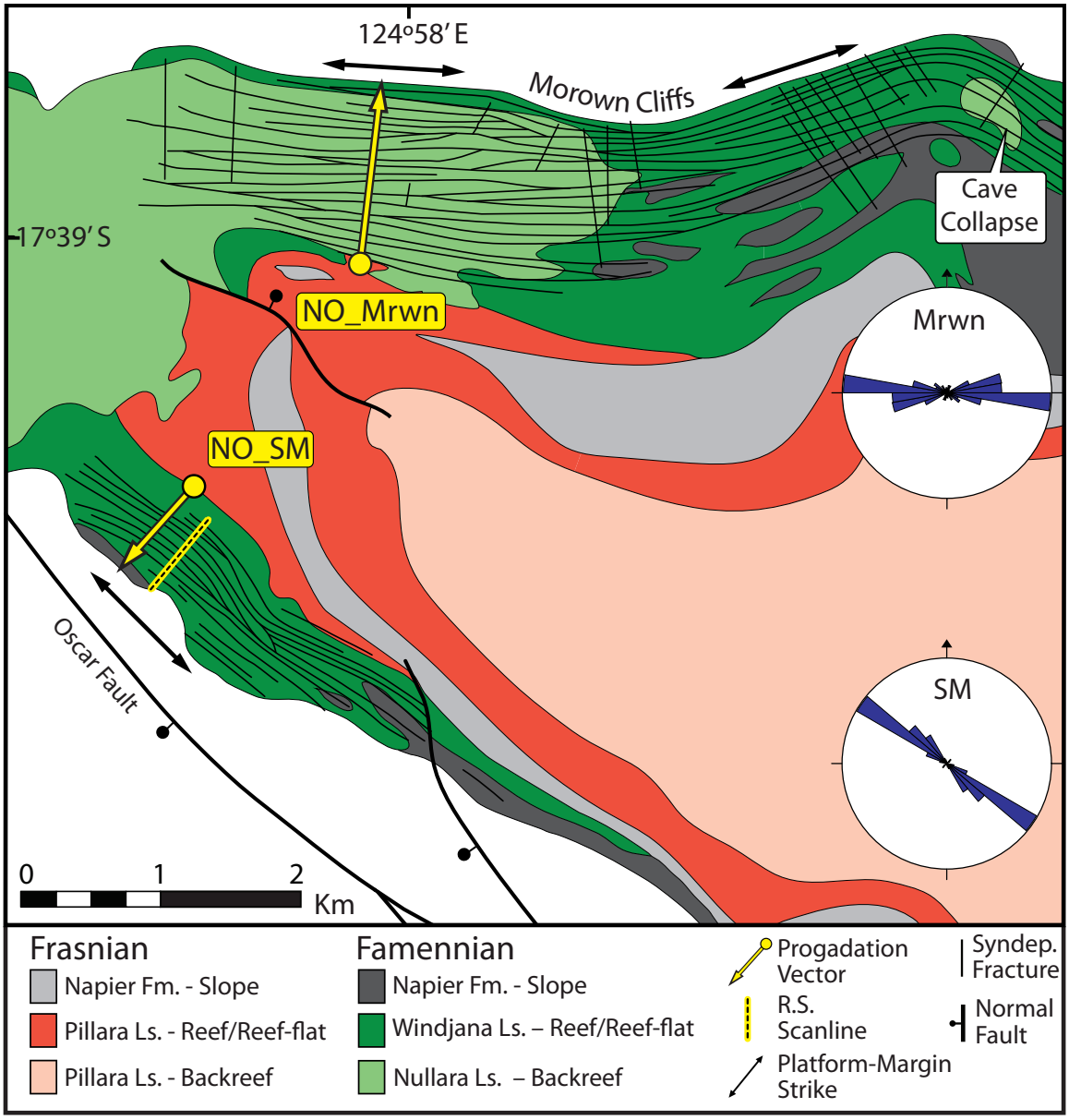

Figure 3.8: Simplified fracture patterns of the Northern Oscar Range.

Geology modified from Playford and Hocking (1999) after Hurley (1986). Along the Morown Cliffs, syndepositional fractures mimic platform morphology and run parallel to the margin, not regional structure. Along the southern margin, fractures also run parallel to the margin; however, given the close proximity to the Oscar Fault, this fracture set is most likely structurally influenced. Scanlines follow platform-margin vector unless otherwise noted.

by a combination of active structural deformation (Type III) and gravitational processes associated with progradation (Type I). The relative contribution of these control types is discussed later.

Billy Munro Gorge

The Billy Munro Gorge platform developed as a progradational, narrow (3.5 × 1 km) promontory with a steep microbial escarpment margin (Figure 3.9). This unique morphology is the result of three distinct phases of Famennian platform evolution within the Billy Munro Gorge area (Frost et al., in prep.): (1) development of a large antiformal, early Famennian deep-water stromatolite bioherm complex; (2) platform nucleation and high-energy shoal-water carbonate development on the positive antecedent topography created by the marginal-slope mound complexes; and (3) rapid platform progradation along antecedent topographic highs and development of an extensive network of syndepositional fractures.

Three distinct syndepositional fracture sets are observed from remote sensing and field mapping in the Billy Munro Gorge platform (Figure 3.9). Set 1, a platform-margin parallel set that mirrors the morphology of the platform, developed in response to gravitational instability of the platform margin associated with compaction of basinal sediments (Type I control). These fractures are best developed near the platform margin and are filled with marine cement and sediment, with apertures of 1.5 m or less. Set 2, WSW-ENE-trending clusters of fractures that run parallel to the long axis of the platform, is thought to have developed from compaction of platform strata over the underlying antecedent topography of the microbial mound complex (Type II control). Set 2 fractures are restricted to a narrow swath at the center of the Billy Munro Gorge promontory, with lengths that exceed 4 km and apertures up to 13 m in width. Set 3, NNW-SSE-trending clusters

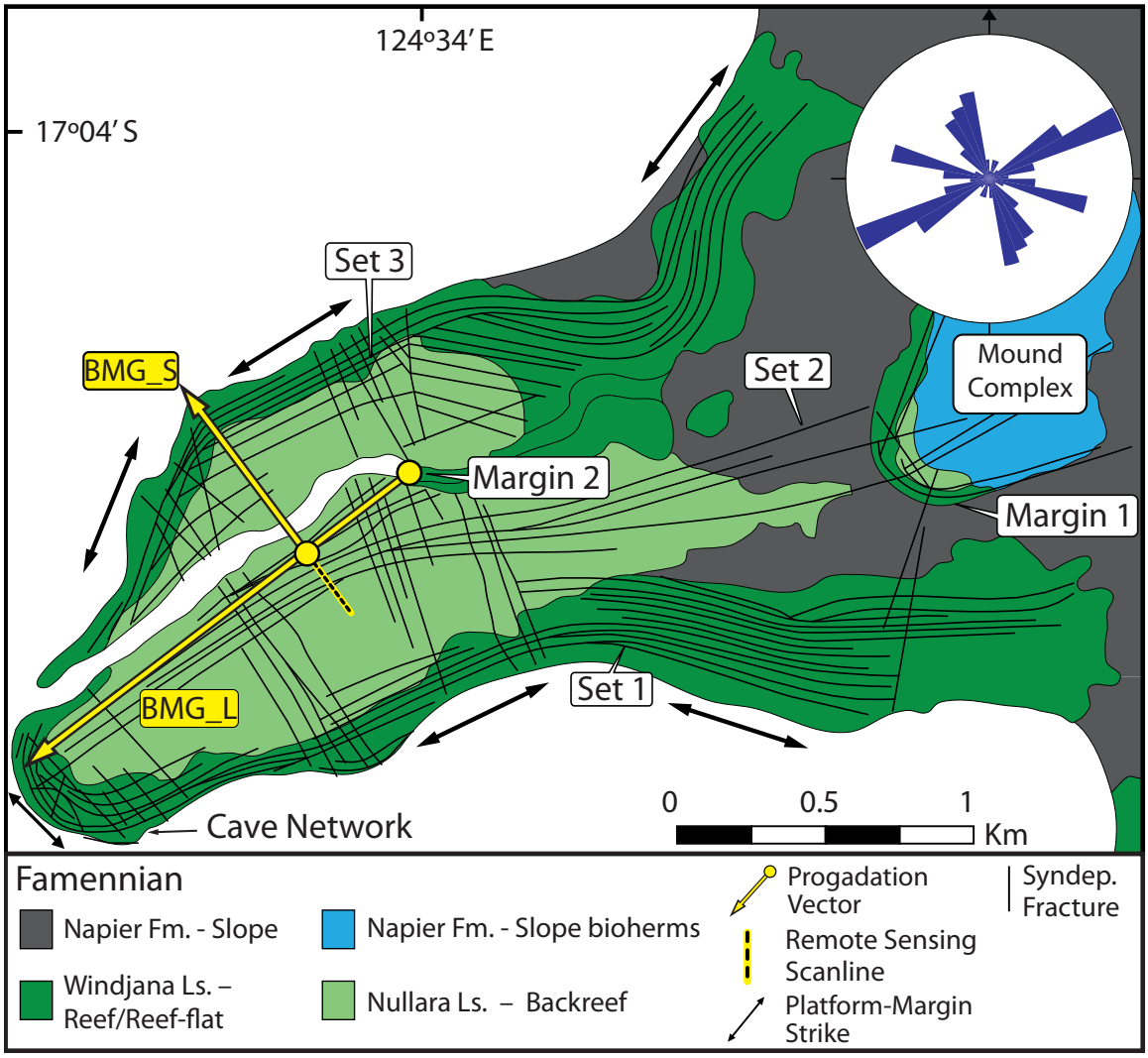

Figure 3.9: Simplified fracture patterns of Billy Munro Gorge.

Geology modified from Playford and Hocking (1999). Three discrete syndepositional fracture sets are recognized: (1) margin parallel fractures, (2) WSW-ENE-trending fractures that run parallel to the long axis of the platform, and (3) NNW-SSE-trending fractures that run perpendicular to the long axis of the promontory. Scanlines follow platform-margin vector unless otherwise noted.

of fractures that run perpendicular to the long axis of the promontory, formed from differential compaction over an older Famennian margin (Type II control), in a fashion similar to that of the compactional hinge of Hunt and Fitchen (1999). The apertures of sets 2 and 3 fractures are filled with platform-derived sediments (grainstone and sandstone), with a minor component of marine cement.

Discrete highs in fracture intensity occur along the fracture swarms associated with sets 2 and 3 (Figure 3.9). Most of the fractures in the Billy Munro Gorge area appear to be dominantly opening mode. Rare syndepositional faults with minor normal offset (<1 m) are observed, with subtle growth features similar to those described by Kosa and Hunt (2005). Syndepositional faults are associated with set 3 fractures and occur basinward of margin 2 (Figure 3.9).

Windjana Gorge

The outcrops of Windjana Gorge preserve a series of retrograding to prograding late Frasnian to Famennian platforms (Playford, 2002; Figure 3.10). The Frasnian succession is characterized by retrograding microbial-stromatoporoid-built platforms that culminate in a major platform-margin collapse event, followed by progradation in the latest Frasnian and throughout the Famennian (Figure 3.2). Frasnian syndepositional fractures are best developed in the early-lithified strata of the reefal-slope, reef, and reef-flat and generally run margin parallel. Owing to margin reconfiguration associated with gravitational collapse, fractures appear to intersect the margin at high angle along collapse scars (Figures 3.10-11). Fractures are well developed in the platform margin and decrease in frequency into the backreef of the backstepping and aggrading Frasnian platforms (e.g., W_Fr-6 and W_Fr-7; Table 3.1). Given the weak fracture development in the Frasnian backreef and the absence of any known syndepositional fault systems, it is inferred

that Frasnian syndepositional fractures in Windjana Gorge formed in response to gravitational instability associated with oversteepening of the platform margin (Type I controls).

The Famennian succession of Windjana Gorge is characterized by a series of prograding microbially constructed platforms. Although erosion associated with Permian glaciation has planed off the backreef section of the Famennian reef complexes, the reef and upper marginal slope remain extremely well preserved (Figures 3.12-13). Syndepositional fracturing is extensive in these facies (e.g., W_Fa-1 and 9559, Table 3.1), with fractures oriented parallel and perpendicular to the platform margin, dipping either steeply toward the platform interior or with subvertical traces. Large-scale syndepositional fractures extend for several kilometers across the top of the range and often crosscut the entire exposed Famennian section (80-90 m; Figures 3.12-13). In some instances, these features appear to terminate into fore-reef bedding planes (Figure 3.13), leading Playford (1984) and Hurley (1986) to propose bedding-plane slippage as a driver for syndepositional fracturing, which is likely manifested as the rare low-angle faults (bedding subparallel) observed in upper-slope strata.

FACIES CONTROL ON FRACTURE PATTERNS

Fracture Patterns in Frasnian Facies

In the retrograding and aggrading Frasnian platforms of Windjana Gorge, fractures are observed in backreef to fore-reef slope strata (Table 3.2;Figure 3.11). The greatest amount of syndepositional extension occurs in the microbial-stromatoporoid boundstones of the reef flat and in the lithoclast breccias of the fore-reef slope (Table 3.2). Syndepositional fracturing in the reef flat is enhanced by elevated early lithification and microbial activity associated with proximity to the

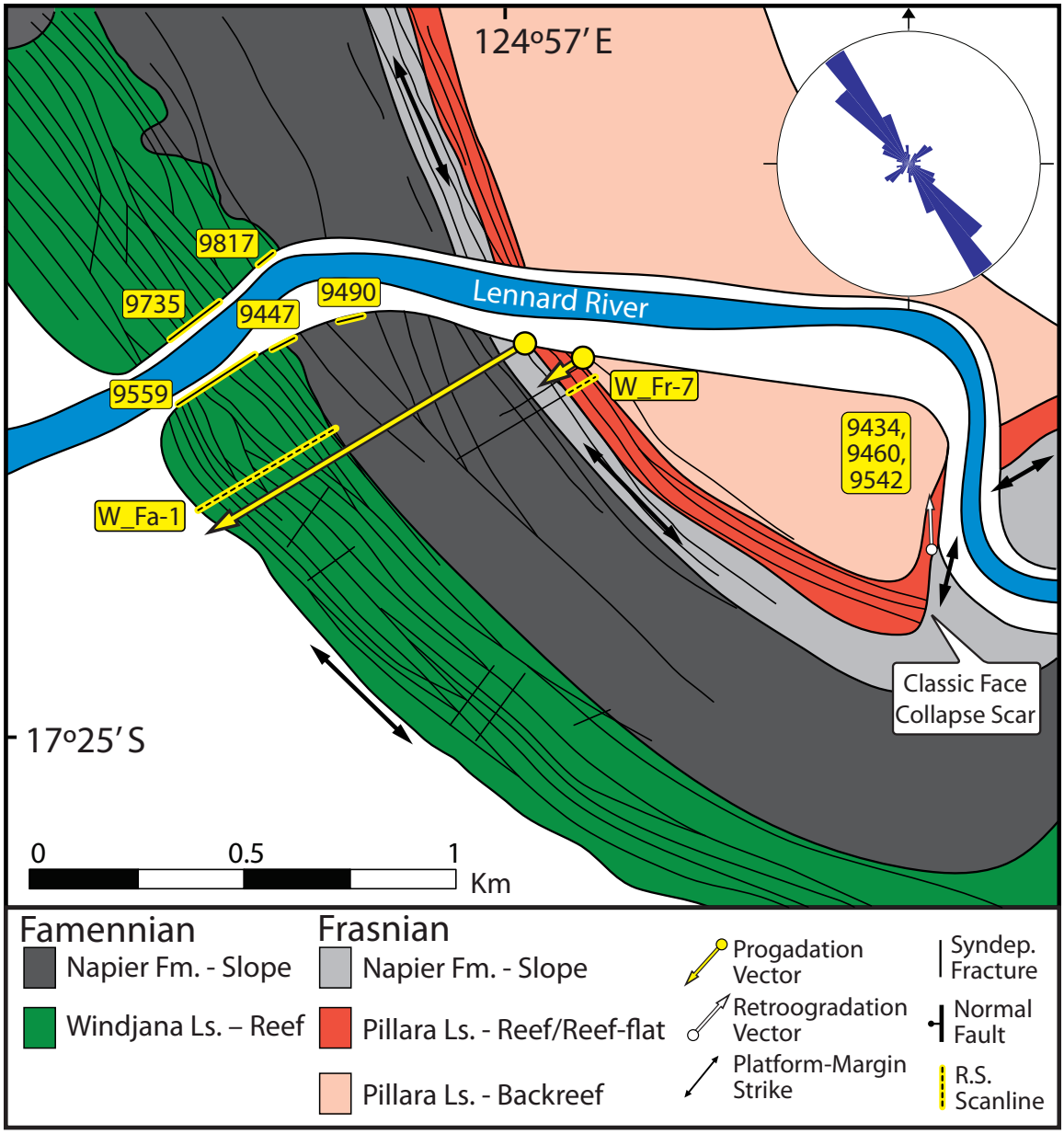

Figure 3.10: Simplified fracture patterns and scanline locations, Windjana Gorge.

Geology modified from Playford and Hocking (1999). Syndepositional fractures run parallel to the platform margin and in some instances intersect a major collapse scar at high angles.

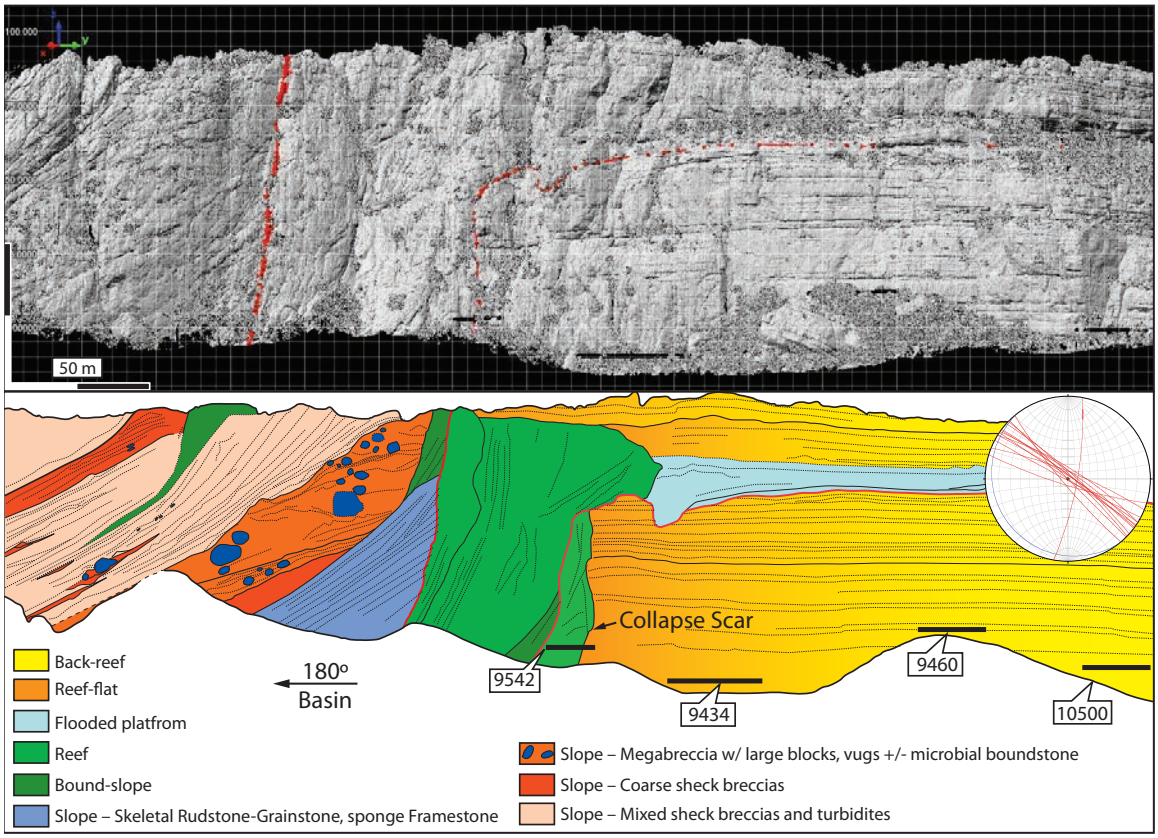

Figure 3.11: Frasnian stratal architecture and scanline locations.

(A) Ground-based lidar DEM of Frasnian for-reef to backreef strata, Classic Face, Windjana Gorge. (B) Facies architecture, scanline locations, and fracture orientation data from the Classic Face. See Figure 3.10 for location.

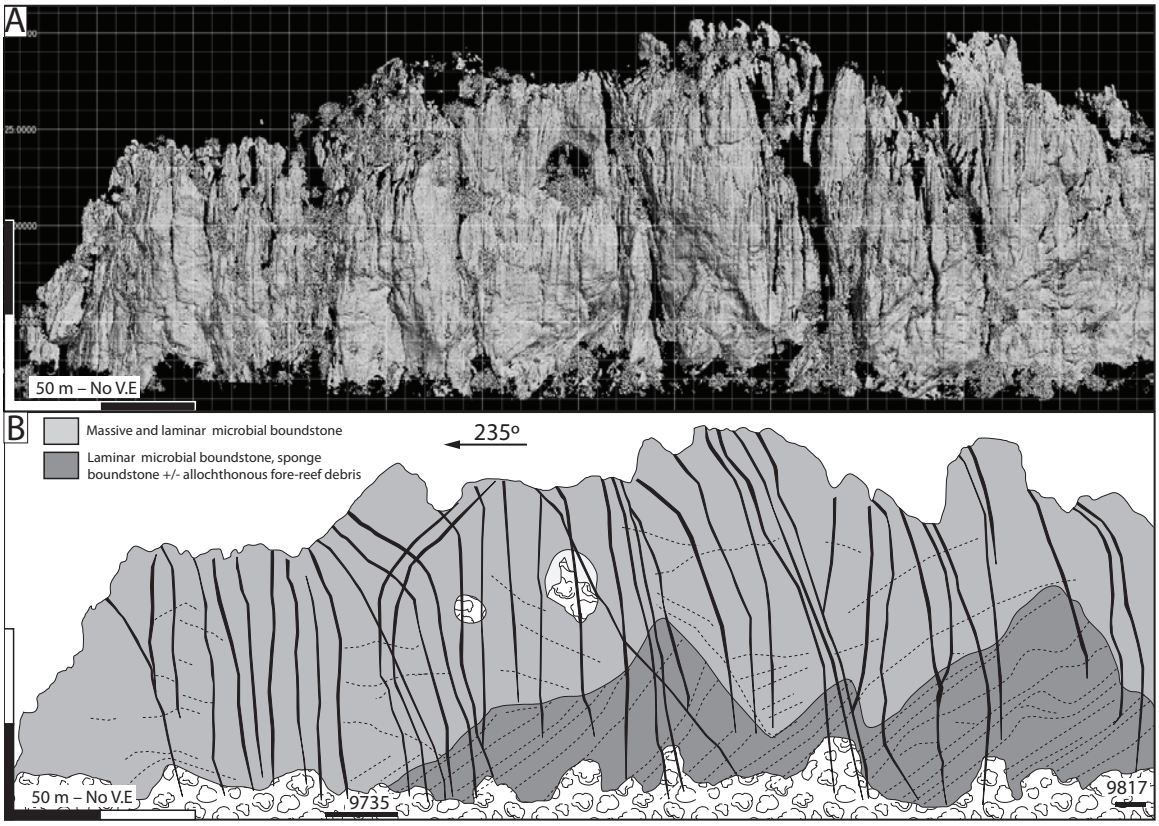

Figure 3.12: Outcrop-scale Famennian fracture patterns.

(A) Ground-based lidar DEM of Famennian reef and upper slope facies, north wall at the western entrance to Windjana Gorge. (B) Syndepositional fracture patterns and scanline locations in prograding Famennian microbial reef facies (grid spacing is 10 m). Many fractures extend upward more than 90 m. See figures 2.5C and 2.5F for examples of fracture fills. See Figure 3.10 for location.

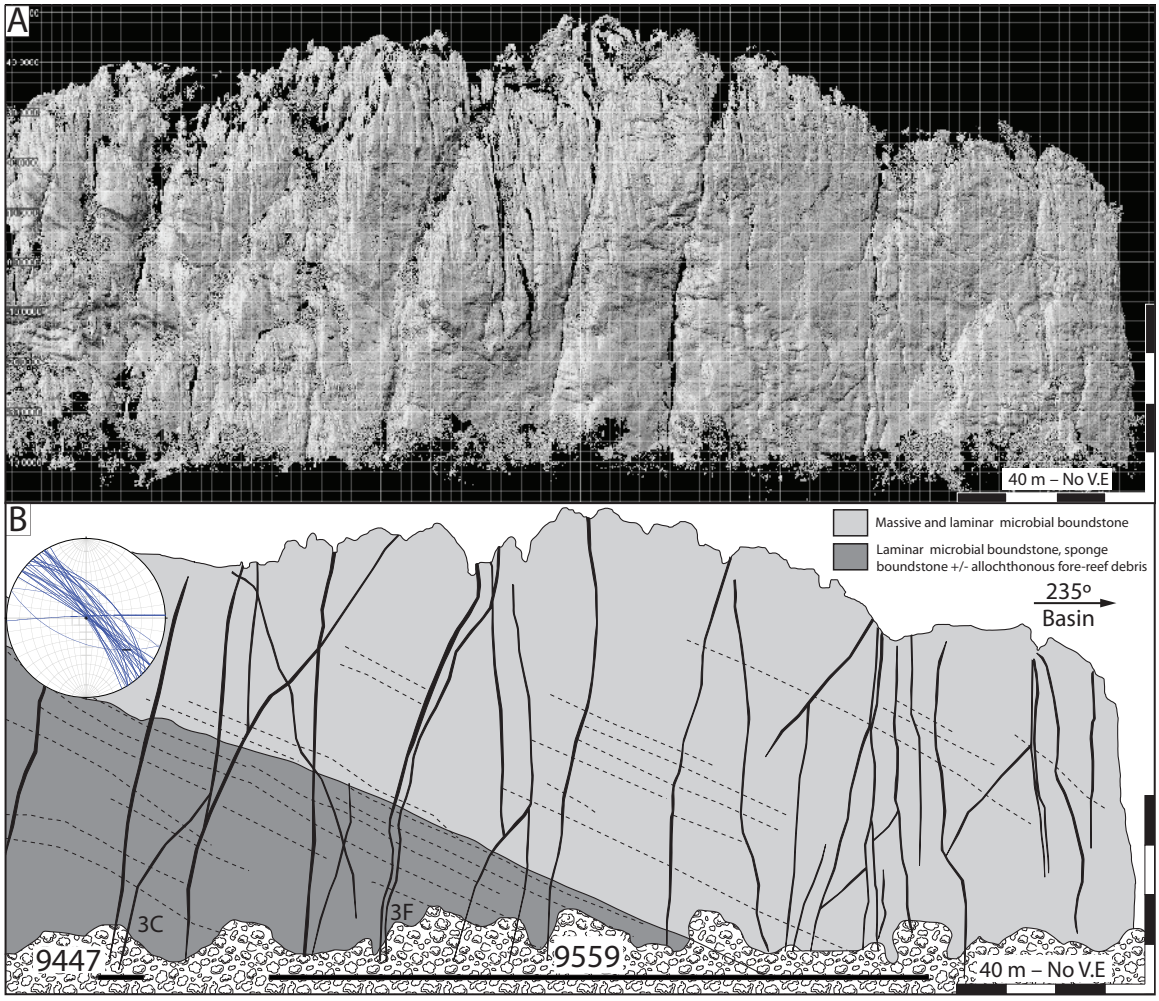

Figure 3.13: Outcrop-scale Famennian fracture patterns.

(A) Ground-based lidar DEM of Famennian reef and upper slope facies, south wall at the western entrance to Windjana Gorge. (B) Syndepositional fracture patterns and scanline locations in prograding Famennian microbial reef facies. Some fractures crosscut the boundary between the upper-slope and the reef facies, while other abruptly terminate into upper slope bedding planes. See Figure 3.10 for location

platform margin (Figure 3.14a). Extensional stress from gravitational instability associated with upward growth of the platform-margin escarpment is manifested in the reef flat as large aperture fractures (high $FI_{0.5}$, low FI; Table 3.2) with a limited number of small aperture fractures.

Syndepositional extension and $FI_{0.5}$ decrease away from the reef flat into the backreef (e.g., scanlines 9460 and 10500; Table 3.2), presumably as a function of decreasing early lithification away from the platform margin (Figure 3.14b). In the backreef, syndepositional fractures crosscut numerous bedding boundaries, and paired scanlines from an early-lithified stromatoporoid biostrome bed and a neighboring terrigenous–peloidal packstone bed (e.g., scanlines 10500a/b; Figure 3.15; Table 3.2) show that early fractures are well developed in both facies. Secondary fractures, however, are strongly affected by lithology with nearly a threefold increase in FI and extension in the biostrome facies compared with that of the packstones (Figure 3.15).

The upper-slope sponge-stromatoporoid boundstone (Figure 3.14C), which mantles a collapse scar in the classic face (Figure 3.11), is dominated exclusively by closely spaced, small syndepositional fractures ($b < 1$ cm). The scarcity of large aperture fractures in this facies may be related to (1) limited early lithification compared with that of surrounding facies, evidenced by minor amounts of marine cement and microbial components; (2) early mechanical properties of the mixed terrigenous-peloidal packstone matrix; or (3) a reduction in stress following platform-margin collapse.

Fore-reef breccias are heavily syndepositionally fractured in the Frasnian (Figure 3.14d; Table 3.2); however, fractures in this setting are not as vertically extensive as observed in other facies. Instead, syndepositional fractures are often restricted to individual debris flow beds, terminating into bedding parallel fractures

			Syndepositional Fractures					*Secondary Fractures*		
Scanline #	Facies	Facies Tract	Extension	FI	*FIn*	S	*Sn*	Extension	FI	S
Famennian				(fracs/m)		(m)			(fracs/m)	(m)
9559	Massive Microbial Bst.	Reef	9.8%	16.5	0.087	0.06	11.5	1.0%	14.9	0.07
9447	Laminar Microbial Bst.	Reef/Upper slope	9.1%	11.2	0.066	0.09	15.1	1.0%	14.6	0.07
9735	Laminar Microbial Bst.	Reef/Upper slope	7.8%	8.2	0.059	0.12	16.9	1.4%	21.3	0.05
9490	Sponge-Microbial Bst.	Upper slope	7.0%	12.1	0.055	0.08	18.2	0.8%	4.3	0.23
9817	Sponge-Microbial Bst.	Upper slope	5.1%	10.5	0.032	0.10	31.3	0.7%	5.5	0.18
			7.8%	11.7	0.060	0.09	18.60	0.98%	12.1	0.12
Frasnian										
9434	Stromatoporoid Frm	Reef/Reef-flat	4.0%	6.8	0.061	0.15	16.4	0.1%	3.4	0.30
9539	Breccia	Fore-reef	3.9%	11.1	nd	0.03	nd	nd	nd	nd
9460	Stromatoporoid Flt.	Backreef	2.9%	9.1	0.029	0.11	34.5	0.3%	6.1	0.16
9542	Stromatoporoid/Sponge Bst.	Reef/Upper slope	2.8%	12.6	0.030	0.08	33.3	0.7%	15.4	0.07
10500a	Stromatoporoid Flt.	Backreef	1.5%	1.8	0.03	0.56	33.4	0.7%	11.2	0.09
10500b	Terrigeneous Pelliodal Ps.	Backreef	1.4%	1.8	0.03	0.57	34.1	0.2%	2.96	0.34
			2.7%	7.2	0.038	0.25	29.4	0.39%	7.8	0.19

Table 3.2: Fracture attributes by facies.

Normalized fracture intensity (FIn) and normalized spacing (Sn) were calculated for kinematic apertures of 0.5 m or larger using the methodology of Ortega et al. (2006).

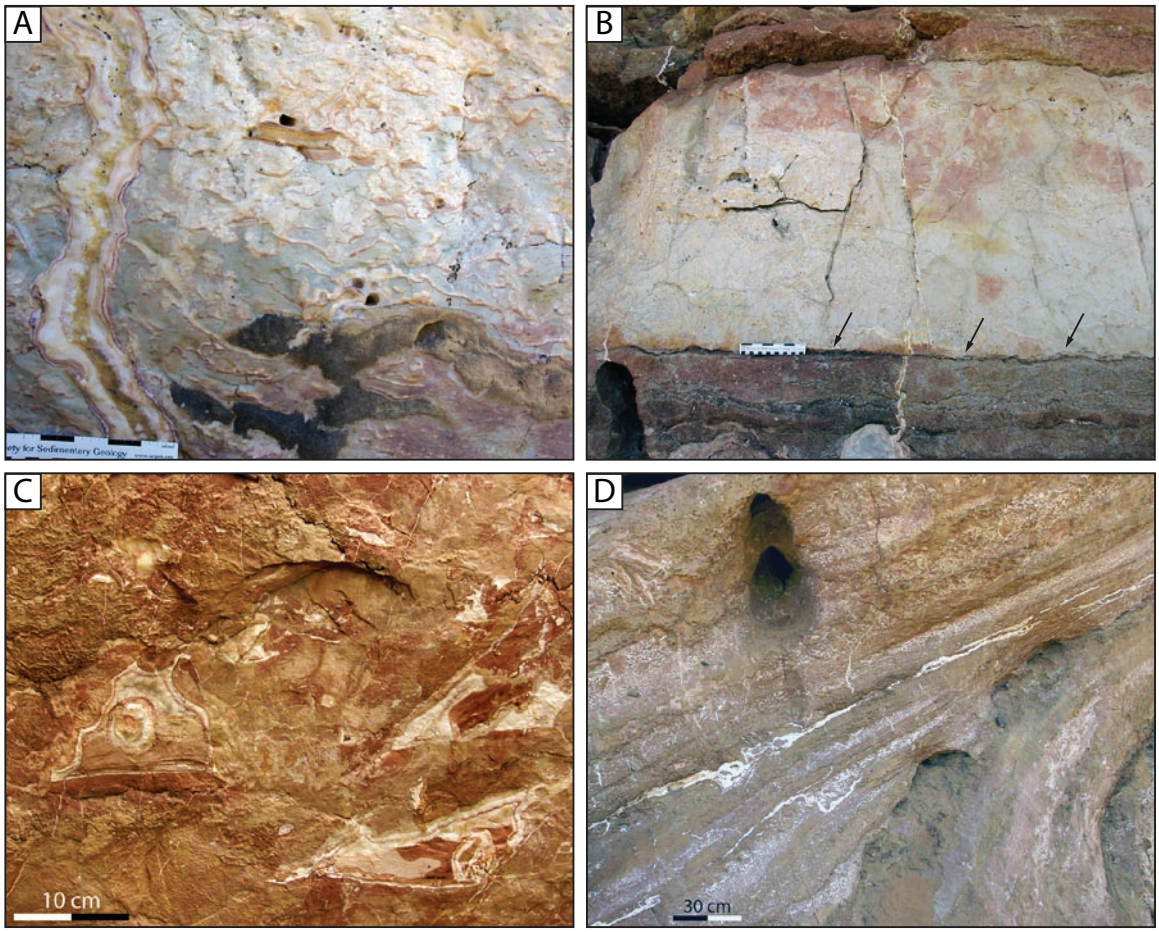

Figure 3.14: Frasnian facies.

(A) Reef flat, scanline 9434, Classic Face. Marine-cement- and dolomite-lined syndepositional fracture, microbial stromatoporoid boundstone. (B) Backreef strata, with alternating stromatoporoid biostromes (lt. gray) and stromatolitic sandstone beds (dark beds); scanline 10500, Classic Face. (C) Bound upper slope; scanline 9542, Classic Face. Small syndepositional fractures (< 5 mm) in sponge boundstone. (D) Fore-reef slope; scanline 9539, north wall of the east entrance to Windjana Gorge. Syndepositional fractures in steeply dipping fore-reef breccia. Fractures often terminate in bedding-parallel fractures referred to as “neptunian sills” (Playford, 1984).

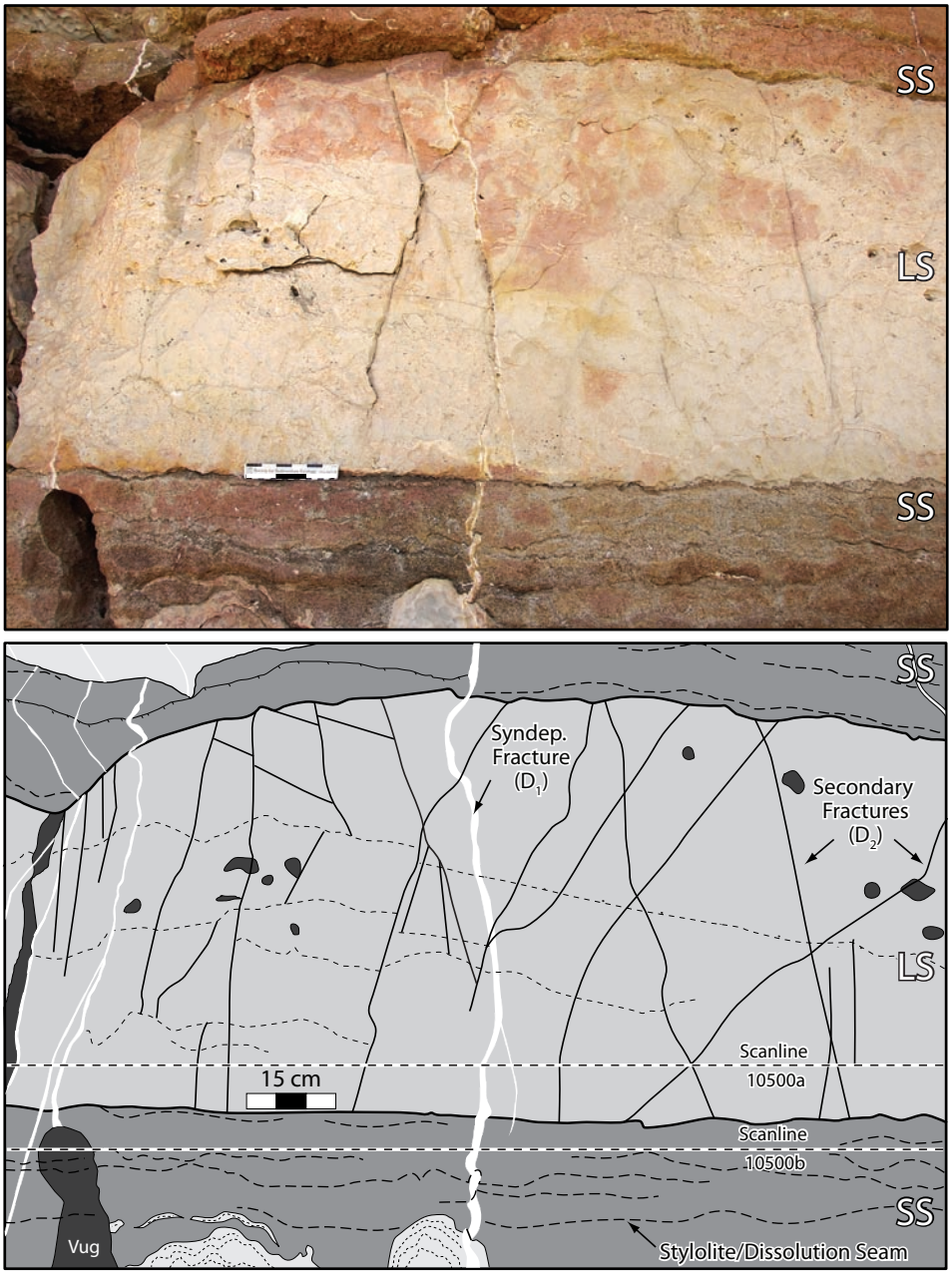

Figure 3.15: Fracture patterns in stromatoporoid, microbial boundstone, Frasnian, Windjana Gorge.

Small syndepositional (5–20 mm) fractures in stromatoporoid biostrome (lt. gray) and stromatolitic sandstone (dark beds). Syndepositional fractures crosscut all layers and are ptygmaticly folded in sandstone beds, suggesting early compaction. Secondary fractures are well developed in biostrome facies (S=0.09m) and to a lesser degree in the sandstone beds (S=0.34m, scanline 10500b), and the majority of these fractures terminate at bedding boundaries.

referred to by Playford (1984) as neptunian sills (Figure 3.14d). These fractures most likely represent bedding-plane slip associated with downslope creep of sediments deposited above the angle of repose and are thought to strongly influence fracturing in this early-lithified facies.

Fracture Patterns in Famennian Facies

Exposures of the prograding Famennian platforms preserved at the west entrance to Windjana Gorge are dominated by microbial reef boundstones (Figures 3.12-13). Three depositional facies with distinct fracture patterns are differentiated within these exposures (Table 3.2: Figure 3.16): (1) Massive microbial boundstone, containing calcimicrobes, sponges, and platform-derived sediment. This facies is the most fractured of all the Famennian facies, and syndepositional extension is accommodated in a series of large-aperture (<70-cm) fractures (Table 3.2). (2) Laminar, microbial boundstone, which consists of microbial lenses and variable amounts of platform-derived sediment (Figure 3.16-17). Syndepositional fractures occur preferentially in the microbial lenses, and large-scale (<50-cm) syndepositional fractures are well developed. Small-scale faults are also present in this facies, running subparallel to bedding with minor offset (Figure 3.16b). (3) Sponge microbial boundstone. This facies is composed of alternating steeply dipping (30°-35°) beds of sponge boundstone and detrital platform-derived sediments. This facies marks the lower contact of the "reef" facies and has a strong fore-reef slope affinity. Syndepositional fractures are well developed in this facies, with dominantly 1- to 15-cm-wide marine-cement-lined fractures, and fractures filled with platform-top sediment are rare. One important feature of this facies is an abundance of what appear to be bedding-parallel slip planes linking syndepositional fractures (Figure 3.16d). Many syndepositional fractures in the Famennian are vertically extensive,

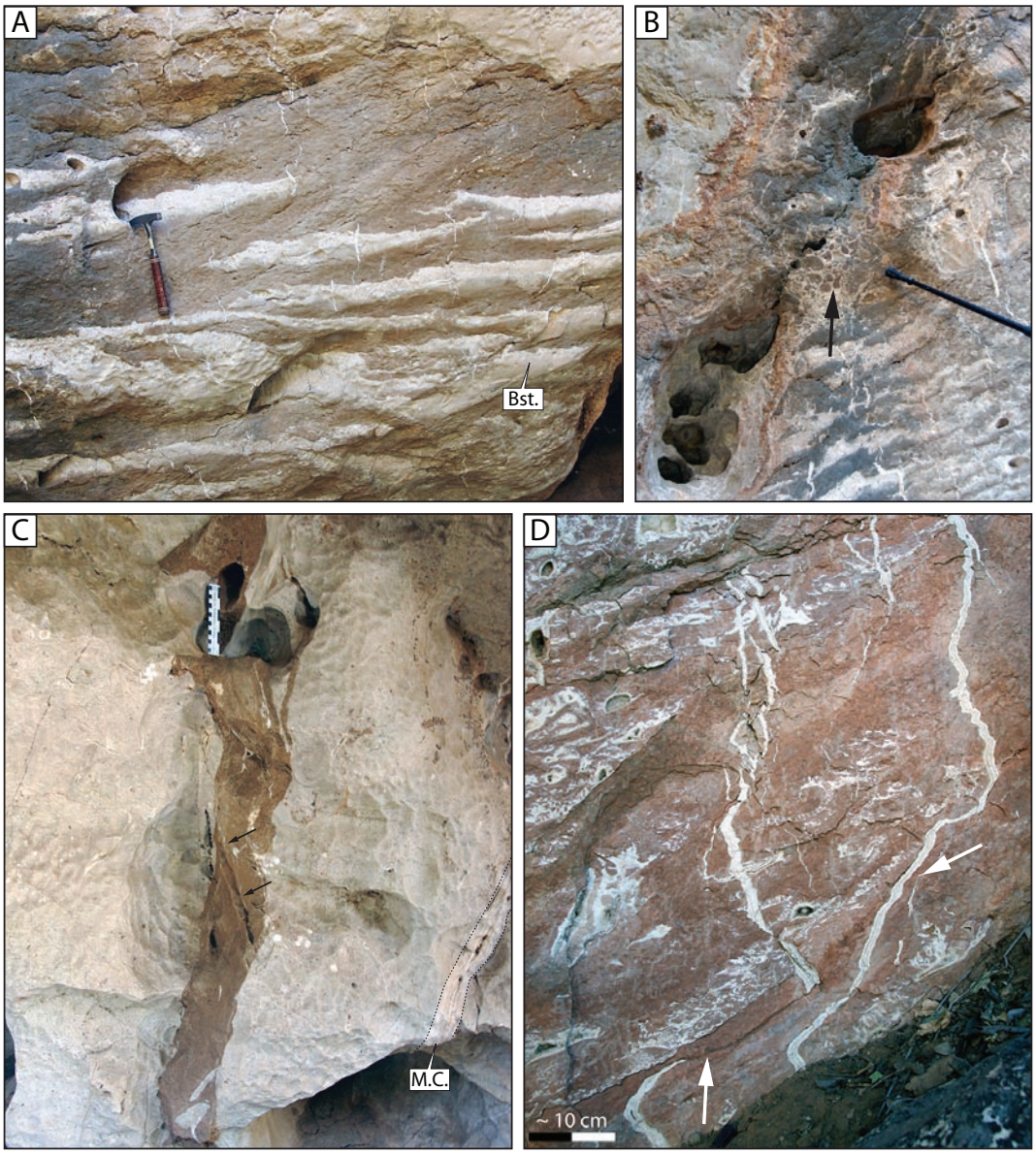

Figure 3.16: Famennian facies at the west entrance of Windjana Gorge.

(A) Laminar microbial boundstone, deep reef–bound slope, scanline 9735. (B) Small-scale basinward-dipping fault with spar balls developed along fault plane (arrow), in laminar microbial boundstone, north wall. (C) Sand and marine cement-filled fractures developed in massive microbial reef boundstone, scanline 9559. Marine cement-lined fractures (arrows) crosscut sand-filled fracture. (D) Syndepositional fractures in steeply dipping (30°–35°) sponge boundstone, upper bound slope, scanline 9817. Apparent downdip slippage along bedding planes (arrows).

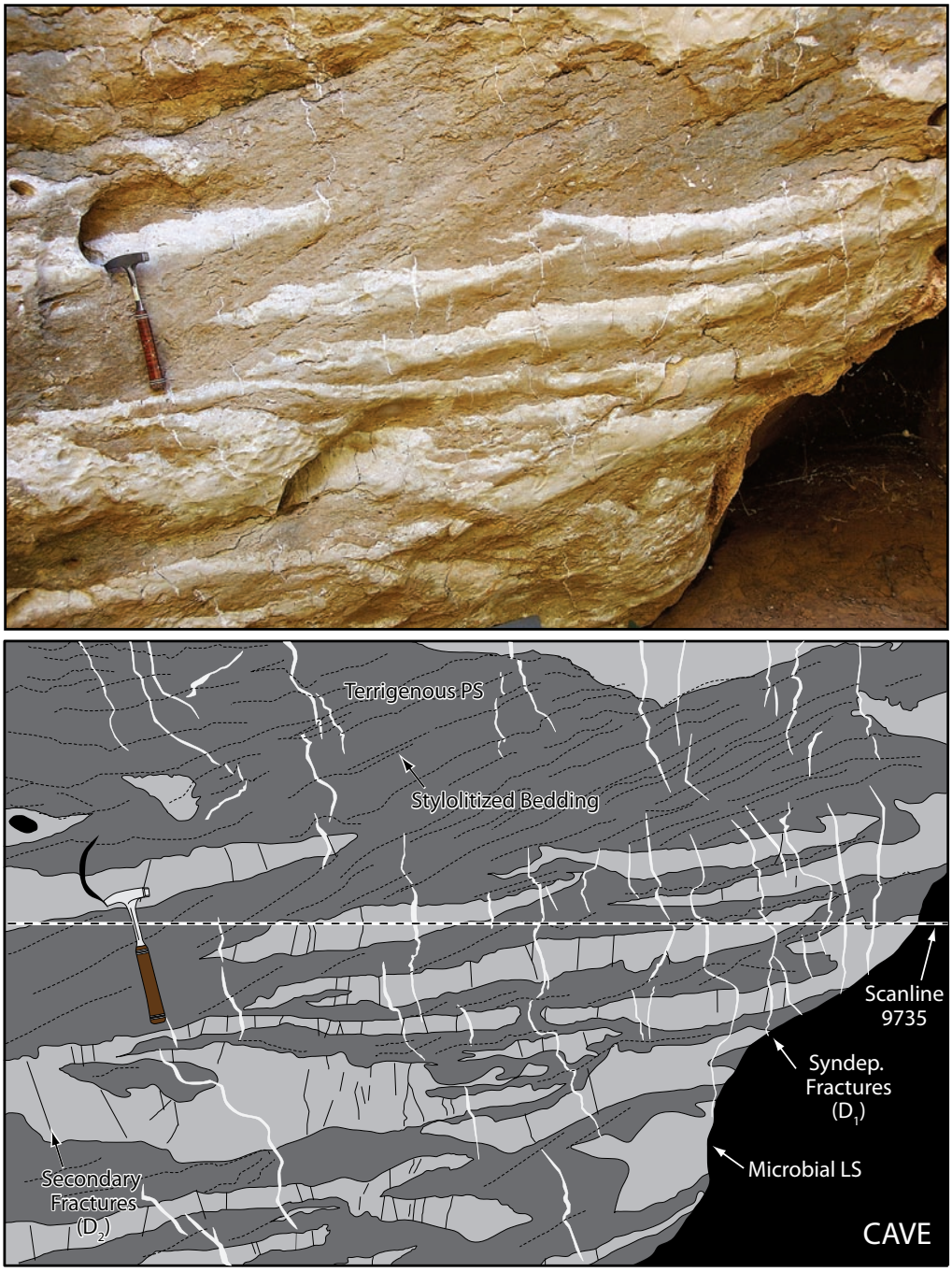

Figure 3.17: Fracture patterns in laminar microbial boundstone, Windjana Gorge.

Syndepositional fractures are best developed in the microbial boundstone shelves and to lesser degree in mixed detrital matrix sediment, while secondary fractures are largely restricted to the microbial lenses. Early fractures are folded and crosscut by dissolution seams and stylolites in the detrital matrix.

with even modest aperture fractures (b >2.5 cm) extending for several tens of meters, crosscutting numerous bedding contacts.

SPATIAL ARRANGEMENT OF FRACTURES

Characterizing the spatial arrangement of syndepositional fractures poses a significant problem in geology. Clusters of early fractures can create zones of enhanced permeability, leading to an altered diagenetic profile compared with that of surrounding areas lacking fracture clusters. Fracture swarms may act as zones of weakness susceptible to reactivation with later tectonic activity, and local zones of high fracture intensity are prone to enhanced dolomitization and karstification. Visual inspection indicates that fractures in the Devonian reef complexes are often clustered, and this observation is verified by simple tests for fracture clustering such as the Kolmogorov-Smirnov test (Figure 3.18). Improved characterization of the degree and dimensions of fracture clusters was obtained using Normalized Correlation Count (NCC; Marrett et al., in press; Gomez, 2007).

NCC is capable of distinguishing between five possible types of fracture clustering: harmonically arranged clusters, self-organized (fractal) clusters, inherited/imposed (plateau) clusters, random clusters, or a combination of the previous four arrangements (Figure 3.19a; Gomez, 2007; Marrett et al., in press). NCC compares the degree of clustering to an expected value of a random arrangement (approximately 1) and can detect repetitive patterns as well as anti-clustering. Spatial correlation at a given length scale (fracture separation or lag) reflects the degree of clustering and is plotted against the 95% confidence interval of 100 random iterations (Marrett et al., in press). For example, in the Frasnian reef flat, spatial correlation is approximately four for length scales of 50 to 60 mm (Figure 3.19b), meaning that fractures are four times more abundant than would be expected with

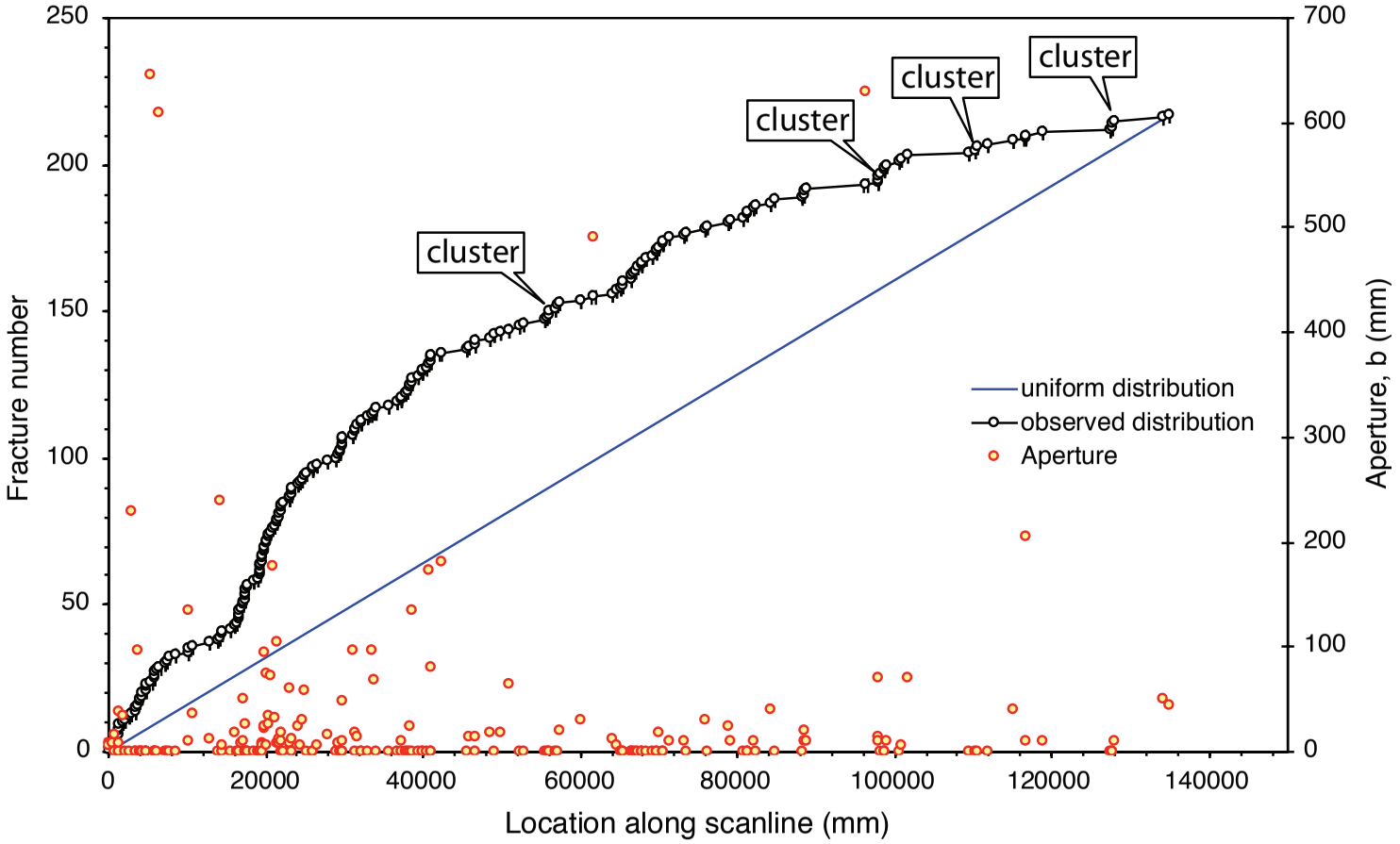

Figure 3.18: Evidence of fracture clustering.

Kolmogorov-Smirnov test of Scanline 9559, Famennian reef, Windjana Gorge. Cumulative fracture number is plotted against location along scanline. Where curve is steeper than the uniform distribution trend line, fractures are clustered. Note that two of the largest aperture fractures occur in close proximity to one another.

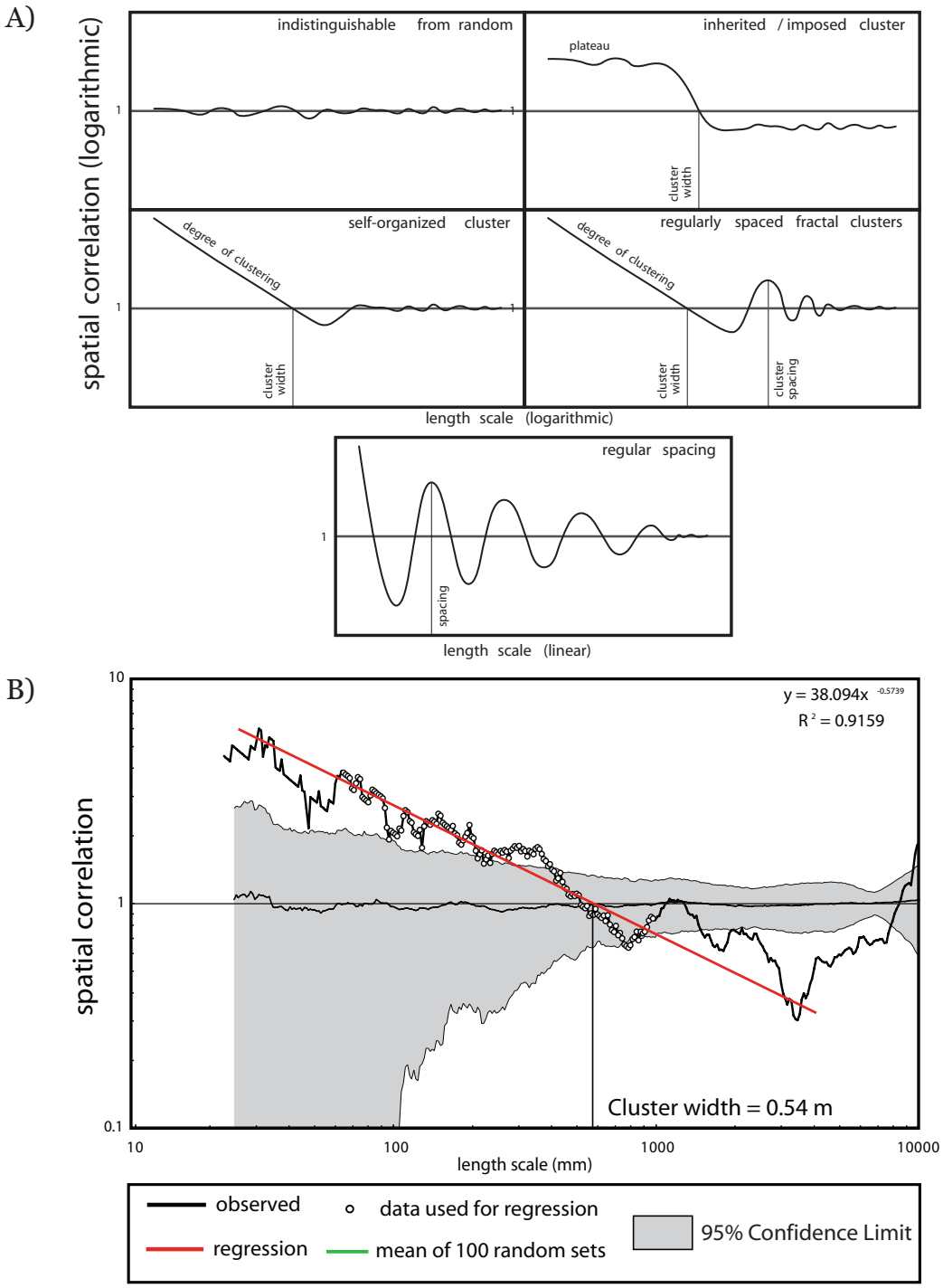

Figure 3.19: Spatial arrangement of fractures in Windjana Gorge.

(A) Proposed types of spatial arrangement, modified from Marrett et al. (in review). (B) Self-organized fracture clustering, scanline 9434, Frasnian reef flat. Cluster width is approximately 54 cm.

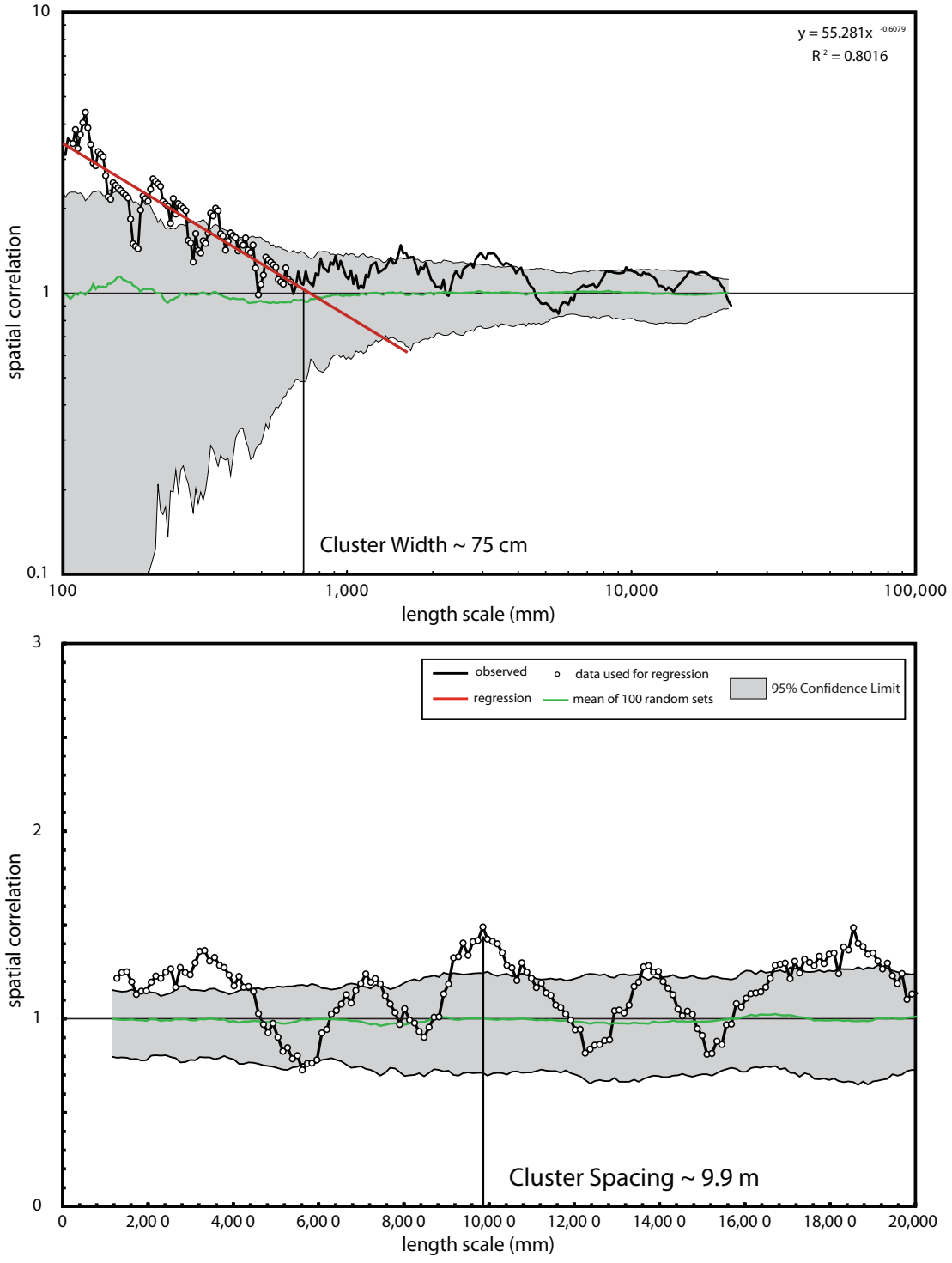

Figure 3.20: Spatial arrangement of fractures in scanline 9559, Windjana Gorge.

Self-organized harmonic fracture clustering, massive microbial boundstone, Famennian reef. Cluster width approximately 75 cm with a spacing of 9.9 m

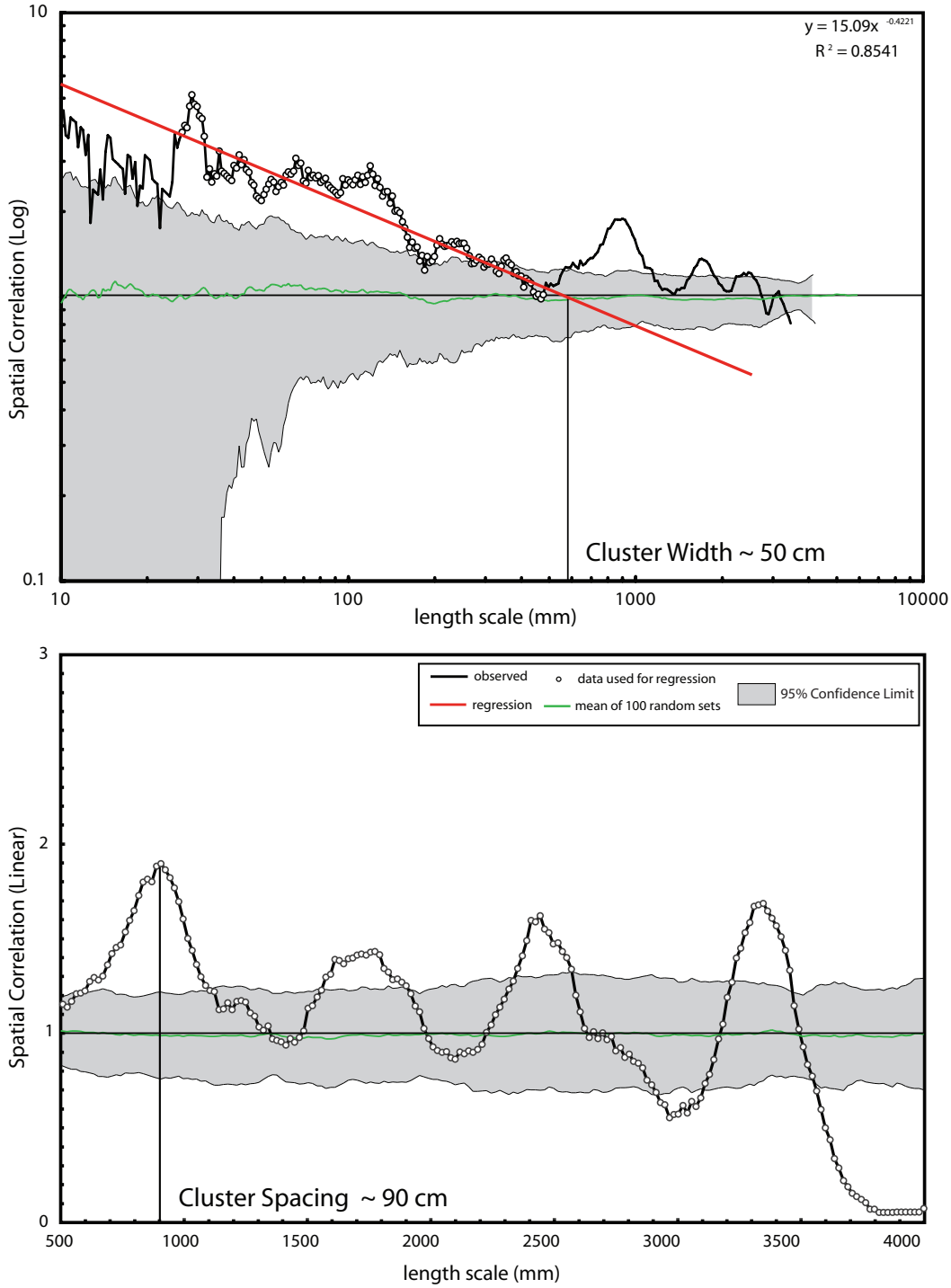

Figure 3.21: Spatial arrangement of fractures in scanline 9447, Windjana Gorge.

Self-organized/inherited harmonic fracture clustering in laminar microbial boundstone, Famennian reef. Cluster width approximately 50 cm with a spacing of 90 cm.

a random arrangement.

In the Famennian microbial reef facies, clustering of fractures is apparent (Figure 3.18), with two of the largest aperture fractures (>60 cm) occurring less than 30 cm apart. Fracture clustering in this facies is verified by NCC, with self-organized clusters approximately 75 cm wide and spaced roughly 10 m apart (Figure 3.20); however there is no obvious control (faults) on the genesis or distribution of fracture clusters in this setting.

In some instances, fracture clusters occur as a function of variable diagenetic and mechanical conditions. For example, in the laminar microbial boundstones of the Famennian reef, fractures are clearly best developed in the early-lithified and brittle microbial lenses (Figure 3.17) and less so in the surrounding detrital packstones leading to the harmonic lateral clusters observed in scanline 9735. NCC analysis shows inherited or imposed clustering, with over length scales of roughly 10 to 50 cm and with a cluster spacing of roughly 90 cm (Figure 3.21). In areas where there is clear evidence of syndepositional faulting such as Geikie Gorge, Tunnel Creek (Ward, 1996), and the Pillara Mine (Miller et al., 2007), syn-depositional fractures cluster around fault planes.

RESULTS AND DISCUSSION

Scales of Mechanical Stratigraphy and Mechanical Unit Evolution

Fracture patterns in carbonates are strongly influenced by the rigidity, thickness, and layering of mechanical units (Ladeira and Price, 1981; Corbett et al., 1987; Narr and Suppe, 1991; Bai and Pollard, 2000; Underwood et al., 2003). A mechanical layer is commonly defined as a package of rock with the same general mechanical properties (i.e., rigidity), with fractures generally terminating at the unit's upper and lower interface. Mechanical layers in many cases do not correlate

directly with stratigraphic horizons and may crosscut bedding planes and lithologic boundaries. The mechanical stratigraphy of a succession of rocks is characterized by (1) the thickness and rigidity of individual mechanical units, (2) the stacking of mechanical layers, and (3) the nature of the interface between mechanical layers (Shackleton et al., 2005). Previous studies have typically addressed thin mechanical layers (5 m or less) in rocks that have been subjected to burial and associated diagenesis (Narr and Suppe, 1991; Underwood et al., 2003).

Syndepositional fractures in the Canning Basin typically crosscut small-scale "apparent" mechanical units such as individual beds and cycle boundaries (0.25-5.0 m scale units; Figures 3.15 and 2.17). In contrast, postdepositional fracture patterns are strongly influenced by these small-scale mechanical layers (Figures 3.15 and 2.17). This observation raises the following questions: (1) At what scale do mechanical layers occur in early fracture systems prior to burial diagenesis? (2) What types of mechanical interfaces are required to terminate large-scale syndepositional fractures? And (3) do the properties of these mechanical layers evolve with continued diagenesis?

The data presented by this study indicate that syndepositional fracture patterns are strongly influenced by depositional facies. However, the small-scale lithologic heterogeneity associated with bedding and high-frequency cycle boundaries (0.25-5.0 m scale units; Figures 3.15 and 2.17) do not provide sufficient mechanical contrast to terminate syndepositional fractures. Instead, syndepositional mechanical unit differentiation depends on early-lithification patterns within a carbonate platform, with extensive syndepositional fracturing restricted to early-cemented zones. During syndepositional fracture development, the mechanical contrast between individual beds was low, with early-lithified strata effectively behaving as one mechanical unit, regardless of bedding or lithology (Figure 3.22a). Moreover,

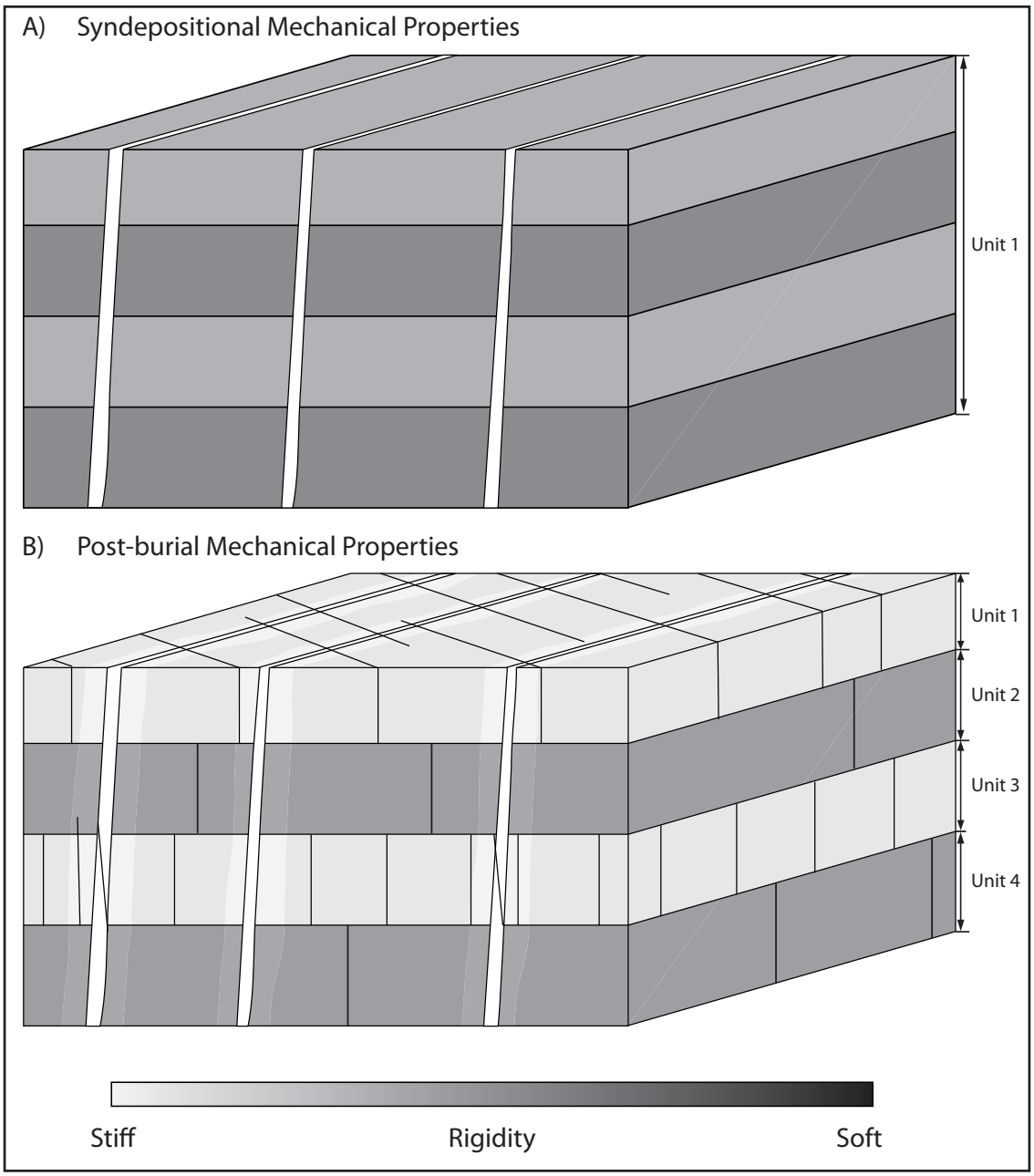

Figure 3.22: Fracture patterns related to mechanical property evolution.

A) During syndepositional fracture development, all layers are rigid enough for fractures to propagate; however, rigidity contrasts at bedding boundaries are insufficient to terminate fractures. Fractures crosscut all layers, with all beds effectively behaving as one mechanical unit. B) Following burial diagenesis, the mechanical contrast between individual beds increases, effectively creating four mechanical units with secondary fractures confined within each of these layers.

fractures are effectively terminated only by large-scale rigidity contrast associated with the transition between early-lithified facies and unlithified facies (e.g., reef to slope). The relationship suggests that mechanical unit differentiation in early fracture systems (prior to burial diagenesis) occurs at roughly the stratigraphic sequence scale (50-200 m0 with the transition between early-lithified unlithified strata defining mechanical unit boundaries.

Secondary fractures in the Devonian reef complexes are far more sensitive to small-scale mechanical heterogeneity, with postburial mechanical layers typically occurring at the bed scale (Figures 3.15-16). Progressive diagenesis associated with burial introduces increased mechanical heterogeneity, and various lithologies begin to develop into unique mechanical layers. Strata that initially behaved as one mechanical unit prior to burial become increasingly partitioned, and multiple mechanical layers develop, strongly affecting secondary fracture patterns (Figure 3.22b) and suggesting that mechanical conditions in the Devonian reef complexes have evolved over time.

Recent studies have shown that mechanical stratigraphy is not static; instead, mechanical properties are dynamic and fluid flow along fracture networks and progressive diagenesis can have a pronounced effect on the temporal evolution of mechanical properties and subsequent fracture patterns (Marrett and Laubach, 2001; Shackleton et al., 2005; Laubach and Ward, 2006). Previous workers in the Canning Basin (Hurley, 1986; Kerans et al., 1986) have proposed that the early-fracture permeability system is responsible for enhancing early-marine cementation. The relationship between early fracture permeability and early lithification effectively creates a feedback loop in which fracturing leads to enhanced early lithification throughout the platform, which in turn promotes increased fracturing. Diagenetic events following early-fracture development introduce mechanical

heterogeneity, and the mechanical stratigraphy for any subsequent period of fracture development will depend largely on the diagenetic history of the system.

Variations in Fracture Pattern as a Function of Stratigraphic Architecture

Ground-based scanline data reveal that syndepositional fracture attributes vary with depositional facies, as well as platform-margin trajectory. In the prograding Famennian facies sampled by this study, average values of extension are approximately 2.9 times higher relative to the Frasnian, fracture intensity is roughly 1.6 times higher, and the spacing of large fractures decreases by a factor of 1.6 (Table 3.2). A similar relationship is described by Hurley (1986) in the Oscar Range, where he demonstrated an approximate twofold increase in extension in the Famennian backreef of the Northern Oscar range compared with the Frasnian of the Southern Oscar Range (6.7% and 3.3%, respectively).

When data from all localities are considered, a statistically significant linear relationship between fracture intensity (FI) and P/A ratio is observed in both the platform margin and platform interior (Frost and Kerans, in review; Figure 3.23). In this relationship, FI increases linearly with P/A ratio, with the highest FI values observed in the platform margins of the most progradational platforms (high P/A) more than double those of the most retrogradational platforms (negative P/A; Table 3.1). All platform-margin data points plot within the same 95% confidence interval (Figure 3.23), regardless of control type and proximity to regional syndepositional structural elements (e.g., Scanline NO-SM).

In the platform interior, the relationship between FI and P/A ratio is observed only for gravitational and antecedent-topography-controlled (Type I and II) systems (Figure 18). Fracture populations controlled by active tectonic deformation (Type III) consistently produce fracture intensities two to three times higher

than predicted by P/A ratio alone and plot well outside the 95% confidence interval for Type I controlled systems.

The relationship between FI and P/A ratio is a function of (1) the architecture and mechanical properties of the material that a platform builds over as it progrades (P/A >1), aggrades (0 > P/A > 1), or retrogrades (P/A < 0) (Figure 3.24) and (2) the control that P/A ratio imparts on the dominant syndepositional fracturing control type (Kosa, pers. comm., 2006). During progradation, early cemented and brittle platform-margin facies grow basinward over unstable and ductile fore-reef and compactable basinal strata. Under these conditions, down-to-the-basin tilting generated by mechanical compaction and bedding-plane slippage generate sufficient extensional stress for early fracture development. With increasing P/A ratios (flatter platform-margin trajectory), progressively larger amounts of unstable slope and basinal strata are loaded and subsequently compacted, leading to increased fracturing (Figure 3.24). Mechanical compaction values as high as 70% are reported for basinal sediments in the Canning Basin (Playford, 1984; Playford and Wallace, 2001), while Goldhammer (1997) showed that mechanical compaction of carbonate muds can occur at very shallow burial depths (e.g., 50% porosity reduction within 100 m of burial).

In aggrading or retrograding margins, where younger platforms build upward or retreat landward over older early-lithified platform-margin or platform-interior strata, fracturing in the platform-margin facies is dominantly driven by stresses associated with gravitational instability of the margin owing to oversteepening and self-erosion of the platform-margin escarpment (Figure 3.24). This style of fracturing is related to escarpment height and consequently is strongest in high-rising aggradational platforms, diminishing in lower relief retrograding platforms.

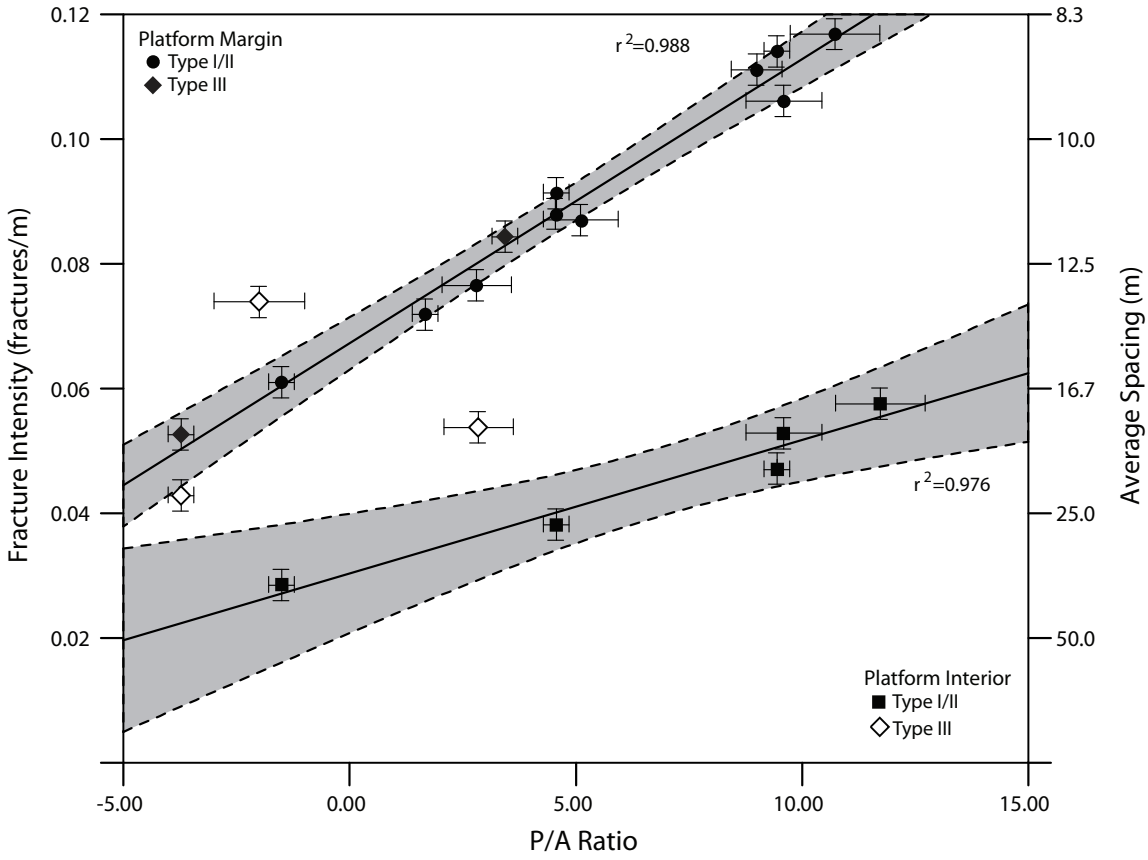

Figure 3.23: Normalized fracture intensity (FIn) for fractures with apertures greater than 0.5 m as a function of progradation/aggradation (P/A) ratio.

Platform-margin (upper curve) and platform interior facies (lower curve) plotted with a linear regression and 95% confidence intervals. Type III data not included in platform interior regression.

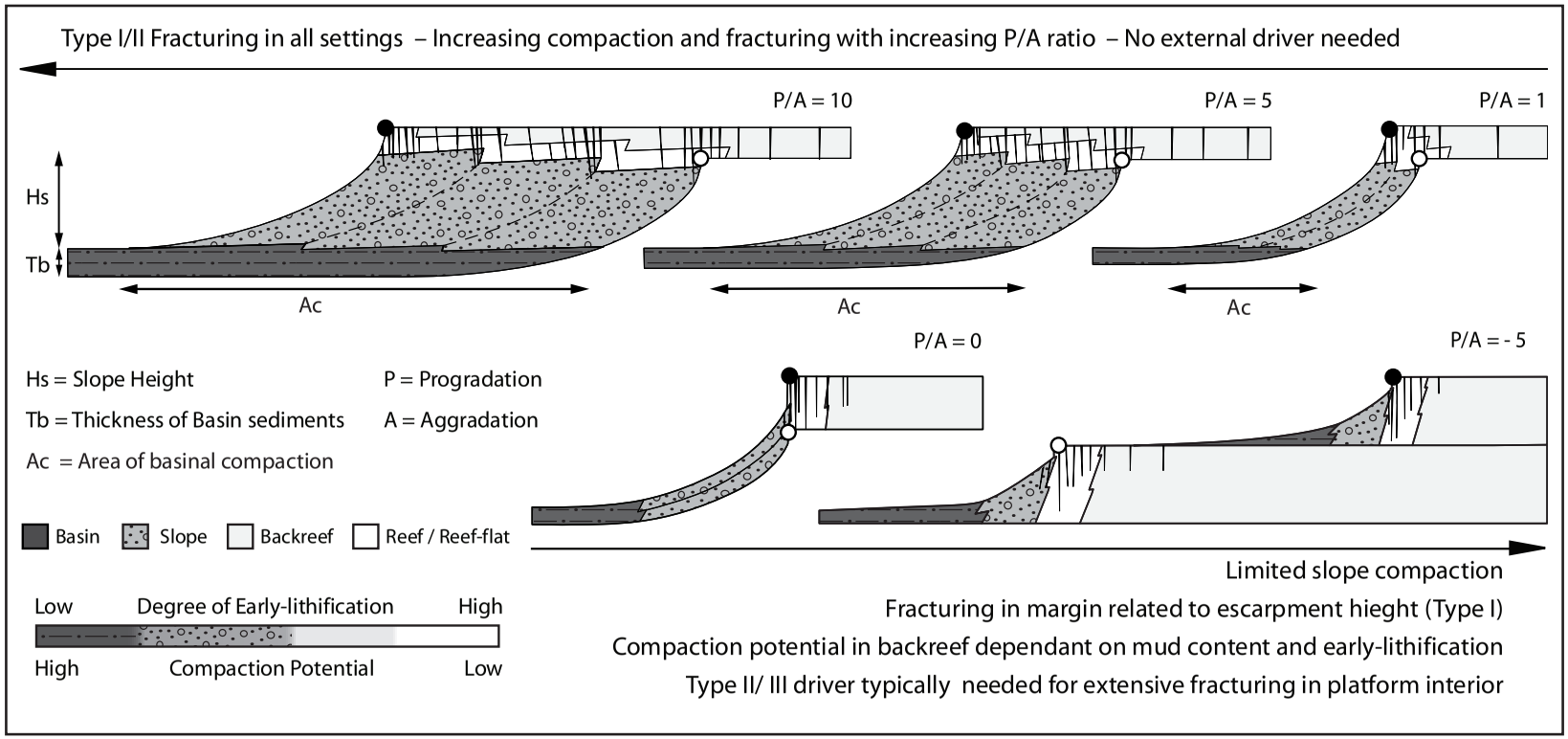

Figure 3.24: Basis for the relationship between P/A ratio and syndepositional fracture patterns.

In prograding platforms, increasing amounts of slope and basinal strata are loaded, leading to increasing compaction, bedding-plane slippage, and subsequently more fracturing. In aggrading and retrograding platforms, compaction of slope and basinal strata is far less important. Here, gravitational instability of the escarpment drives fracturing in the platform margin, while external drivers are required for extensive fracturing in the backreef.

In the platform interior of aggrading and retrograding platforms, compaction-related syndepositional fracturing is highly dependent on the mechanical properties of the platform interior facies. Compaction potential of backreef strata is critical. If backreef strata are early-lithified, compactional controls on syndepositional fracturing are generally ineffective, and fractures are weakly developed in the absence of external controls (e.g., scanlines 9434, 9460; Figure 3.10). Fracturing under these conditions depends on differential compaction over rigid antecedent topography and/or syndepositional faulting, with highs in fracture intensity occurring near faults (e.g., scanline SO_Fr-7; Figure 3.7) or over basement topography (e.g., scanline SO_FR-6; Figure 3.7).

The very high degree of correlation observed in Canning Basin between FI and P/A is related to the similarity of the gross mechanical properties throughout the Devonian reef complexes. Despite major changes in reef-building organisms across the Frasnian-Famennian boundary (Playford, 2002), key factors such as degree of early lithification of the platform margin did not change dramatically. In areas where there are significant temporal variations of large-scale mechanical properties (e.g., variations in early lithification or reflux dolomitization), it is unclear how the relationship between syndepositional fracturing and stratigraphic architecture would be affected, and more study is needed.

Comparison to Other Settings

The syndepositional fracture patterns observed in the Canning Basin display many similarities to other settings, as well as several key differences. The most obvious comparison is to the Permian-age Capitan System of Texas and New Mexico, which is characterized by prograding and aggrading high-relief, early-lithified carbonate platforms (Kerans and Tinker, 1999). Syndepositional deformation

in backreef strata of strongly progradation platforms (P/A ratio of 13–25; Tinker, 1998; Kerans and Tinker, 1999) has been described by Hunt and Fitchen (1999), Hunt et al. (2002), and Kosa and Hunt (2005).

Syndepositional growth faulting associated with compaction of basinal and slope strata is the dominant style of deformation in the Capitan backreef, and purely opening-mode fracturing is less common (Kosa and Hunt, 2005). Compaction-related growth faulting is rare in the Canning Basin and is restricted to the most progradational platforms (e.g., Billy Munro Gorge). There are two possible explanations for the differing styles of deformation in these two settings. Either the mechanical properties (degree of early lithification) of the Capitan system favor growth faulting rather than fracturing or, as P/A ratio increases, the style of early-deformation changes—namely, that stress from higher amounts of compaction is accommodated by growth faults rather than by purely opening-mode fractures. Kosa and Hunt (2005) reported that in many cases, Yates growth faults grew by interaction with inherited fractures in older reef strata. Given this observation, it seems plausible that the transition from fracturing to growth faulting as the dominant styles of early deformation is linked to P/A ratio, with the most progradational platforms being fault dominated and low P/A platforms fracture dominated (Figure 3.24).

CONCLUSIONS

Results presented here suggest that fracture patterns and mechanical stratigraphy are dynamic, time-sensitive variables. The strong relationship between FI and P/A ratio demonstrated here implies that stratigraphic architecture is a fundamental and intrinsic control on syndepositional deformation in carbonate platforms and that external drivers are not required for fracture development.

Our data predict that the highest degrees of fracturing should occur in high P/A settings and along active syndepositional structural elements. In these settings, syndepositional deformation will profoundly alter local diagenesis and platform-margin collapse patterns and will create conditions susceptible to secondary fracturing and paleokarst. The lowest fracture intensities are predicted in platforms with low or negative P/A ratios in tectonically stable settings. By deriving fracture intensity as a function of observable criteria, such as platform-margin trajectory and tectonic setting, results presented here take a significant first step toward developing predictive relationships between syndepositional fracture development and stratigraphic architecture in the subsurface using seismic or well data.

Chapter Four: Evidence for Stratigraphic Controls on Syndepositional Fracture Patterns

ABSTRACT

Syndepositional fractures are a ubiquitous feature of high-relief, reef-rimmed carbonate-platform and platform-margin systems and exert a profound influence on many facets of platform evolution. In this study we demonstrate a statistically significant relationship between syndepositional fracture development and variations in stratigraphic architecture, approximated here by platform-margin trajectory. Syndepositional fracturing increases significantly with progradation, with a two-fold increase in fracture intensity observed between the most retrogradational to progradational carbonate platforms. In the platform margin, syndepositional fracturing varies systematically with platform-margin trajectory, regardless of proximity to regional structure, whereas, in the platform interior, structurally controlled settings consistently display fracture intensities significantly higher than predicted by platform-margin trajectory alone. The results presented here suggest a first-order relationship between long-term changes in stratigraphic architecture and syndepositional fracture development in high-relief carbonate platforms and imply that while external structural drivers may enhance early fracturing, they are not required.

This chapter is in review in the *Journal of Sedimentary Research*

INTRODUCTION

Syndepositional fractures, often referred to as neptunian dikes, are a ubiquitous feature in early-lithified, high-relief carbonate platforms, directly impacting margin collapse, slope megabreccia deposition, and early diagenesis, including extensive marine cementation and dolomitization, mechanical property evolution, and karstification. Traditional models typically attribute fracture development to regional tectonic deformation and relate fracture characteristics (e.g., spacing, orientation, and termination) to variations in bed-scale mechanical properties. The large-scale syndepositional fracture populations observed in many carbonate platforms present a paradox, because these features typically crosscut numerous small, mechanical layers and often develop high fracture intensities in the absence of coeval regional structural deformation. While syndepositional fracturing is often acknowledged to be stratigraphically controlled, no quantitative relationships between stratigraphic architecture and syndepositional fracturing have been reported, and current models provide only empirical relationships that predict increased fracturing in the platform margin relative to platform interior and slope facies (Playford et al., 1989) and enhanced deformation in strongly prograding platforms (Hurley, 1986; Hunt and Fitchen, 1999; Kosa et al., 2003).

On the basis of fracture data collected from outcrops in Devonian reef complexes of Western Australia's Canning basin, we document a very strong link between syndepositional fracturing and variations in sequence-scale stratigraphic architecture, approximated here by platform margin trajectory. Our data illustrate that platform-margin trajectory governs the Type and relative influence of various syndepositional fracture mechanisms, and subsequently the degree of fracture development. We assert that syndepositional fracturing is a fundamental and

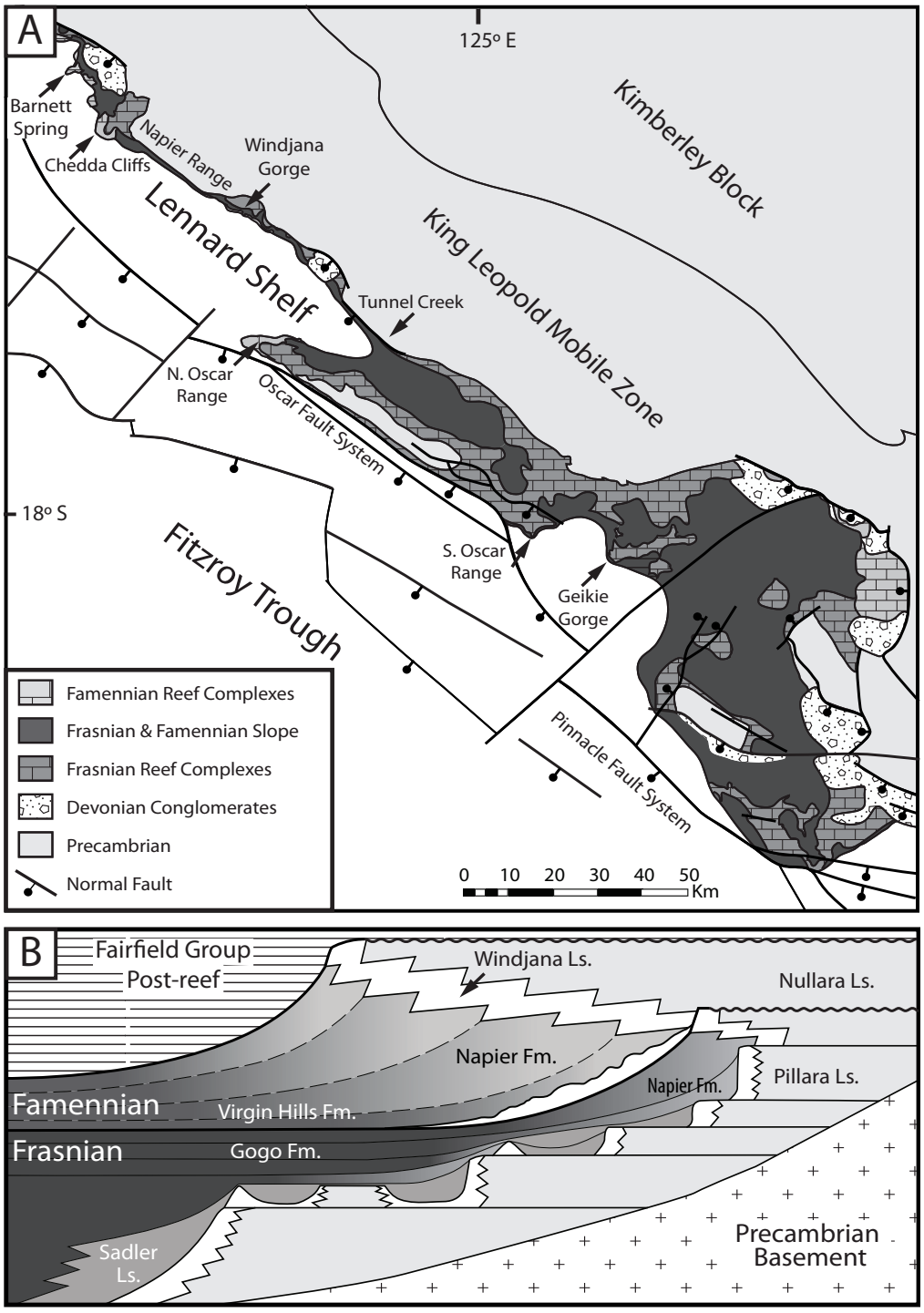

Figure 4.1: Study area geology and stratigraphy.

(A) Geology of the Devonian reef complexes of the Lennard Shelf, modified after Playford and Hocking (1999). (B) Stratigraphy of the Devonian reef complexes, modified after Playford (2002).

intrinsic response of high-relief carbonate platforms to long-term variations in stratigraphic architecture that in many scenarios requires no external structural drivers.

SETTING

The Devonian reef complexes of the Canning Basin outcrop are a series of retrograding platforms and pinnacle reefs of Givetian (Middle Devonian) to late Frasnian (Late Devonian) age and latest Frasnian- to Famennian-age prograding platforms (Figure 4.1; Playford, 2002, and references therein). The reef complexes fringe the mountainous Precambrian Kimberley Block, as well as smaller, isolated, Precambrian emergent uplifts (e.g., Oscar Range) and are bounded to the southwest by large-scale Upper Devonian extensional fault systems and the deeply subsident Fitzroy Trough. Glaciation in the Early Permian removed many of the younger sediments overlying the Devonian reef complexes, which, following broad, regional Cenozoic uplift, are now represented as flat-topped limestone ranges (Playford, 2002). Much of the original depositional topography is relatively undeformed, with syndepositional fractures well exposed along the dip-oriented polished walls of river gorges and along the top of most of the limestone ranges. Differential weathering and vegetation accentuate the fracture planes, creating linear depressions that are easily resolvable from satellite imagery.

SYNDEPOSITIONAL FRACTURES

Syndepositional fractures are common in many carbonate systems throughout the geologic record (Smart et al., 1988; Playford et al., 1989; Hunt and Fitchen, 1999; Cozzi, 2000; De La Porta et al., 2004; Collins et al., 2006; Guidry et al., 2007)

and are a hallmark of early-lithified and brittle platform-margin facies of steep, reef-rimmed carbonate platforms. Fracture timing has been established as syndepositional by recognition of (1) Upper Devonian marine cements (Hurley, 1986) and (2) coeval, platform-derived sediment, encrusting marine microbial colonies and benthic organisms (Playford, 1984) lining fracture walls. Syndepositional fractures in the Canning Basin are dominantly opening mode; however, a minor component of normal offset is also commonly observed in tectonically active areas (Miller et al., 2007) and backreef strata of strongly prograding platforms (Kosa et al., 2003). Fractures typically crosscut bedding and reach heights exceeding 90 m, while kinematic apertures of up to 20 m and fracture trace lengths 5 km long have been reported (Hurley, 1986; Playford et al., 1989). These fractures stand in contrast to the Canning Basin's secondary (postdepositional) fracture set, which is strongly influenced by meter-scale bedding, with fracture heights rarely exceeding a few centimeters and with apertures filled with blocky equant spar and generally less than 2.5 mm in width.

We propose three primary syndepositional fracture mechanisms: (1) gravitational instability and compaction (Type I), (2) differential compaction over rigid antecedent topography (Type II), and (3) active structural deformation (Type III). Each control Type represents an end member with unique fracture patterns (Kosa et al., 2003); however, any given fracture set can be the product of one or all of these drivers. Type I fractures run parallel and, to a lesser degree, orthogonal to the platform-margin and are generated by stress associated with oversteepening and defacement of the active platform-margin escarpment (Schlager and Camber, 1986) and by extensional stress associated with down-to-the-basin tilting related to early compaction of basinal sediments and ductile slope strata (Playford et al., 1989). Type II fractures are generated by differential compaction and flexure of

early-cemented strata over rigid antecedent topography, such as older platform escarpments (Hunt and Fitchen, 1999; Rusciadelli and Di Simone, 2007), fore-reef bioherm complexes, drowned reef spines, or crystalline basement topography (Hurley, 1986). Type II fractures typically occur in discrete swarms focused over the crest of the underlying topographic element. Type III fractures are generated by stress associated with syndepositional tectonics, are orientated parallel to the active deformation feature or regional stress field (Hurley, 1986; Cozzi, 2000; Ward; 1996; Miller et al., 2007), and a component of vertical displacement is often observed. Type I and Type II are passive deformation mechanisms and intrinsic to the stratigraphic architecture of many carbonate systems, while Type III is an extrinsic mechanism requiring active regional structural deformation.

METHODS

Four study areas along the Napier and Oscar Ranges (Figure 4.2) were selected to investigate the relationship between syndepositional fracturing and stratigraphic architecture, and fracture attribute data were collected at two scales of observation: (1) outcrop scale (apertures 0.2 mm and larger) and (2) remote-sensing scale (apertures 0.5 m and larger). Outcrop fracture data were collected along the polished canyon walls of Windjana Gorge (Figure 4.2), and fracture attributes (orientation, extension, intensity, and aperture scaling) were analyzed along 12 one-dimensional scanlines using the methodology of Ortega et al. (2006). Syndepositional fractures were differentiated from secondary fractures on the basis of fill and crosscutting relationships, and attributes from each population are reported separately (see Table 4.2). Platform-wide examination of large-scale fracture populations was conducted on high-resolution (~1-m-pixel) IKONOS satellite imagery, and fracture intensity and average spacing were analyzed in 11

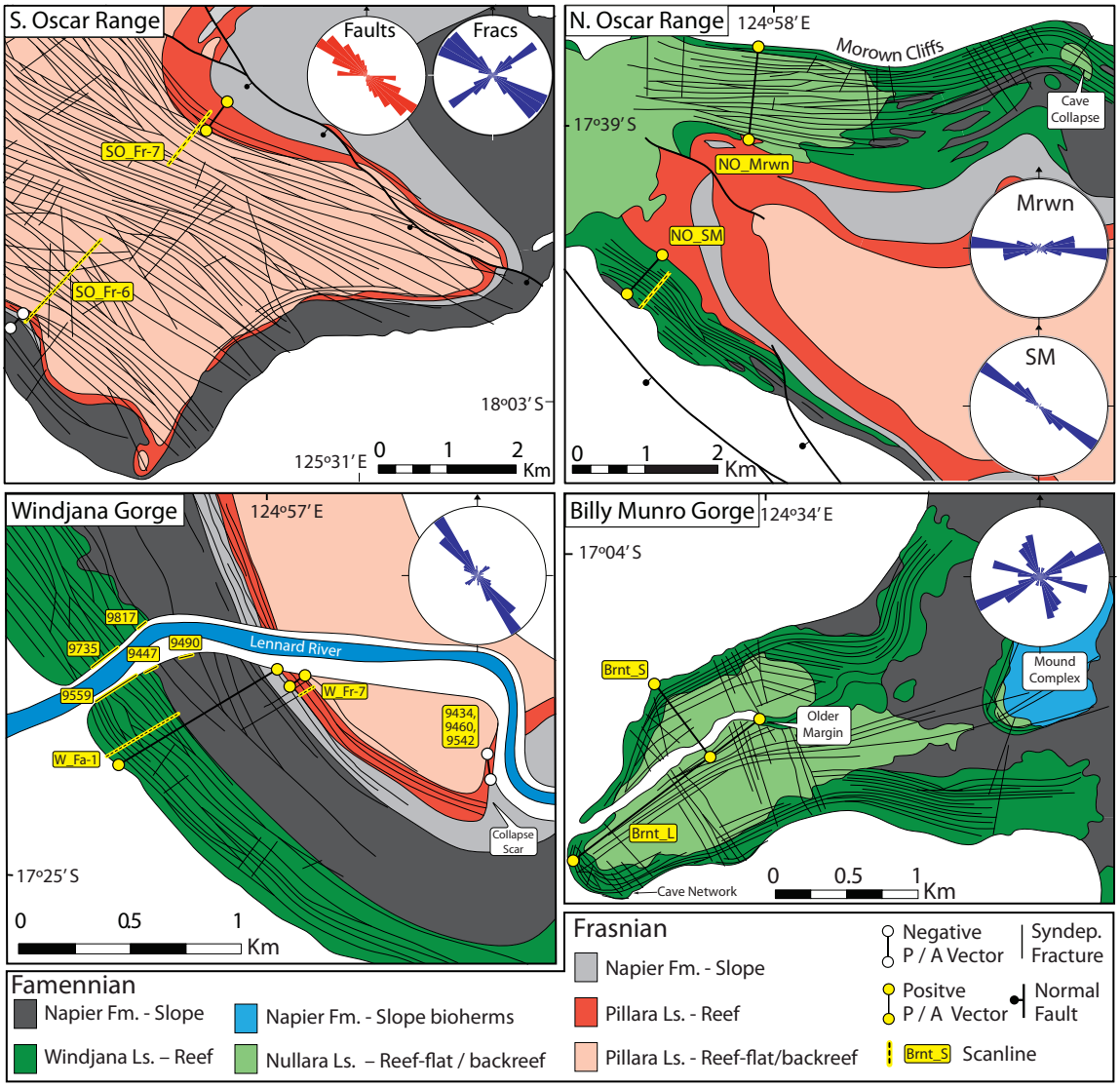

Figure 4.2: Simplified fracture patterns of the Devonian reef complexes.

Geology modified from Playford and Hocking (1999). Scanlines follow platform-margin vector unless otherwise noted. Scanlines not pictured: Mick Malcolm Gap, Chedda Cliffs, and Tunnel Creek.

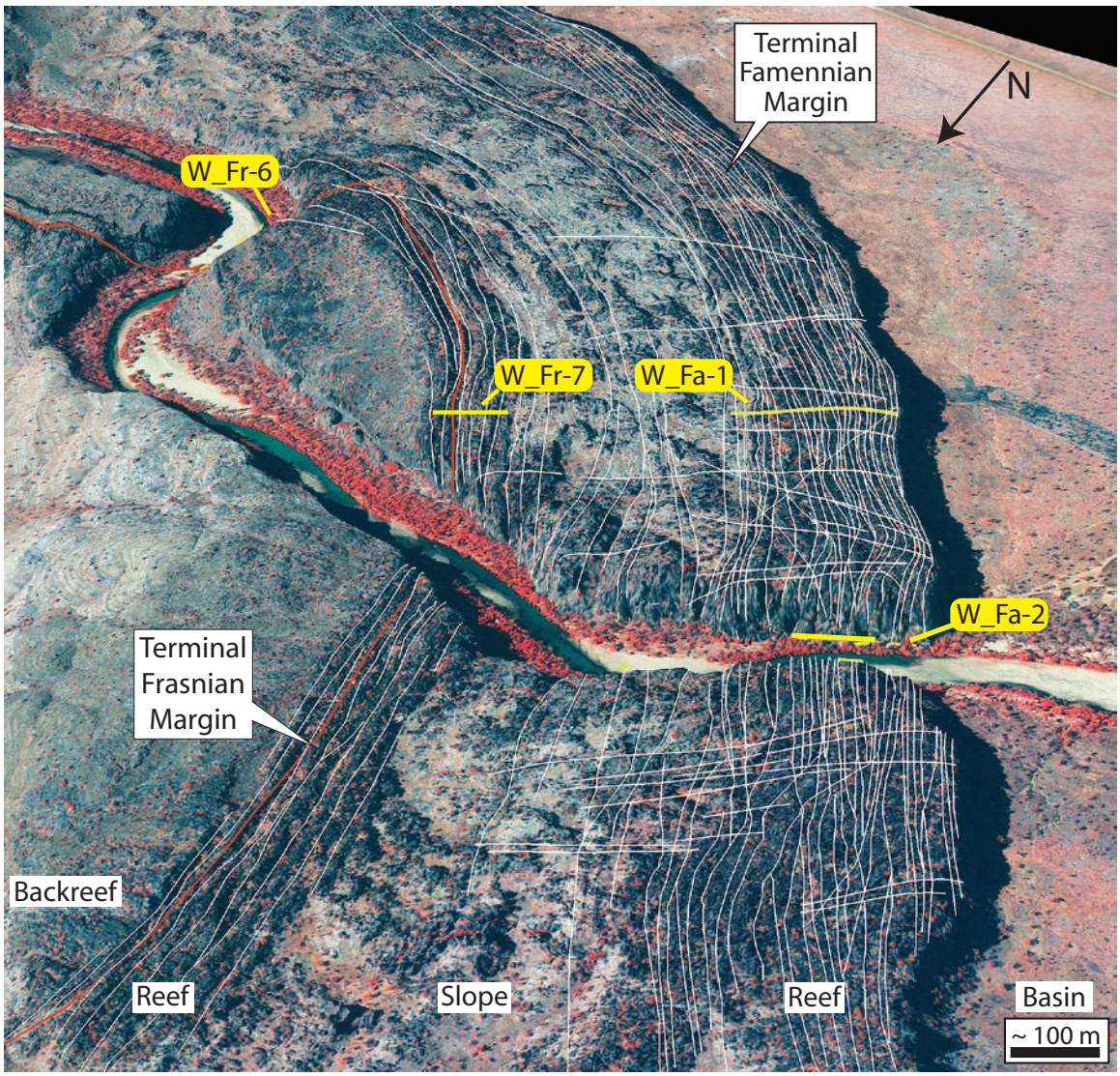

Figure 4.3: Syndepositional fractures of Windjana Gorge.

Cliff face is approximately 90 m tall. Image constructed from false-color Ikonos satellite imagery, high-resolution ground-based lidar, and 90-m SRTM data.

one-dimensional scanlines using ArcGIS (Figures 4.2 and 4.3). Remote-sensing interpretations were calibrated to ground-based scanlines, field mapping, and published data (Hurley, 1986) in order to ensure that only syndepositional fractures were recorded.

Fracture intensity (*FI*; Ladeira and Price, 1981) was used to compare syndepositional fracturing at different localities, given its relative ease of acquisition at both scales of observation. FI values vary by nearly three orders of magnitude between the remote-sensing scale (low FI) and outcrop (high FI), owing to disparate resolutions of the two methods. *Normalized fracture intensity* (*FIn*; Ortega et al., 2006) was calculated for each ground-based scanline to allow direct comparison between the two different scales of observation. FIn was calculated for apertures of 0.5 m and larger ($FIn_{0.5}$), and results from Windjana Gorge demonstrate that FIn calculated from ground-based scanlines accurately predicts (within 99%) FI at the remote-sensing scale (Table 4.1). Because of incomplete mechanical boundary preservation from modern erosion, FI was not normalized for mechanical unit thickness (*sensu* Narr and Suppe, 1991).

Progradation to aggradation (P/A) ratio quantifies platform-margin trajectory and serves as a proxy for stratigraphic architecture (Tinker, 1998; Kerans and Tinker, 1999; De La Porta et al., 2004). P/A ratio was calculated from field mapping, satellite imagery, or published data (Table 4.1). In the absence of a platform section, the mean thickness of time-equivalent sections was applied. Owing to differential stratigraphic preservation, aggradation values do not necessarily reflect total thickness and are best thought of as minimum values. Absolute rates are not calculated for this study because of limited chronostratigraphic data, and P/A ratios reported here represent long-term trends.

Scanline	Locality	Method	Control	Progradation (m)	Aggradation (m)	P/A Ratio	Fracture Intensity (fractures/m)		Average Spacing (m)	
Famennian Platforms							Reef	Platform	Reef	Platform
BMG_L	Billy Munro (Long axis)	RS	I, II	1759	160	11.0	0.119	0.058	8.4	17.4
BMG_S	Billy Munro (Short axis)	RS	I, II	685	160	4.3	0.089	0.038	11.2	26.2
MMG	Mick Malcom Gap	RS	I	1450	160	9.1	0.109	0.053	9.1	18.9
Chd	Chedda Cliffs	RS	I	1729	200[1]	8.6	0.109	ND	9.2	ND
NO_Mrwn	N Oscars (MRWN)	RS	I	1511	168[3]	9.0	0.112	0.048	8.9	20.8
NO_SM	N Oscars (SWM)	RS	I, III	550	168[3]	3.3	0.084	ND	11.9	ND
W_Fa-1	Windjana Gorge	RS	I	704	169[#]	4.1	0.088	ND	11.4	ND
9559	Windjana Gorge	G	I	613	148[#]	4.1	0.087[$]	ND	11.5	ND
Famennian Platforms										
W_Fr-7	Windjana Gorge	RS	I	167[3]	233[3]	0.7	0.072	ND	13.9	ND
9434 / 9460	Windjana Gorge	G	I	–82	74	-1.1	0.051[$]	0.029[$]	16.4	34.5
SO_Fr-6	S Oscars (Fr6)	RS	III, II, I	–1326[2]	547[2]	-2.4	0.054	0.043	18.4	23.3
SO_Fr-7	S Oscars (Fr7)	RS	III, II, I	328[2]	256[2]	1.3	0.075	0.054	13.4	18.5
TC-1	Tunnel Creek	G	III, II	–100[4]	50[4]	-2.0	ND	0.074[$]	ND	13.5

$ Normalized fracture intensity for fractures greater than 0.50 m. [1] Chow et al., 2004; [2]Hurley, 1986; [3]Playford and Hocking, 1999; [4]Ward 1996.

Table 4.1: Normalized fracture intensity and platform-margin trajectory data for the Devonian Reef Complexes.

			Syndepositional Fractures					*Secondary Fractures*		
Scanline #	Facies	Facies Tract	Extension	FI	*FIn*	S	*Sn*	Extension	FI	S
Famennian				(fracs/m)		(m)			(fracs/m)	(m)
9559	Massive Microbial Bst.	Reef	9.8%	16.5	0.087	0.06	11.5	1.0%	14.9	0.07
9447	Laminar Microbial Bst.	Reef/Upper slope	9.1%	11.2	0.066	0.09	15.1	1.0%	14.6	0.07
9735	Laminar Microbial Bst.	Reef/Upper slope	7.8%	8.2	0.059	0.12	16.9	1.4%	21.3	0.05
9490	Sponge-Microbial Bst.	Upper slope	7.0%	12.1	0.055	0.08	18.2	0.8%	4.3	0.23
9817	Sponge-Microbial Bst.	Upper slope	5.1%	10.5	0.032	0.10	31.3	0.7%	5.5	0.18
			7.8%	11.7	0.060	0.09	18.60	0.98%	12.1	0.12
Frasnian										
9434	Stromatoporoid Frm	Reef/Reef-flat	4.0%	6.8	0.061	0.15	16.4	0.1%	3.4	0.30
9539	Breccia	Fore-reef	3.9%	11.1	nd	0.03	nd	nd	nd	nd
9460	Stromatoporoid Flt.	Backreef	2.9%	9.1	0.029	0.11	34.5	0.3%	6.1	0.16
9542	Stromatoporoid/Sponge Bst.	Reef/Upper slope	2.8%	12.6	0.030	0.08	33.3	0.7%	15.4	0.07
10500a	Stromatoporoid Flt.	Backreef	1.5%	1.8	0.03	0.56	33.4	0.7%	11.2	0.09
10500b	Terrigeneous Pelliodal Ps.	Backreef	1.4%	1.8	0.03	0.57	34.1	0.2%	2.96	0.34
			2.7%	7.2	0.038	0.25	29.4	0.39%	7.8	0.19

Table 4.2: Fracture attributes by lithofacies for ground-based scanlines in Windjana Gorge.

Normalized fracture intensity (FIn) and average spacing (Sn) calculated for fractures apertures greater than 0.50 m.

RESULTS AND DISCUSSION

Ground-based scanline data reveal that syndepositional fracture attributes vary with depositional facies, as well as platform-margin trajectory. In the prograding platforms of the Famennian, the massive microbial reef boundstones are the most fractured (FI=16.5 fractures/m; $FIn_{0.5}$= 0.09 fractures/m) and accommodate the most extension (9.8%). In the retrograding Frasnian platforms, the microbial-stromatoporoid boundstones of the reef flat accommodate the most extension (3.0%) in a series of large-aperture fractures ($FIn_{0.5}$= 0.05 fractures/m), while the upper bound slope is dominated by abundant small, syndepositional fractures with relatively few large-aperture fractures (FI=12.6 fractures/m, $FIn_{0.5}$= 0.03 fractures/m). Average extension and fracture intensity values are approximately 2.5 times higher in the prograding Famennian platforms than in the retrograding platforms of the Frasnian.

At the 95% confidence level, when data from all localities are considered, a statistically significant linear relationship between fracture intensity and P/A ratio is observed in both platform-margin and platform-interior settings (Figure 4.4). The platform-margin of the most progradational platforms (high P/A) show FI values more than double those of the most retrogradational platforms (negative P/A). All platform-margin data points plot within the same 95% confidence interval (Figure 4.4), regardless of control Type or proximity to regional syndepositional structural elements. In the platform interior, a similar relationship between FI and P/A ratio is observed for Type I and II systems (Figure 4.4). However, Type III fracture populations consistently produce fracture intensities two to three times higher than predicted by P/A ratio alone and plot well outside the 95% confidence interval for Type I controlled systems. The very high degree of correlation observed

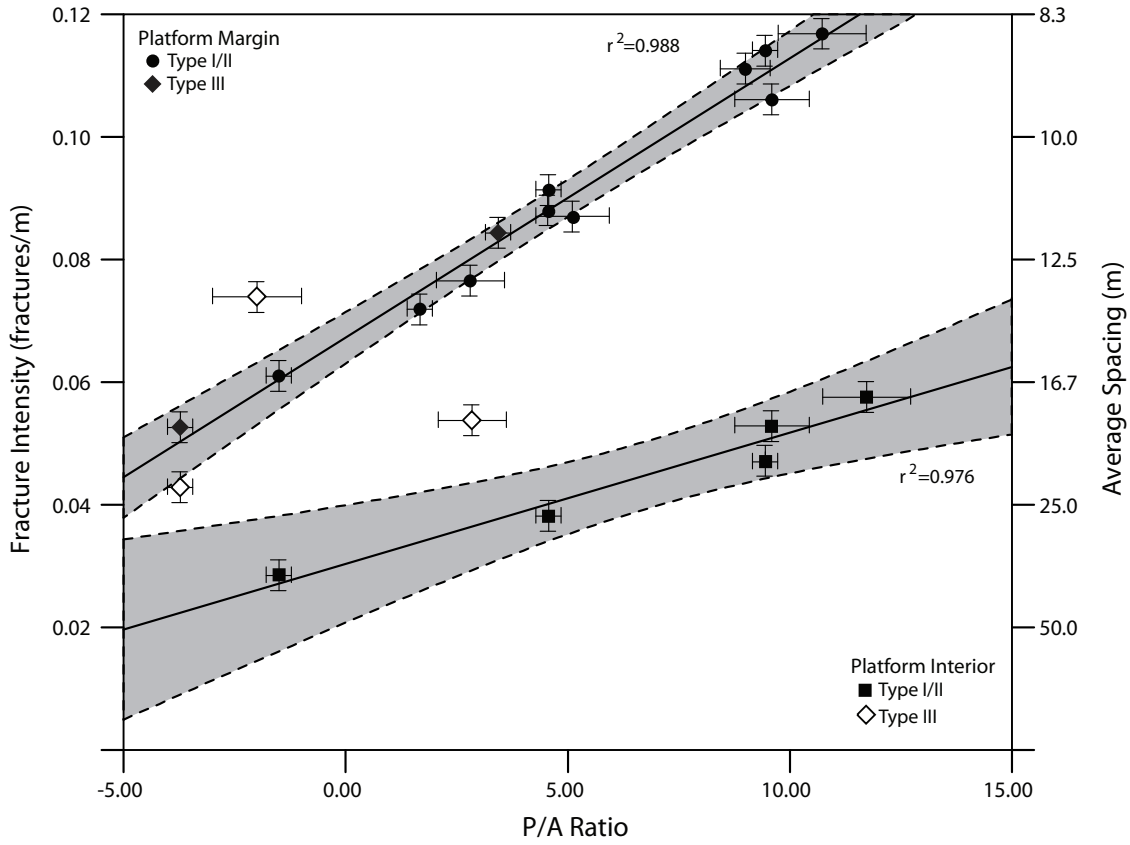

Figure 4.4: Normalized fracture intensity (FIn) for fractures greater than 0.5 m as a function of progradation/aggradation (P/A) ratio.

Platform margin (upper curve) and platform interior facies (lower curve) plotted with a linear regression and 95% confidence intervals. Type III data not included in platform interior regression.

between FI and P/A is related to the similarity of gross mechanical properties (e.g., compactibility, degree of early lithification) throughout the Devonian reef complexes.

The relationship between FI and P/A ratio is a function of (1) the architecture and mechanical properties of the material that a platform builds over as it progrades (P/A >1), aggrades (0 > P/A > 1), or retrogrades (P/A < 0) (Figure 4.4), and (2) the effect that P/A ratio imparts to the dominant Type and relative intensity of syndepositional fracturing controls. During progradation, early cemented and brittle platform-margin facies grow basinward over unstable and ductile fore-reef and compactible basinal strata; under these conditions, down-to-the-basin tilting generated by mechanical compaction generates sufficient extensional stress for early fracture development. With increasing P/A ratios (flatter trajectory), progressively larger amounts of unstable slope and basinal sediments are loaded and subsequently compacted, leading to increased fracturing (Figure 4.5). Mechanical compaction values as high as 70% are reported for basinal sediments in the Canning Basin (Playford 1984; Playford and Wallace, 2001), while Goldhammer (1997) showed that mechanical compaction of carbonate muds can occur at very shallow burial depths (e.g., 50% porosity reduction within 100 m of burial). Direct loading of basinal sediments generally does not occur at low P/A ratios of less than 3 (Figure 4.5); however, once this threshold is crossed, significant early compaction and down-to-the-basin tilting can occur, depending on the thickness of the basinal sediments.

In aggrading or retrograding margins, where younger platforms build upward or retreat landward over older, early-lithified platform-margin or platform-interior strata, fracturing in the platform-margin facies is dominantly driven by stresses associated with gravitational instability of the margin owing to oversteepening and

self-erosion of the platform-margin escarpment (Figure 4.5). This style of fracturing is related to escarpment height and, consequently, is strongest in high-rising aggradational platforms, diminishing in lower relief retrograding platforms. In the platform interior of aggrading and retrograding platforms, compaction-related syndepositional fracturing is highly dependent on the mechanical properties of the platform interior facies, and, given the limited early compaction of typical backreef facies (Hurley, 1986; Goldhammer, 1999), syndepositional fractures are weakly developed in the absence of external controls (e.g., W_Fr6; Figure 4.2). Instead, fracturing in this setting depends on differential compaction over rigid antecedent topography and/or syndepositional faulting, which are the most important fracture mechanisms, and discrete highs in fracture intensity occur near faults (e.g., SO_Fr-7; Figure 4.2) or over basement topography (e.g., SO_Fr-6; Figure 4.2).

IMPLICATIONS AND CONCLUSIONS

The data we present here have broad implications for a number of processes in steep-rimmed carbonate systems. Syndepositional fracturing of the platform margin is intimately linked to platform-margin morphology and escarpment development (Schlager and Camber, 1986; Playford et al., 1989), while George et al. (1995) showed that intensified slope instability and fracturing associated with prograding platforms can generate high-frequency platform-margin collapse. Syndepositional fracture networks often strongly alter local diagenetic patterns by creating early permeability pathways that allow fluids to circulate through the platform. This enhanced early fluid-flow system can have profound effects on processes such as reflux dolomitization (Kosa et al., 2003) and groundwater circulation (Smart et al., 1988). Reactive transport models have shown that groundwater circulation

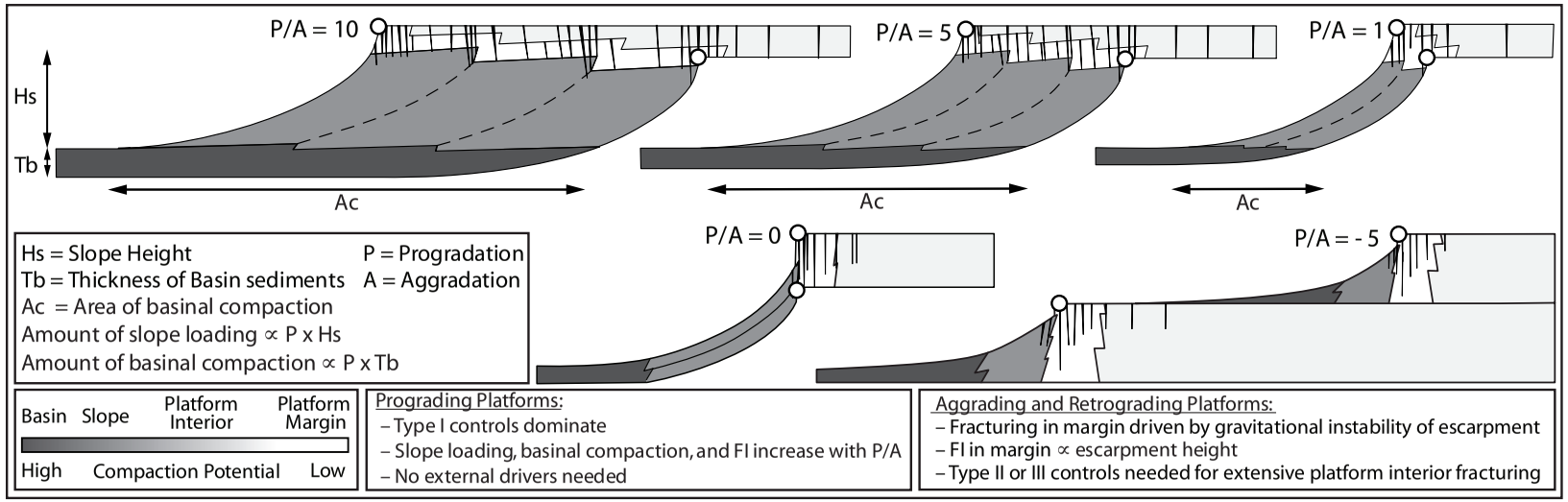

Figure 4.5: Proposed basis for the relationship between P/A ratio and syndepositional fracture patterns.

In prograding platforms, increasing amounts of slope and basinal strata are loaded, leading to increasing compaction and, subsequently, more fracturing. In aggrading and retrograding platforms, compaction of slope and basinal strata is far less important; here gravitational instability of the escarpment drives fracturing in the platform margin, while external drivers are required for extensive fracturing in the backreef.

within carbonate platforms is highly sensitive to vertical fracture permeability (Jones and Xiao, 2006) and can produce dissolution halos along fracture planes (Whitaker and Smart, 1997). In strongly progradational margins, where fracture permeability is increased, groundwater convection cells can develop, significantly altering platform-wide diagenetic patterns (Collins et al., 2006; Jones and Xiao, 2006). Fluid flow along early fracture networks can have a pronounced effect on mechanical evolution and subsequent fracture patterns (Shackleton et al., 2005), and increased syndepositional fracturing and associated diagenesis in prograding platforms may produce mechanical conditions more susceptible to secondary fracturing, with the highest secondary fracture intensity and extension (21.3 fractures/m, 1.4% respectively) occurring in the prograding Famennian microbial reef facies of Windjana Gorge. During exposure events, syndepositional fracture networks are conducive to dissolution and enhanced karst development (Smart et al., 1988; Whitaker and Smart, 1997; Playford, 2002; Kosa et al., 2003, Guidry et al., 2007), with the strongest prograding and most fractured margins being the most susceptible to karstification (e.g., Morown Cliffs, Billy Munro Gorge; Figure 4.2).

Our results suggest that drivers intrinsic to carbonate systems, coupled with variations in stratigraphic architecture, are sufficient to generate syndepositional fractures in high-relief carbonate platforms, and external tectonic drivers are not required. We assert that fracture development in the platform margin is dominantly governed by gravitational (Type I) mechanisms, and while external structural (Type III) drivers may enhance margin fracturing, they do not significantly affect the relationship between FI and P/A ratio, suggesting that stratigraphic architecture is a first-order control on fracturing in this setting. In the platform interior, syndepositional patterns are also strongly related to stratigraphic architecture;

however, in aggrading and retrograding platforms, gravitational drivers are generally ineffective in producing extensive syndepositional fractures, and either antecedent topography (Type II) or external tectonic stress (Type III) is required to explain extensive fracturing. The significant vertical and lateral extent of many syndepositional fractures (often > 90 m and > 1 km, respectively) and frequent crosscutting of bedding boundaries suggest that meter-scale mechanical layers are often ineffective in terminating these features, and we suggest that mechanical stratigraphy should be considered not only at the bed scale, but at the sequence scale as well. On the basis of the results presented here, we propose that long-term variations in stratigraphic packaging (e.g., 2nd-order transgression vs. regression) will produce temporal variations in syndepositional fracture patterns, and, given the effect that syndepositional fractures have on both depositional and early diagenetic processes, it is imperative that they be considered when characterizing carbonate-platform evolution, diagenesis, and deformation.

Appendix: Famennian measured sections

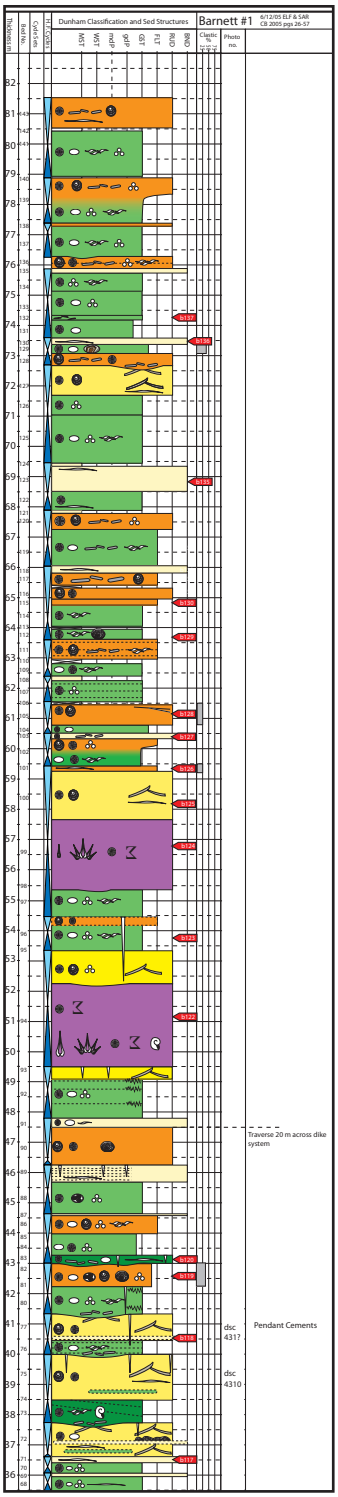

- Fenestral Laminite
- Tepee Horizon
- Beachrock
- Coated grain, microbial FS/RS
- Bubble fenestral, ooid GS/FS
- Bioclastic, ooid GS
- Sandy ooid lithoclast FS/RS
- Megalodont FS/RS
- Lithiotid FS/RS
- Stromatolitic BS
- Renalcis BS
- Stromatactis BS

- Lithiotid Bivalve
- Megalodont Bivalve
- Gastropod
- Undiff. Bioclast
- Pisoid
- Ooid
- Composite Grain
- Oncoid
- Lithoclast
- Beachrock or Tepee Slab

- Tepee Structure
- Sheet Crack
- Laminar Fenestrae
- Bubble Fenestrae
- Undiff. Fenestrae
- Ripple Lamination
- Tabular Cross-bedding

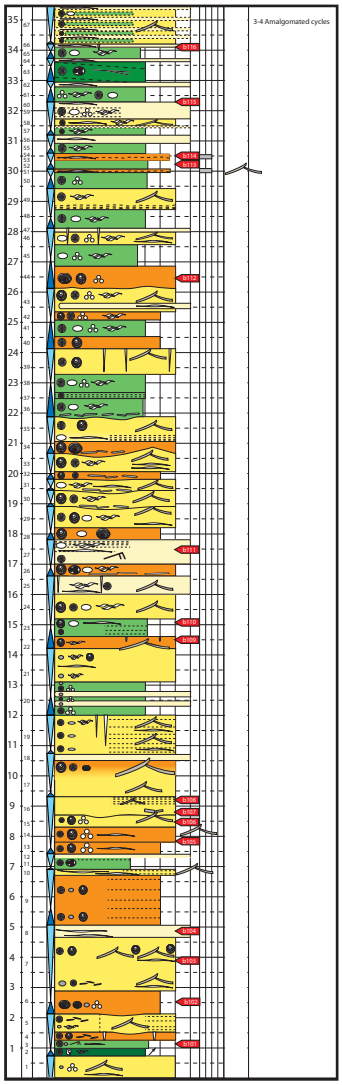

Measured Section B-1

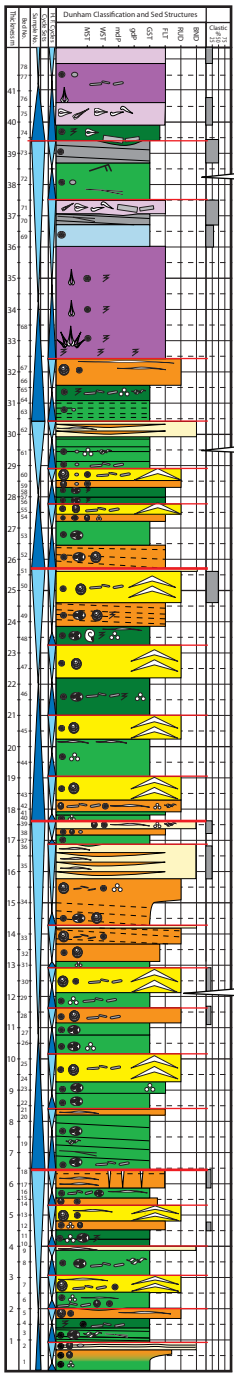

- Fenestral Laminite
- Tepee Horizon
- Beachrock
- Coated grain, microbial FS/RS
- Bubble fenestral, ooid GS/FS
- Bioclastic, ooid GS
- Sandy ooid lithoclast FS/RS
- Megalodont FS/RS
- Lithiotid FS/RS
- Stromatolitic BS
- Renalcis BS
- Stromatactis BS

- Lithiotid Bivalve
- Megalodont Bivalve
- Gastropod
- Undiff. Bioclast
- Pisoid
- Ooid
- Composite Grain
- Oncoid
- Lithoclast
- Beachrock or Tepee Slab

- Tepee Structure
- Sheet Crack
- Laminar Fenestrae
- Bubble Fenestrae
- Undiff. Fenestrae
- Ripple Lamination
- Tabular Cross-bedding

Measured Section B-2

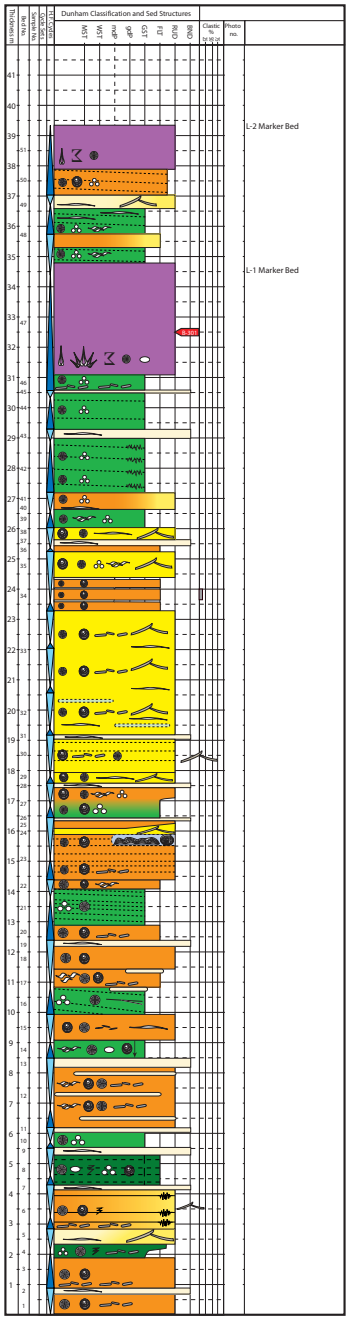

- Fenestral Laminite
- Tepee Horizon
- Beachrock
- Coated grain, microbial FS/RS
- Bubble fenestral, ooid GS/FS
- Bioclastic, ooid GS
- Sandy ooid lithoclast FS/RS
- Megalodont FS/RS
- Lithiotid FS/RS
- Stromatolitic BS
- Renalcis BS
- Stromatactis BS

- Lithiotid Bivalve
- Megalodont Bivalve
- Gastropod
- Undiff. Bioclast
- Pisoid
- Ooid
- Composite Grain
- Oncoid
- Lithoclast
- Beachrock or Tepee Slab

- Tepee Structure
- Sheet Crack
- Laminar Fenestrae
- Bubble Fenestrae
- Undiff. Fenestrae
- Ripple Lamination
- Tabular Cross-bedding

Measured Section B-3

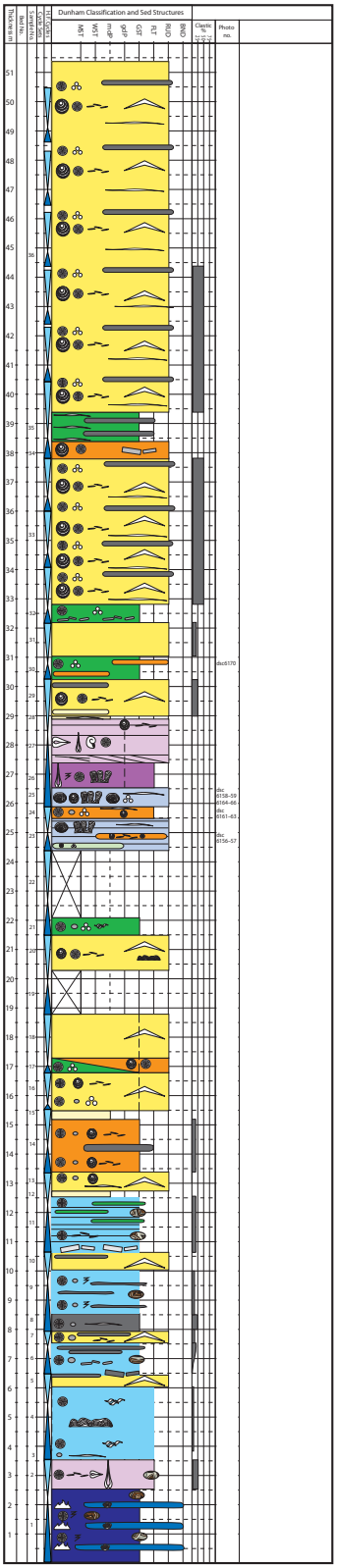

- Fenestral Laminite
- Tepee Horizon
- Beachrock
- Coated grain, microbial FS/RS
- Bubble fenestral, ooid GS/FS
- Bioclastic, ooid GS
- Sandy ooid lithoclast FS/RS
- Megalodont FS/RS
- Lithiotid FS/RS
- Stromatolitic BS
- Renalcis BS
- Stromatactis BS

- Lithiotid Bivalve
- Megalodont Bivalve
- Gastropod
- Undiff. Bioclast
- Pisoid
- Ooid
- Composite Grain
- Oncoid
- Lithoclast
- Beachrock or Tepee Slab

- Tepee Structure
- Sheet Crack
- Laminar Fenestrae
- Bubble Fenestrae
- Undiff. Fenestrae
- Ripple Lamination
- Tabular Cross-bedding

Measured Section B-4

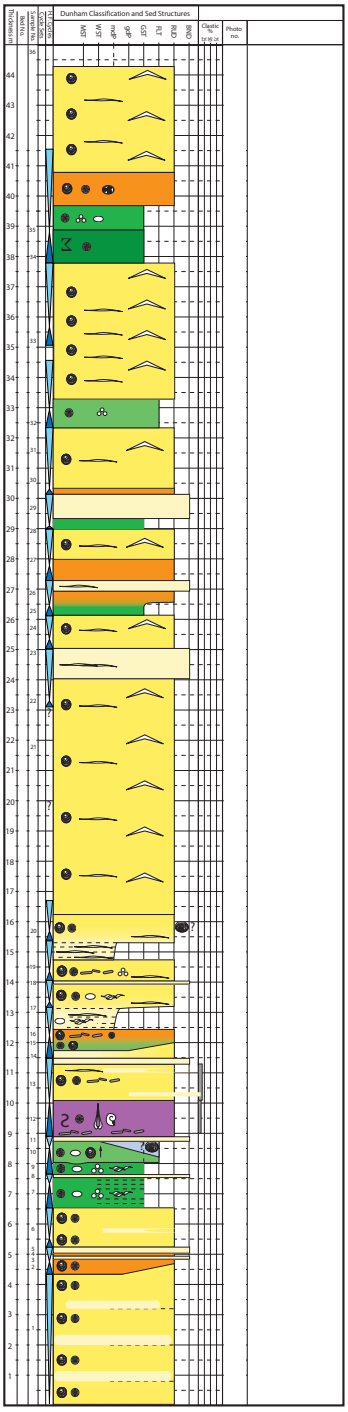

- Fenestral Laminite
- Tepee Horizon
- Beachrock
- Coated grain, microbial FS/RS
- Bubble fenestral, ooid GS/FS
- Bioclastic, ooid GS
- Sandy ooid lithoclast FS/RS
- Megalodont FS/RS
- Lithiotid FS/RS
- Stromatolitic BS
- Renalcis BS
- Stromatactis BS

- Lithiotid Bivalve
- Megalodont Bivalve
- Gastropod
- Undiff. Bioclast
- Pisoid
- Ooid
- Composite Grain
- Oncoid
- Lithoclast
- Beachrock or Tepee Slab

- Tepee Structure
- Sheet Crack
- Laminar Fenestrae
- Bubble Fenestrae
- Undiff. Fenestrae
- Ripple Lamination
- Tabular Cross-bedding

Measured Section B-5

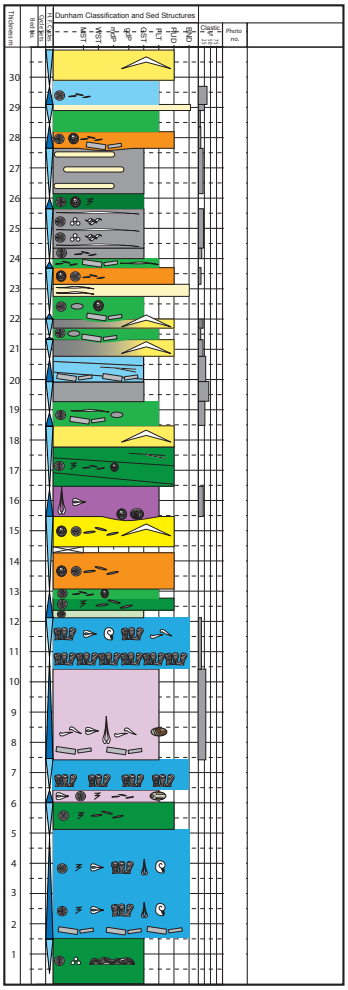

Measured Section B-6

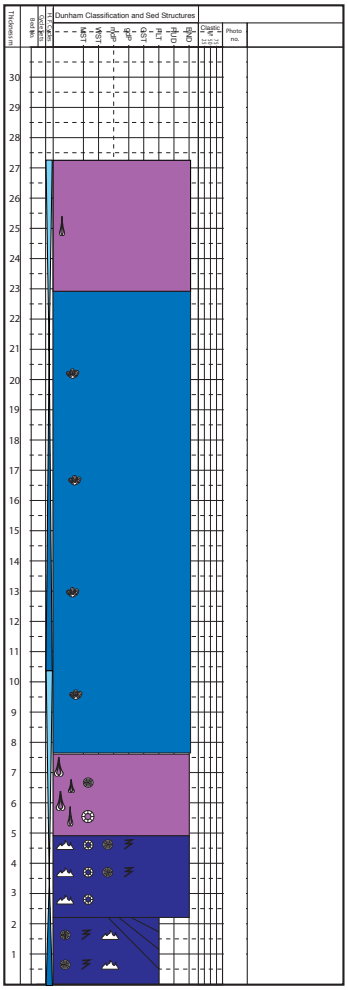

- Fenestral Laminite
- Tepee Horizon
- Beachrock
- Coated grain, microbial FS/RS
- Bubble fenestral, ooid GS/FS
- Bioclastic, ooid GS
- Sandy ooid lithoclast FS/RS
- Megalodont FS/RS
- Lithiotid FS/RS
- Stromatolitic BS
- Renalcis BS
- Stromatactis BS

- Lithiotid Bivalve
- Megalodont Bivalve
- Gastropod
- Undiff. Bioclast
- Pisoid
- Ooid
- Composite Grain
- Oncoid
- Lithoclast
- Beachrock or Tepee Slab

- Tepee Structure
- Sheet Crack
- Laminar Fenestrae
- Bubble Fenestrae
- Undiff. Fenestrae
- Ripple Lamination
- Tabular Cross-bedding

Measured Section B-7

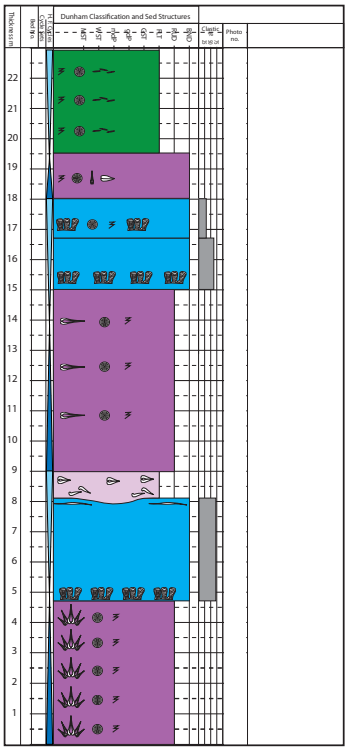

- Fenestral Laminite
- Tepee Horizon
- Beachrock
- Coated grain, microbial FS/RS
- Bubble fenestral, ooid GS/FS
- Bioclastic, ooid GS
- Sandy ooid lithoclast FS/RS
- Megalodont FS/RS
- Lithiotid FS/RS
- Stromatolitic BS
- Renalcis BS
- Stromatactis BS

- Lithiotid Bivalve
- Megalodont Bivalve
- Gastropod
- Undiff. Bioclast
- Pisoid
- Ooid
- Composite Grain
- Oncoid
- Lithoclast
- Beachrock or Tepee Slab

- Tepee Structure
- Sheet Crack
- Laminar Fenestrae
- Bubble Fenestrae
- Undiff. Fenestrae
- Ripple Lamination
- Tabular Cross-bedding

Measured Section B-8

References

Adams, E. W., J. P. Grotzinger, W. A. Watters, S. Schroder, D. S. McCormick, and H. A. Al-Siyabi, 2005, Digital characterization of thrombolite-stromatolite reef distribution in a carbonate ramp system (terminal Proterozoic, Nama Group, Namibia): AAPG Bulletin, v. 89, p. 1293-1318.

Adams, E. W., S. Schroder, J. P. Grotzinger, and D. S. McCormick, 2004, Digital Reconstruction and Stratigraphic Evolution of a Microbial-Dominated, Isolated Carbonate Platform (Terminal Proterozoic, Nama Group, Namibia): Journal of Sedimentary Research, v. 74, p. 479-497.

Assereto, R.L., and R. L. Folk, 1980, Diagenetic fabrics of aragonite, calcite, and dolomite in an ancient peritidal-spelean environment; Triassic Calcare rosso, Lombardia, Italy: Journal of Sedimentary Petrology, v. 50, p. 371-394.

Assereto, R. L., and C. G. S. C. Kendall, 1977, Nature, origin and classification of peritidal tepee structures and related breccias: Sedimentology, v. 24, p. 153-210.

Baceta, J. I., V. P. Wright, S. J. Beavington-Penney, and V. Pujalte, 2007, Palaeohydrogeological control of paleokarst macro-porosity genesis during a major sea-level lowstand: Danian of the Urbasa-Andia plateau, Navarra, North Spain: Sedimentary Geology, v. 199, p. 141.

Bai, T., 2000, Fracture spacing in layered rocks; a new explanation based on the stress transition, in D. D. Pollard, ed., Journal of Structural Geology, International, Pergamon: Oxford-New York, International, p. 43.

Barnaby, R. J., and W. B. Ward, 2007, Outcrop analog for mixed siliciclastic, and carbonate ramp reservoirs stratigraphic hierarchy, facies architecture, and geologic heterogeneity: Grayburg Formation, Permian Basin, U.S.A.: Journal of Sedimentary Research, v. 77, p. 34-58.

Bellian, J. A., C. Kerans, and D. C. Jennette, 2005, Digital Outcrop Models: Applications of Terrestrial Scanning Lidar Technology in Stratigraphic Modeling: Journal of Sedimentary Research, v. 75, p. 166-176.

Brown, S. A., I. M. Boserio, K. S. Jackson, and K. W. Spence, eds., 1984, The geological evolution of the Canning Basin; implications for petroleum exploration: The Canning Basin, W.A., p.85-96.

Brownlaw, R. L. S., R. M. Hocking, and J. S. Jell, 1996, High frequency sea-level fluctuations in the Pillara Limestone, Guppy Hill, Lennard Shelf, northwestern Australia: Historical Biology, v. 11, p. 187-212.

Chen, D., and M. E. Tucker, 2003, The Frasnian-Famennian mass extinction; insights from high-resolution sequence stratigraphy and cyclostratigraphy in South China: Palaeogeography, Palaeoclimatology, Palaeoecology, v. 193, p. 87-111.

Chow, N., and A. D. George, 2004, Tepee-shaped agglutinated microbialites; an example from a Famennian carbonate platform on the Lennard Shelf, northern Canning Basin, Western Australia: Sedimentology, v. 51, p. 253-265.

Chow, N., A. D. George, and K. M. Trinajstic, 2004, Tectonic control on development of a Frasnian–Famennian (Late-Devonian) paleokarst surface, Canning Basin reef complexes, northwestern Australia: Australian Journal of Earth Sciences, v. 51, p. 911-917.

Collins, J. F., J. A. M. Kenter, P. M. Harris, G. Kuanysheva, D. J. Fischer, and K. L. Steffen, 2006, Facies and Reservoir-quality Variations in the Late Visean to Bashkirian Outer Platform, Rim, and Flank of the Tengiz Buildup, Precaspian Basin, Kazakhstan, in P. M. Harris, and L. J. Weber, eds., Giant Hydrocarbon Reservoirs of the World: From Rocks to Reservoir Characterization and Modeling; American Association of Petroleum Geologists Memoir 88, p. 55-95.

Cook, H. E., V. G. Zhemchuzhnikov, W. G. Zempolich, V. Y. Zhaimina, V. M. Buvtyshkin, E. A. Kotova, L. Y. Golub, A. Y. Zorin, P. J. Lehmann, D. V. Alexeiev, A. Giovannelli, M. Viaggi, N. Fretwell, P. A. LaPointe, and J. J. Corboy, 2002, Devonian and Carboniferous carbonate platform facies in the Bolshoi Karatau, southern Kazakhstan; outcrop analogs for coeval carbonate oil and gas fields in the North Caspian Basin, western Kazakhstan, in W. G. Zempolich, and H. E. Cook, eds., Paleozoic carbonates of the Commonwealth of Independent States (CIS); subsurface reservoirs and outcrop analogs: Special Publication - Society for Sedimentary Geology 74, p. 81-122.

Copp, I. A., 2000, Subsurface facies analysis of Devonian reef complexes Lennard Shelf, Canning Basin, Western Australia: Report - Geological Survey of Western Australia.

Copper, P., 2002, Reef development at the Frasnian/Famennian mass extinction boundary: Palaeogeography. Palaeoclimatology. Palaeoecology, v. 181, p. 27-65.

Corbett, K. P., M. Friedman, and J. Spang, 1987, Fracture development and mechanical stratigraphy of Austin Chalk, Texas: AAPG Bulletin, v. 71, p. 17-28.

Corsetti, F. A., and J. P. Grotzinger, 2005, Origin and Significance of Tube Structures in Neoproterozoic Post-glacial Cap Carbonates: Example from Noonday Dolomite, Death Valley, United States: Palaios v. 20, p. 348-362.

Craig, J., J. W. Downey, A. D. Gibbs, and J. R. Russell, 1984, The application of Landsat imagery in structural interpretation of the Canning Basin, W.A.: The Canning Basin W.A.: Proceedings of the GSA/PESA Canning Basin Symposium, p. 57-71.

Daugherty, D. R., 1986, Characteristics and origins of joints and sedimentary dikes of the Bahama Islands: Proceedings of the Symposium on the Geology of the Bahamas, p. 45-56.

Della Porta, G., J. A. M. Kenter, and J. R. Bahamonde, 2004, Depositional facies and stratal geometry of an Upper Carboniferous prograding and aggrading high-relief carbonate platform (Cantabrian Mountains, N. Spain): Sedimentology, v. 51, p. 267-295.

Demicco, R. V., and L. A. Hardie, eds., 1994, Sedimentary structures and early diagenetic features of shallow marine carbonate deposits: SEPM Atlas Series, v. 1, Society of Sedimentary Geology, 265 p.

Doglioni, C., and R. K. Goldhammer, 1988, Compaction-induced subsidence in the margin of a carbonate platform: Basin Research, v. 1, p. 237-246.

Donaldson, J. A., and B. D. Ricketts, 1979, Beachrock in Proterozoic dolostone of the Belcher Islands, Northwest Territories, Canada: Journal of Sedimentary Research, v. 49, p. 1287-1294.

Dörling, S. L., M. C. Dentith, D. I. Groves, P. E. Playford, J. R. Vearncombe, P. Muhling, and D. Windrim, 1996, Heterogeneous brittle deformation in the Devonian carbonate rocks of the Pillara Range, Canning Basin; implications for the structural evolution of the Lennard Shelf: Australian Journal of Earth Sciences, v. 43, p. 15-29.

Drummond, B. J., M. A. Etheridge, P. J. Davies, and M. F. Middleton, 1988, Half-graben model for the structural evolution of the Fitzroy Trough, Canning Basin, and implications for resource exploration: APEA Journal, v. 28, p. 76-86.

Drummond, B. J., M. J. Sexton, T. J. Barton, and R. D. Shaw, 1991, The nature of faulting along the margins of the Fitzroy Trough, Canning Basin, and implications for the tectonic development of the trough: Exploration Geophysics, v. 22, p. 111±115.

Dunham, R. J., 1969, Vadose pisolite in the Capitan reef (Permian), New Mexico and Texas: Special Publication - Society of Economic Paleontologists and Mineralogists, v. 14, p. 182-191.

Dunham, R. J., 1972, Capitan Reef, New Mexico and Texas; facts and questions to aid interpretation and group discussion: Publication - Society of Economic Paleontologists and Mineralogists, Permian Basin Chapter, v. 72, p. 72-14.

Dunn, P. A., 1992, Cyclic stratigraphy and early diagenesis; an example from the Triassic Latemar Platform, northern Italy: Doctoral thesis, Johns Hopkins University, Baltimore, MD, 993 p.

Egenhoff, S. O., A. Peterhansel, T. Bechstaedt, R. Zuhlke, and J. Grotsch, 1999, Facies architecture of an isolated carbonate platform; tracing the cycles of the Latemar (Middle Triassic, northern Italy): Sedimentology, v. 46, p. 893-912.

Emmerich, A., V. Zamparelli, T. B. dt, and R. Zhlke, 2005, The reefal margin and slope of a Middle Triassic carbonate platform: the Latemar (Dolomites, Italy): Facies, v. 50, p. 573-614.

Esteban, M., and L. C. Pray, 1977, Origin of the pisolite facies of the shelf crest, in M. E. Hileman, and S. J. Mazzullo, eds., Publication - Society of Economic Paleontologists and Mineralogists, Permian Basin Chapter, v. 77-16.

Eyles, N., 2001, Permian-Carboniferous tectono-stratigraphic evolution and petroleum potential of the northern Canning Basin, Western Australia: AAPG Bulletin, v. 85, p. 989.

Fischer, A. G., 1964, The Lofer cyclothems of the Alpine Triassic: Kansas Geological Survey Bulletin, v. 1, p. 107-149.

Fraser, N. M., D. J. Bottjer, and A. G. Fischer, 2004, Dissecting “Lithiotis” Bivalves: Implications for the Early Jurassic Reef Eclipse: Palaios, v. 19, p. 51-67.

Frost, E. L., and C. Kerans, In review, Evidence For Stratigraphic Controls on Syndepositional Fracture Patterns: Journal of Sedimentary Research.

Frost, E. L., C. Kerans, and X. Janson, In prep., Evolution and Architecture of a Famennian (Late Devonian) Carbonate Platform, Canning Basin, Western Australia: Sedimentology.

George, A. D., 1999, Deep-water stromatolites, Canning Basin, northwestern Australia: Palaios, v. 14, p. 493-505.

George, A. D., and N. Chow, 2002, The depositional record of the Frasnian/ Famennian boundary interval in a fore-reef succession, Canning Basin, Western Australia: Palaeogeography, Palaeoclimatology, Palaeoecology, v. 181, p. 347-374.

George, A. D., N. Chow, and K. M. Trinajstic, 2002, Integrated approach to platform-basin correlation and deciphering the evolution of Devonian reefs, northern Canning Basin, Western Australia, in M. Keep, and S. Moss, J., eds., The sedimentary basins of Western Australia 3; proceedings of the West Australian basins symposium, v. 3: Perth, West. Aust., Australia, Petroleum Exploration Society of Australia, p. 817-835.

George, A. D., P. Playford, E., and C. M. Powell, 1995, Platform-margin collapse during Famennian reef evolution, Canning Basin, Western Australia: Geology, v. 23, p. 691-694.

George, A. D., P. E. Playford, and C. M. Powell, 1994, Carbonates breccias and quartzo-feldspathic sandstones of the marginal slope, Devonian reef complex, Canning Basin, Western Australia, in P. G. Purcell, and R. R. Purcell, eds., The sedimentary basins of Western Australia., v. 1: Perth, West. Aust., Australia, Petroleum Exploration Society of Australia, p. 727-738.

George, A. D., P. E. Playford, C. M. Powell, and P. M. Tornatora, 1997, Lithofacies and sequence development on an Upper Devonian mixed carbonate-siliciclastic fore-reef slope, Canning Basin, Western Australia: Sedimentology, v. 44, p. 843-867.

George, A. D., and C. M. Powell, 1997, Paleokarst in an Upper Devonian reef complex of the Canning Basin, Western Australia: Journal of Sedimentary Research, v. 67, p. 935-944.

Ginsburg, R. N., 1953, Beachrock in south Florida: Journal of Sedimentary Research, v. 23, p. 85-92.

Goldhammer, R. K., 1997, Compaction and decompaction algorithms for sedimentary carbonates: Journal of Sedimentary Research, v. 67, p. 26-35.

Goldhammer, R. K., M. T. Harris, P. A. Dunn, and L. A. Hardie, 1993a, Sequence stratigraphy and systems tract development of the Latemar Platform, Middle Triassic of the Dolomites (northern Italy); outcrop calibration keyed by cycle stacking patterns, in R. G. Loucks, and J. F. Sarg, eds., Carbonate sequence stratigraphy; recent developments and applications: AAPG Memoir, v. 57: Tulsa, American Association of Petroleum Geologists, p. 353-387.

Goldhammer, R. K., P. J. Lehmann, and P. A. Dunn, 1993b, The origin of high-frequency platform carbonate cycles and third-order sequences (Lower Ordovician El Paso Gp, West Texas); constraints from outcrop data and stratigraphic modeling: Journal of Sedimentary Petrology, v. 63, p. 318-359.

Gomez, L. A., 2007. Characterization and prediction of the spatial arrangement of opening-mode fractures. The University of Texas at Austin, Ph.D. dissertation.

Guidry, S. A., M. Grasmueck, D. G. Carpenter, A. M. G. Jr., S. L. Bachtel, and D. A. Viggiano, 2007, Karst and Early Fracture Networks in Carbonates, Turks and Caicos Islands, British West Indies: Journal of Sedimentary Research, v. 77, p. 508-524.

Guppy, D. J., A. W. Lindner, J. H. Rattigan, and J. N. Casey, 1958, The Geology of the Fitzroy Basin, Western Australia: Bureau of Mineral Resources, Geology, and Geophysics, Western Australia, Bulletin, v. 36, 73 p.

Handford, C. R., A. C. Kendall, D. R. Prezbindowski, J. B. Dunham, and B. W. Logan, 1984, Salina-margin tepees, pisoliths, and aragonite cements, Lake MacLeod, Western Australia; their significance in interpreting ancient analogs: Geology, v. 12, p. 523-527.

Harris, P. M., 1979, Facies anatomy and diagenesis of a Bahamian ooid shoal, Sedimenta, p. 163.

Hocking, R. M., and P. E. Playford, 1998, Devonian reef complexes of the Canning Basin (Geologic Maps): Geological Survey of Western Australia Bulletin, v. 145.

Hocking, R. M., and P. E. Playford, 2002, Cycle types in carbonate platform facies, Devonian reef complexes, Canning Basin, Western Australia: Geological Survey of Western Australia Annual Review, p. 74-80.

Holmes, A. E., and N. Christie-Blick, 1993, Origin of sedimentary cycles in mixed carbonate-siliciclastic systems; an example from the Canning Basin,

Western Australia, in R. G. Loucks, and J. F. Sarg, eds., Carbonate sequence stratigraphy; recent developments and applications: AAPG Memoir, v. 57, p. 181-212.

Hunt, D., and W. M. Fitchen, 1999, Compaction and the dynamics of carbonate-platform development; insights from the Permian Delaware and Midland basins; southeastern New Mexico and West Texas, U.S.A.: Special Publication - Society for Sedimentary Geology, v. 63, p. 75-106.

Hunt, D. W., W. M. Fitchen, and E. Kosa, 2002, Syndepositional deformation of the Permian Capitan reef carbonate platform, Guadalupe Mountains, New Mexico, USA: Sedimentary Geology, v. 154, p. 89-126.

Hunt, D. W., W. M. Fitchen, and E. Kosa, 2003, Syndepositional deformation of the Permian Capitan reef carbonate platform, Guadalupe Mountains, New Mexico, USA: Sedimentary Geology, v. 154, p. 89-126.

Hurley, N. F., 1986, Geology of the Oscar Range Devonian Reef Complex, Canning Basin, Western Australia., University of Michigan, 269 p.

Hurley, N. F., and K. C. Lohmann, 1989, Diagenesis of Devonian reefal carbonates in the Oscar Range: Canning Basin, Western Australia: Journal of Sedimentary Petrology, v. 59, p. 127-146.

Janson, X., C. Kerans, J. A. Bellian, and W. Fitchen, 2007, Three-dimensional geological and synthetic seismic model of Early Permian redeposited basinal carbonate deposits, Victorio Canyon, west Texas: AAPG Bulletin, v. 91, p. 1405-1436.

Joachimski, M. M., S. Breisig, and W. Buggisch, 2003, Climatic changes in the late Frasnian; trigger of the Frasnian-Famennian crisis: Abstracts with Programs - Geological Society of America, v. 35, p. 207.

Joachimski, M. M., and W. Buggisch, 1993, Anoxic events in the late Frasnian; causes of the Frasnian-Famennian faunal crisis? Geology, v. 21, p. 675-678.

Joachimski, M. M., and W. Buggisch, 2002, Conodont apatite ∂18O signatures indicate climatic cooling as a trigger of the Late Devonian mass extinction: Geology, v. 30, p. 711-714.

Joachimski, M. M., R. D. Pancost, K. H. Freeman, C. Ostertag-Henning, and W. Buggisch, 2002, Carbon isotope geochemistry of the Frasnian-Famennian transition: Palaeogeography, Palaeoclimatology, Palaeoecology, v. 181, p. 91-109.

Jones, G. D., and Y. Xiao, 2006, Geothermal convection in the Tengiz carbonate platform, Kazakhstan: Reactive transport models of diagenesis and reservoir quality: AAPG Bulletin v. 90, p. 1251-1272.

Kendall, C. G. S. C., and J. Warren, 1987, A review of the origin and setting of tepees and their associated fabrics: Sedimentology, v. 34, p. 1007-1027.

Kennard, J.M., Southgate, P.N., Jackson, M.J., O'Brien, P.E., Christie-Blick, N., Holmes, A.E., Sarg, J.F., 1992. New sequence perspective on the Devonian reef complex and the Frasnian-Famennian boundary, Canning Basin, Australia. Geology. v. 20, Issue 12, pp.1135-1138

Kenter, J. A. M., P. M. Harris, and G. Della Porta, 2005, Steep microbial boundstone-dominated platform margins; examples and implications: Sedimentary Geology, v. 178, p. 5-30.

Kerans, C., 1985, Petrology of Devonian and Carboniferous carbonates of the Canning and Bonaparte Basins: Report of the Western Australian Mining and Petroleum Research Institute, v. 12, 203 p.

Kerans, C., and W. M. Fitchen, 1995, Sequence hierarchy and facies architecture of a carbonate-ramp system; San Andres Formation of Algerita Escarpment and western Guadalupe Mountains, West Texas and New Mexico: Report of Investigations - Texas, University, Bureau of Economic Geology, v. 235, 86 p.

Kerans, C., N. F. Hurley, and P. E. Playford, 1986, Marine diagenesis in Devonian reef complexes of the Canning Basin, Western Australia: Reef diagenesis: Berlin, Springer-Verlag, 357-380 p.

Kerans, C., and S. Tinker, 1997, Sequence stratigraphy and characterization of carbonate reservoirs: SEPM Short Course Notes, v. 40, p. 130.

Kerans, C., and S. W. Tinker, eds., 1999, Extrinsic stratigraphic controls on development of the Capitan Reef Complex: Geological Framework of the Capitan Reef: SEPM, Special Publication, v. 65, 15-36 p.

Kosa, E., D. Hunt, W. M. Fitchen, M.-O. Bockel-Rebelle, and G. Roberts, 2003, The heterogeneity of paleocavern systems developed along syndepositional fault zones; the Upper Permian Capitan Platform, Guadalupe Mountains, U.S.A: Special Publication - Society for Sedimentary Geology, v. 78, p. 291-322.

Kosa, E., and D. W. Hunt, 2005, Growth of syndepositional faults in carbonate strata; Upper Permian Capitan Platform, New Mexico, USA: Journal of

Structural Geology, v. 27, p. 1069-1094.

Kosa, E., and D. W. Hunt, 2006, Heterogeneity in Fill and Properties of Karst-Modified Syndepositional Faults and Fractures: Upper Permian Capitan Platform, New Mexico, U.S.A.: Journal of Sedimentary Research, v. 76, p. 131-151.

Ladeira, F.L., and Price, N.J., 1981, Relationship between fracture spacing and bed thickness: Journal of Structural Geology, v. 3, p. 179-183.

Laubach, S. E., and M. E. Ward, 2006, Diagenesis in porosity evolution of opening-mode fractures, Middle Triassic to Lower Jurassic La Boca Formation, NE Mexico: Tectonophysics, v. 419, p. 75.

Logan, B. W., and V. Semeniuk, 1976, Dynamic metamorphism; processes and products in Devonian carbonate rocks, Canning Basin, Western Australia: Special Publication - Geological Society of Australia, 137 p.

Marrett, R., Gale, J., and Gomez, L. in review, Spatial arrangement of fractures III – correlation analyses. Journal of Structural Geology.

Marrett, R., and S. E. Laubach, 2001, Fracturing during burial diagenesis: Guidebook - Bureau of Economic Geology, University of Texas at Austin, v. 28, p. 109-123.

Marrett, R., O. J. Ortega, and C. M. Kelsey, 1999, Extent of power-law scaling for natural fractures in rock: Geology, v. 27, p. 799-802.

Middleton, M. F., 1987. Seismic stratigraphy of Devonian reef complexes, northern Canning Basin, Western Australia. AAPG Bulletin, V. 71, Issue 12, pp.1488-1498

Miller, J. McL., Nelson, E. P., Hitzman, M., Muccilli, P., and Hall, W. D. M., 2007, Orthorhombic fault–fracture patterns and non-plane strain in a synthetic transfer zone during rifting: Lennard shelf, Canning basin, Western Australia. Journal of Structural Geology 29, 1002-1021.

Narr, W., and J. Suppe, 1991, Joint spacing in sedimentary rocks: Journal of structural geology, v. 13, p. 1037-1048.

Ortega, O. J., R. A. Marrett, and S. E. Laubach, 2006, A scale-independent approach to fracture intensity and average spacing measurement: AAPG Bulletin, v. 90, p. 193-208.

Playford, P., E., N. F. Hurley, C. Kerans, and M. F. Middleton, 1989, Reefal platform development, Devonian of the Canning Basin, Western Australia, in P. D. Crevello, J. L. Wilson, J. F. Sarg, and J. F. e. Read, eds., Controls on carbonate platform and basin development: Special Publication - Society of Economic Paleontologists and Mineralogists, v. 44, p. 187-202.

Playford, P. E., 1980, Devonian 'great barrier reef' of Canning Basin, Western Australia: AAPG Bulletin, v. 64, p. 814-840.

Playford, P. E., 1981, Devonian reef complexes of the Canning Basin, Western Australia: Geological Society of Australia, Fifth Australian Geological Convention Guidebook, p. 64.

Playford, P. E., 1984, Platform-margin and marginal-slope relationships in Devonian reef complexes of the Canning Basin: The Canning Basin W.A., p. 189-214.

Playford, P.E., 2002, Palaeokarst, pseudokarst, and sequence stratigraphy in Devonian reef complexes of the Canning Basin, Western Australia, in M. Keep, and S. Moss, J., eds., The sedimentary basins of Western Australia; proceedings of the West Australian basins symposium., v. 3: Perth, West. Aust., Australia, Petroleum Exploration Society of Australia, p. 763-793.

Playford, P. E., and A. E. Cockbain, 1969, Algal stromatalites: deepwater forms in the Devonian of Western Australia: Science, v. 165, p. 1008-1010.

Playford, P. E., A. E. Cockbain, E. C. Druce, and J. L. Wray, 1976, Devonian stromatolites from the Canning Basin, Western Australia, in M. R. Walter, ed., Stromatolites.: Netherlands, Elsevier Sci. Publ. Co.: Amsterdam, Netherlands, p. 543.

Playford, P. E., A. E. Cockbain, R. M. Hocking, and M. W. Wallace, 2001, Novel paleoecology of a postextinction reef; Famennian (Late Devonian) of the Canning Basin, northwestern Australia; discussion and reply: Geology, v. 29, p. 1155-1156.

Playford, P. E., and R. Hocking, 2006, Discussion and Reply: Tectonic control on development of a Frasnian-Famennian (Late Devonian) palaeokarst surface, Canning Basin reef complexes, northwestern Australia: Australian Journal of Earth Sciences, v. 53, p. 665-669.

Playford, P. E., C. Kerans, and N. F. Hurley, 1984, Neptunian dikes and sills in Devonian reef complexes of Canning Basin, Western Australia: AAPG Bulletin, v. 68, p. 517.

Playford, P. E., and D. C. Lowry, 1966, Devonian reef complexes of the Canning Basin, Western Australia, Bulletin - Geological Survey of Western Australia, p. 150.

Playford, P. E., and M. W. Wallace, 2001, Exhalative Mineralization in Devonian Reef Complexes of the Canning Basin, Western Australia: Economic Geology, v. 96, p. 1595-1610.

Playton, T. E., In Prep, Depositional Elements, Variations, and Controls for Reefal Carbonate Foreslope Systems, The University of Texas, Austin.

Pomar, L., 2001, Types of carbonate platforms: a genetic approach: Basin Research, v. 13, p. 313-334.

Purcell, P. G., 1984, The Canning Basin, W.A.; an introduction, in P. G. Purcell, ed., The Canning Basin, W.A.

Read, J. F., 1973a, Carbonate Cycles, Pillara Formation (Devonian), Canning Basin, Western Australia: Bulletin of Canadian Petroleum Geology, v. 21, p. 38-51.

Read, J. F., 1973b, Paleo-Environments and Paleography, Pillara Formation (Devonian), Western Australia: Bulletin of Canadian Petroleum Geology, v. 21, p. 344-394.

Rusciadelli, G., and S. Di Simone, 2007, Differential compaction as a control on depositional architectures across the Maiella carbonate platform margin (central Apennines, Italy): Sedimentary Geology, v. 196, p. 133.

Schlager, W., 2003, Benthic carbonate factories of the Phanerozoic: International Journal of Earth Sciences, v. 92, p. 445-464.

Schlager, W., and O. Camber, 1986, Submarine slope angles, drowning unconformities, and self-erosion of limestone escarpments: Geology, v. 14, p. 762-765.

Sepkoski, J. J., 1986, Phanerozoic overview of mass extinction: Life Sciences Research Reports, v. 36, p. 277-295.

Shackleton, J. R., M. L. Cooke, and A. J. Sussman, 2005, Evidence for temporally changing mechanical stratigraphy and effects on joint-network architecture: Geology, v. 33, p. 101-104.

Shaw, R. D., M. J. Sexton, and I. Zeilinger, 1995, The Tectonic Framework of the Canning Basin, WA, Including 1: 2 Million Structural Elements Map of the Canning Basin, Record, Australian Geological Survey Organization.

Shen, J.-W., and G. E. Webb, 2004, Famennian (Upper Devonian) calcimicrobial (Renalcis) reef at Miaomen, Guilin, Guangxi, South China: Palaeogeography, Palaeoclimatology, Palaeoecology, v. 204, p. 373-394.

Shin, E. A., 1968, Practical singnificance of birdseye structures in carbonate rocks: Journal of Sedimentary Research, v. 38, p. 215-223.

Smart, P. L., R. J. Palmer, F. Whitaker, and V. P. Wright, eds., 1988, Neptunian dikes and fissure fills; an overview and account of some modern examples: Paleokarst: New York, NY, Springer-Verlag, 149-163 p.

Smith, D. B., 1974, Origin of Tepees in Upper Permian Shelf Carbonate Rocks of Guadalupe Mountains, New Mexico: AAPG Bulletin, v. 58, p. 63-70.

Southgate, P. N., J. M. Kennard, M. J. Jackson, P. E. O'Brien, and M. J. Sexton, 1993, Reciprocal lowstand clastic and highstand carbonate sedimentation, subsurface Devonian reef complex, Canning Basin, Western Australia, in R. G. Loucks, and J. F. Sarg, eds., Carbonate sequence stratigraphy; recent developments and applications: AAPG Memoir, v. 57, p. 157-179.

Stanton, R. J., Jr., and L. C. Pray, 2004, Skeletal-Carbonate Neptunian Dikes of the Capitan Reef: Permian, Guadalupe Mountains, Texas, U.S.A.: Journal of Sedimentary Research, v. 74, p. 805-816.

Stephens, Nat P., Sumner, D. Y., 2003a. Late Devonian carbon isotope stratigraphy and sea level fluctuations, Canning Basin, Western Australia. Palaeogeography, Palaeoclimatology, Palaeoecology, V. 191, Issue 2, pp.203-219

Stephens, N. P., and D. Y. Sumner, 2003b, Famennian microbial reef facies, Napier and Oscar ranges, Canning Basin, Western Australia: Sedimentology, v. 50, p. 1283-1302.

Teichert, C., 1941, Upper Devonian goniatite succession of Western Australia: American Journal of Science, v. 239, p. 148-153.

Teichert, C., 1943, The Devonian of Western Australia; a preliminary review: American Journal of Science, v. 241, p. 69-94.

Teichert, C., 1947, Stratigraphy of Western Australia: AAPG Bulletin, v. 31, p. 1-70.

Tinker, S. W., 1998, Shelf-to-basin facies distributions and sequence stratigraphy of a steep-rimmed carbonate margin; Capitan depositional system, McKittrick Canyon, New Mexico and Texas: Journal of Sedimentary Research, v. 68, p. 1146-1174.

Osleger, D. A., and S. W. Tinker, 1999, Three-dimensional architecture of Upper Permian high-frequency sequences, Yates-Capitan shelf margin, Permian Basin, U.S.A., in P. M. Harris, A. H. Saller, and J. A. Simo, eds., Advances in carbonate sequence stratigraphy; application to reservoirs, outcrops and models: Special Publication - Society for Sedimentary Geology, v. 63, Society for Sedimentary Geology (SEPM), p. 169-185.

Underwood, C. A., M. L. Cooke, J. A. Simo, and M. A. Muldoon, 2003, Stratigraphic controls on vertical fracture patterns in Silurian dolomite, northeastern Wisconsin: AAPG Bulletin, v. 87, p. 121-142.

Wade, A., 1924, Petroleum Prospects, Kimberley District of Western Australia and Northern Territory: Commonwealth of Australia, Melbourne, 63 p.

Wallace, M. W., C. Kerans, P. E. Playford, and A. McManus, 1991, Burial diagenesis in the Upper Devonian reef complexes of the Geikie Gorge region, Canning Basin, Western Australia: AAPG Bulletin, v. 75, p. 1018-1038.

Ward, W. B., 1996, Platform evolution and diagenesis of Frasnian carbonate platforms, Devonian reef complexes, Napier Range, Canning Basin, Western Australia, State University of New York at Stony Brook, 566 p.

Ward, W. B., 1999. Tectonic control on backstepping sequences revealed by mapping of Frasnian backstepped platforms, Devonian reef complexes, Napier Range, Canning Basin, Western Australia, In: Harris, P.M., Saller, A.H., Simo, J.A. (Eds.), Advances in Carbonate Sequence Stratigraphy: Applications to Reservoirs, Outcrops, and Models. V. 63, pp.47-74

Webb, G. E., 2001, Famennian mud-mounds in the proximal fore-reef slope, Canning Basin, Western Australia: Sedimentary Geology, v. 145, p. 295-315.

Whalen, M. T., J. Day, G. P. Eberli, and P. Homewood, 2002, Microbial carbonates as indicators of environmental change and biotic crises in carbonate systems; examples from the Late Devonian, Alberta Basin, Canada.: Palaeogeography, Palaeoclimatology, Palaeoecology, v. 181, p. 127-151.

Whalen, M. T., G. P. Eberli, F. S. P. van Buchem, E. W. Mountjoy, and P. W. Homewood, 2000, Bypass margins, basin-restricted wedges, and platform-to-basin correlation, Upper Devonian, Canadian Rocky Mountains; implications for sequence stratigraphy of carbonate platform systems: Journal of Sedimentary Research, v. 70, p. 913-936.

Wilson, J. L., 1975, Carbonate facies in geologic history: New York, N.Y., Springer-Verlag, 471 p.

Wood, R., 1998, Novel reef fabrics from the Devonian Canning Basin, Western Australia: Sedimentary Geology, v. 121, p. 149-156.

Wood, R., 2000, Novel paleoecology of a postextinction reef; Famennian (Late Devonian) of the Canning Basin, northwestern Australia: Geology, v. 28, p. 987-990.

Zempolich, W. G., H. E. Cook, V. G. Zhemchuzhnikov, V. Y. Zhaimina, A. Y. Zorin, V. M. Buvtyshkin, E. A. Kotova, L. Y. Golub, A. Giovannelli, M. Viaggi, P. J. Lehmann, N. Fretwell, D. V. Alexeiev, and P. A. LaPointe, 2002, Biotic and abiotic influence on the stratigraphic architecture and diagenesis of middle to upper Paleozoic carbonates of the Bolshoi Karatau Mountains, Kazakhstan and the Southern Urals, Russia; implications for the distribution of early ma, in W. G. Zempolich, and H. E. Cook, eds., Paleozoic carbonates of the Commonwealth of Independent States (CIS); subsurface reservoirs and outcrop analogs: Special Publication - Society for Sedimentary Geology 74, p. 123-180.

Vita

Edmund "Ned" Locke Frost III was born in Washington DC in August of 1974 to Ed and Roon Frost. The author graduated high school from the Berwick Academy in South Berwick Maine and completed a Bachelor of Arts Degree in Geology at the University of Colorado at Boulder in December of 1998. Before attending graduate school, Ned worked as a field geophysicist and as a land surveyor in the Boulder-Denver area. Ned was awarded best student poster at the 2006 American Association of Petroleum Geologist's international meeting in Perth, best student presentation at the 2007 American Association of Petroleum Geologist's annual meeting in Long Beach CA, and was voted best Ph.D. speaker for the Department of Geological Science's spring 2007 technical sessions. Ned was the recipient of the American Association of Petroleum Geologist's Richard C. Hasson Memorial Grant (2006), a Geological Society of America student grant (2005), and a ConocoPhillips fellowship (2005-2007). During his tenure at the University of Texas, Ned worked as a research assistant for the Bureau of Economic Geology's Reservoir Characterization Research Laboratory.

Permanent address: 1622 Missouri Street, Houston, TX 77006

This dissertation was typed by the author.